DOE/BC/14899-36
(DE96001235)

SUPRI HEAVY OIL RESEARCH PROGRAM

TR 106

Annual Report for the Period
February 8, 1995 to February 7, 1996

By
William E. Brigham
Louis M. Castanier

June 1996

Performed Under Contract No. DE-FG22-93BC14899

Stanford University
Stanford, California

Bartlesville Project Office
U. S. DEPARTMENT OF ENERGY
Bartlesville, Oklahoma

DOE/BC/14899-36
Distribution Category UC-122

SUPRI Heavy Oil Research Program

TR 106

Annual Report for the Period
February 8, 1995 to February 7, 1996

By
William E. Brigham
and
Louis M. Castanier

June 1996

Work Performed Under Contract No. DE-FG22-93BC14899

Prepared for
U.S. Department of Energy
Assistant Secretary for Fossil Energy

Thomas B. Reid, Project Manager
Bartlesville Project Office
P.O. Box 1398
Bartlesville, OK 74005

Prepared by
Stanford University
088 Green Earth Sciences
Stanford, CA 94305-2220

TABLE OF CONTENTS

OBJECTIVES

The goal of the Stanford University Petroleum Research Institute is to conduct research directed toward increasing the recovery of heavy oils. Presently, SUPRI is working in five main directions:

1. FLOW PROPERTIES STUDIES — To assess the influence of different reservoir conditions (temperature and pressure) on the absolute and relative permeability to oil and water and on capillary pressure.

2. IN-SITU COMBUSTION — To evaluate the effect of different reservoir parameters on the *in-situ* combustion process. This project includes the study of the kinetics of the reactions.

3. STEAM WITH ADDITIVES — To develop and understand the mechanisms of the process using commercially available surfactants for reduction of gravity override and channeling of steam.

4. FORMATION EVALUATION — To develop and improve techniques of formation evaluation such as tracer tests and pressure transient tests.

5. FIELD SUPPORT SERVICES — To provide technical support for design and monitoring of DOE sponsored or industry initiated field projects.

FOREWORD

We have published several papers and technical reports during the past year. In order to avoid repetition, the present report consists of abstracts of the reports and copies of the technical papers presented or published. The narrative describing the work in progress is of course original.

PROJECT 1: FLOW PROPERTY STUDIES

To assess the influence of different reservoir conditions (temperature and pressure) on the absolute and relative permeability to oil and water and on capillary pressure.

1.1 A Preliminary Study of Relative Permeability in Geothermal Rocks

(C. Satik, W. Ambusso, L. Castanier and R. Horne)

1.1.1 SUMMARY

The paper presented at the Geothermal Resources Council Meeting, Reno (October 8-11, 1995), and the 21st Workshop on Geothermal Engineering, Stanford (January 22 - 24, 1995), is a short summary of this work.

A PRELIMINARY STUDY OF RELATIVE PERMEABILITY IN GEOTHERMAL ROCKS

Cengiz Satik, Willis Ambusso, Louis M. Castanier and Roland N. Horne

Stanford Geothermal Program
Stanford University
Stanford, CA 94305-2220

ABSTRACT

This paper reports preliminary experimental and numerical efforts towards obtaining steam-water relative permeability and capillary pressure functions under steady-state and adiabatic conditions. In the experimental direction, steady-state nitrogen-water relative permeability experiments were conducted in a Berea sandstone core as a first step. Results obtained from this type of experiment will be compared to those from steam-water relative permeability experiments in order to explore the importance of phase change and heat transfer. Using a high resolution X-ray computer tomography (CT) equipment, saturation distributions along the core were obtained and relative permeabilities for both nitrogen and water were calculated. Preliminary results showed strong end effects for the core length and total flow rate used in the experiment, which therefore suggested either to use of a longer core or to work at a higher total flow rate. Along with the experiment, numerical simulations of simultaneous injection of steam and water into a core were also carried out by using a commercial thermal simulator. At steady-state flow conditions, effects of steam quality and total injection rate on saturation profiles were investigated. Numerical simulation results suggested a core length of 38.10 cm for a flat saturation profile region to exist under typical experimental conditions.

INTRODUCTION

Reliable measurement of steam-water relative permeability functions is of great importance in geothermal reservoir simulation to match or forecast production performance of geothermal reservoirs. Accordingly, the subject has attracted attention in the past and several experimental and theoretical attempts have been made to study this important problem. In spite of the large number of reported studies, there still remains considerable uncertainty about the exact form of these functions due to the difficulties encountered in the interpretation of results and the lack of understanding of microscopic pore-level phenomena such as phase change, heat transfer and capillarity.

Unsteady- or steady-state methods are traditionally used to determine relative permeability. Both methods measure the relative permeabilities as a function of saturation. Unsteady-state methods are based on the Buckley-Leverett (B-L) theory, therefore, they are restricted by its assumptions. These methods have commonly been used for immiscible, isothermal and noncondensing types of displacement processes. Steady-state methods measure relative permeabilities that are independent of time. During steady-state experiments two fluids are injected simultaneously at a known fraction until steady-state conditions are reached. At steady state, relative permeabilities are calculated by using a theory that relies on Darcy's law extended for multi phase flow. The corresponding saturation values should also be determined. The main assumption of these methods is the requirement for existence of a flat saturation profile, which can be achieved by using a sufficiently long core or high flow rates. Otherwise, the *capillary end-effects* commonly observed in many experiments may complicate interpretation of the results.

Steady-state methods have been used to determine steam-water relative permeabilities under adiabatic conditions. Even though such experiments are simpler, previous literature has pointed out major difficulties, particularly in the interpretation of results. Problems have arisen in the determination of accurate saturation profiles and also in the treatment of phase change, heat transfer, capillarity and injection rate. Two typical problems have been studied in the past: one involving an injection of a subcooled liquid which undergoes a phase change inside the porous medium after the injection, and another involving simultaneous injection of steam and water.

An early attempt was reported by Arihara (1974) who was unable to measure saturation directly but calculated it instead. The calculation was performed by first measuring the temperature profile along the core to obtain fluid properties, enthalpy and pressure,

and by using steady-state, single-component, non-isothermal and adiabatic flow equations, combined with a relative permeability ratio and a water-oil permeability vs. saturation curve. Trimble and Menzie (1975) developed relative permeability curves for Boise and Berea sandstone cores. They reported unusually low steam relative permeability. Later on, Chen(1976) made an important advance by measuring water saturation directly using a capacitance probe technique, but he assumed a nearly linear relationship between the capacitance probe signal and the water saturation. Counsil (1979) used Chen's method to obtain the water saturation for the process of in-situ evaporation of flowing water. He obtained steady-state steam-water relative permeabilities for a synthetic sandstone core under adiabatic conditions. Counsil (1979) also measured nitrogen-water relative permeabilities and concluded that steam-water relative permeabilities are very different from those of nitrogen-water at high water saturations. His data indicated steam relative permeability being large in all but a narrow region of high water saturation. Later, Monsalve et al. (1984) studied the effects of surfactants on steam-water systems and concluded that relative permeability to water increased with increasing surfactant concentration rather than holding constant. Additionally, Monsalve (1984) observed that steam relative permeability decreased drastically at a certain water saturation, results similar to those of Counsil (1979). Verma (1986) reported a study of relative permeability for two-phase concurrent flow of steam and water. He compared his results with those from oil/water, gas/water and gas/oil systems. He found out that wetting phase relative permeability curves were in good agreement while steam relative permeability was significantly higher than that of non-wetting phase. Recently, Sanchez (1987) reported steady-state adiabatic steam-water relative permeability experiments for an unconsolidated Ottawa sand pack. Sanchez (1987) measured liquid saturations by analyzing the output of a 10 microliter pulse input of NaCl-36 through an HPLC sample injector. He concluded that steam-water relative permeabilities can be represented accurately by gas-liquid permeability for high permeability reservoirs. Very recently, similar results were also reported by Piquemal (1994) who attempted to determine steam-water relative permeabilities in an unconsolidated sandstone.

The wide discrepancy observed in the previous experimental results suggests that the interpretation of the data may not be correct. Additionally, a major problem of obtaining reliable saturation profiles has been emphasized. Recognizing that saturation and temperature profiles are dependent on parameters such as injection rate and temperature, steam

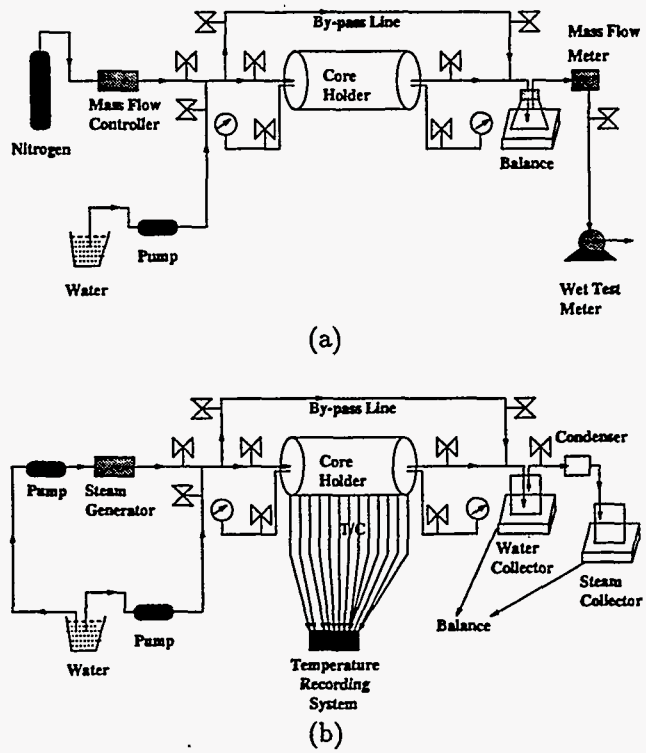

Figure 1: Schematics of experimental apparatus for (a) nitrogen-water and (b) steam-water injection.

quality, system pressure, core permeability and length and also that determining accurate saturation profiles is crucial, we initiated a systematic study to determine steady-state steam-water relative permeabilities directly. With the use of our X-ray computer tomography (CT) scanner equipment, which is capable of producing high-resolution images, we can overcome the difficulty of obtaining accurate saturation distributions along the core samples while multi-phase experiments are being conducted. This paper reports our preliminary results towards the final goal. First, we describe our experimental apparatus and procedure. Next, we discuss some preliminary results from a nitrogen-water injection experiment. Finally, we report some numerical simulation results for the problem of simultaneous injection of steam and water.

EXPERIMENTAL APPARATUS AND PROCEDURE

The experimental apparatus used for the preliminary nitrogen-water relative permeability measurements is shown in Figure 1a. It consist of a core holder, two pressure transducers, a liquid pump, a mass flow

controller, a mass flow meter, a balance and a wet-test meter. Two pressure taps located at the inlet and outlet ends of the core holder were used to measure the water phase pressure during the experiment. Nitrogen injection and production rates are controlled and monitored with the use of mass flow-controller, flowmeter and wet-test meter while a liquid pump was used to inject water into the core and a balance was used to measure water production rate. However, a different experimental apparatus is required for steam-water relative permeability experiments. A schematic of the tentative experimental design for the steam-water relative permeability experiments is shown in Figure 1b. This design will consist of a core holder, two liquid pumps, a steam generator and steam and water collection systems. Pressures will be measured at the inlet and outlet ends of the core while temperatures will be measured by thermocouples inserted at various locations along the core. Several heat flux sensors will be placed along the length of the core holder to measure heat losses.

During an experiment, the core holder is placed inside the high resolution X-ray computer tomography (CT) equipment in order to obtain in-situ saturation profiles along the core. The principles of the use of X-ray CT are described in Johns et al. (1993). Here, we shall summarize this method briefly. The X-ray CT method, as a nondestructive imaging method, enables us to construct an internal image of an object. Simply, an X-ray source is revolved around the object to take various projections at many angles and the data collected are then used to reconstruct the internal image. As X-ray beam travels through the object, changes in density and/or thickness of the material cause differences in X-ray attenuation. The image data obtained with the scanner are normalized to CT numbers whose unit is called a Hounsfield.

The experimental procedure as follows. First, air inside the pore space is displaced out by injecting several pore volumes of CO_2 and then the core is scanned at predetermined locations to obtain dry-core CT (CT_{dry}) values. Next, water is injected into the core to remove CO_2 and to eventually saturate it completely. This step continues until the core is completely saturated with water, at which time the core is X-ray scanned again at the same locations to obtain wet-core CT (CT_{wet}) values and, inlet and outlet end pressure readings are taken at this time. Steady-state relative permeability experiments involve injection of varying fractions of nitrogen and water (or steam and water), at a constant total flow rate, into the core. Measurements done at each step result in a single data point on relative permeability vs. saturation curve. Starting from completely water saturated core and injecting nitrogen at increasing fractions will give rise to a drainage process while the opposite procedure gives rise to an imbibition process. Each step continues until steady-state conditions at which injection and production rates become the same for both nitrogen and water and also inlet and outlet end pressures stabilize. At the onset of steady-state conditions, another X-ray scanning is done along the core at the same locations to obtain CT (CT_{exp}) values corresponding to the particular gas-water fraction. To complete the step, inlet and outlet end pressure readings are taken again. Next, the nitrogen-water fraction is changed, keeping total flow rate constant, and the procedure is repeated.

After the experiment is completed, interpretation software is used to calculate the porosity and saturation distributions from the CT values obtained with the scanner. To calculate porosity the following expression is used:

$$\phi = \frac{CT_{wet} - CT_{dry}}{CT_{water} - CT_{air}} \tag{1}$$

where CT_{water}, CT_{air} are CT numbers for water and air, respectively. Similarly, the expression used to calculate saturations is:

$$S_g = \frac{CT_{wet} - CT_{exp}}{CT_{wet} - CT_{dry}} \tag{2}$$

and

$$S_w = 1 - S_g \tag{3}$$

where S_g and S_w denote gas and water saturations, respectively. Relative permeabilities for water and nitrogen can be calculated by using Darcy's law,

$$k_{rw} = \frac{\mu_w q_w L}{kA\Delta p_w} \tag{4}$$

for water and

$$k_{rg} = \frac{\mu_g q_g L}{kA\Delta p_g} \tag{5}$$

for gas. Here k_r, μ, q, k, A, L and Δp are relative permeability, flow rate, permeability, cross sectional area and length of the core and pressure drop, respectively. Subscripts w and g denote water and gas, respectively. In these equations, all of the parameter values are either measured or determined by using the experimental data. For the preliminary experiment, we measured water and gas flow rates and water pressure drop but calculated nitrogen pressure drop by using a nitrogen-water capillary pressure curve.

PRELIMINARY RESULTS

EXPERIMENTAL

A preliminary experiment was conducted to measure nitrogen-water relative permeability. The core

used in this experiment was a Berea sandstone, the length and diameter of which were 25.4 cm and 5.08 cm, respectively. The total injection rate of fluids was 12 cc/min. Porosity and saturation distributions, and relative permeability were obtained by using the results of this experiment, as discussed below.

First, the absolute permeability of the core was calculated by using Equation 4 with $k_{rw} = 1$ and also with the results of the wet-core step. The value was calculated to be 601 mD. Next, the porosity distributions along the core were obtained by inserting the CT values in Equation 1. In Figure 2, we show the porosity distributions at four different locations through the

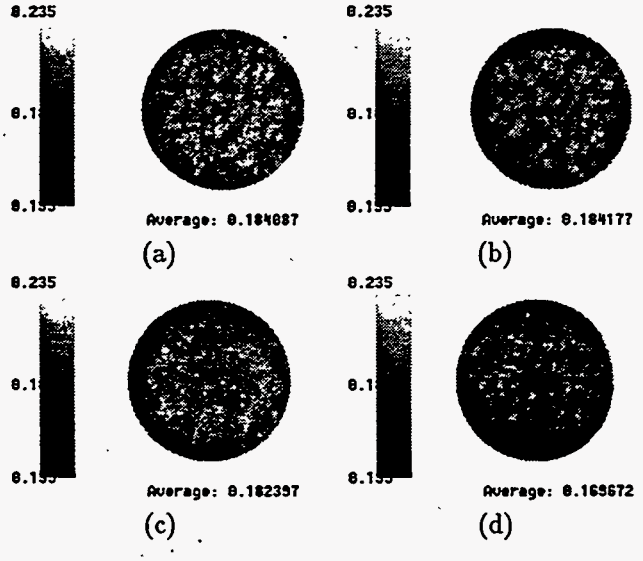

Figure 2: Porosity distributions obtained from X-ray CT scanning at (a) 0.2 cm, (b) 8.2 cm, (c) 16.2 cm and (d) 25.2 cm from the inlet end of the core.

core (at 0.2, 8.2, 16.2 and 25.2 cm from the inlet end of the core). Average porosity was calculated to be 18.50 %. During the experiment, we obtained a total of 26 slices from the X-ray CT scanning. All of those slices indicated a fairly homogenous core with average porosity decreasing slightly (from 18.4087 % to 16.9672 %) towards the outlet.

Saturation distributions were also calculated by using Equations 2a and b. In Figure 3, we show nitrogen saturation distributions at four different locations along the core (0.2, 8.2, 16.2 and 25.2 cm from the inlet end of the core). Nitrogen saturation is higher closer to the inlet and decreases closer towards the oulet. Saturation distributions shown in the figure are consistent with the porosity distributions (Figure 2). Small gas saturations spots observed in Figures 3b, c and d correspond to smaller porosity values, implying gas (non-wetting) phase residing in large pores with water (wetting) phase residing in smaller pores.

Average water saturation distributions calculated using Equation 2b for four different values of f_g (gas fraction), defined as the fraction of the gas flow rate to the total flow rate), are shown in Figure 4. All of the saturation distributions shown in the figure indicates very strong inlet end effects (saturations starting from about 60 % at the inlet and increasing with distance) and a possible weak outlet end effect. Flat saturation profiles do not exist probably due to the strong end effects. Moreover, water saturation changes significantly as f_g increases from 0.16 to 0.3333 although further increase in f_g (up to 0.84) does not seem to change the saturation levels significantly. These preliminary results suggest either using a longer core or operating at a higher total flow rate to obtain a flatter saturation profile.

A summary of the preliminary experiment is given in Table 1. Water pressure drops were measured directly

Table 1: Summary of preliminary results for a nitrogen-water relative permeability experiment.

f_g	ΔP_w, psi	ΔP_g, psi	k_{rw}	k_{rg}
0	5	0	1.0	0.0
0.16	16	20.17	0.312	0.0009
0.33	19	23.50	0.210	0:00155
0.50	15	19.67	0.1999	0.0028
0.67	11	15.67	0.1817	0.0046
0.84	6	10.27	0.1666	0.0089

during the experiment. Gas pressure drops, however, were calculated by using a nitrogen-water capillary pressure curve obtained for Berea sandstone (borrowed from the study of Oak et al. (1990)). Finally, relative permeabilities for each phase were calculated by using Equations 4 and 5. Water relative permeabilities decreases monotonically as f_g increases while gas relative permeabilities are almost zero. This implies a very sharp increase in the f_g vs. S_g curve within a very narrow gas saturation range.Therefore, it is necessary to increase the f_g value to between 0.84 and 1.0 to have an increase in gas relative permeability.

NUMERICAL

To investigate the effects of various parameters and to determine a proper core length along which a flat saturation profile may exist, we carried out numerical simulations by using a commercial thermal simulator. Simultaneous injection of steam and water under adiabatic conditions were simulated. In the context of this

Table 2: Typical parameter values used in the numerical simulations.

ρ_w	=	$960.85\ \mathrm{kg/m^3}$
C_{pw}	=	$4.2092 * 10^3\ \mathrm{J/kg-K}$
λ_w	=	$0.6808\ \mathrm{W/m-K}$
μ_w	=	$2.4799 * 10^{-4}\ \mathrm{N-s/m^2}$
L_V	=	$2.2568 * 10^6\ \mathrm{J/kg}$
ρ_s	=	$0.5886\ \mathrm{kg/m^3}$
C_{ps}	=	$4.2092 * 10^3\ \mathrm{J/kg-K}$
λ_s	=	$0.6808\ \mathrm{W/m-K}$
μ_s	=	$2.4799 * 10^{-4}\ \mathrm{N-s/m^2}$
ρ_r	=	$2200.0\ \mathrm{kg/m^3}$
C_{pr}	=	$8.3732 * 10^2\ \mathrm{J/kg-K}$
λ_r	=	$6.808\ \mathrm{W/m-K}$
k	=	400 mD
ϕ	=	0.20
A	=	$5.08 * 10^{-4}\ \mathrm{m^2}$
L	=	0.381 m
p_{init}	=	$1.0133 * 10^5\ \mathrm{N/m^2}$
T_{init}	=	294.15 K

paper, we shall discuss only the effects of steam quality and total injection rates. Parameter values used in the simulations are given in Table 2. In the table, $\rho, C_p, \lambda, L_v, p$ and T denote density, specific heat capacity, thermal conductivity, latent heat of evaporation, pressure and temperature, respectively. Subscripts w, s and r represent water and steam phases, and rock, respectively.

In Figure 5, we show water saturation, temperature and pressure profiles obtained from numerical simulation for parameter values given in Table 2 and for a total injection rate (m_i) of 5 kg/D and a mass steam quality (X_s) of 0.25. In order to simulate end effects numerically, the capillary pressure was set to zero and the permeability was assigned a large value of 20000 mD in both the first and last grid blocks. The water saturation profile shows both inlet (an increse in water saturation) and outlet (first an increase or buildup followed by a decrease in water saturation) end effects which are restricted to narrow regions, otherwise a flat saturation profile is observed. To interpret our results, we followed a recent study of Parlar et al. (1990), which showed an analytical attempt to understand the end effects for steady-state, vapor-liquid concurrent flows in porous media. Because capillary pressure is zero at the inlet and oulet ends and is non-zero otherwise steam entering the core condenses at the inlet, causing a sudden temperature drop (Figure 5b). However, towards the outlet end, the effect is the opposite such that capillary pressure becomes zero from a nonzero value. This will induce first a saturation buildup and then a saturation decrease at the outlet, which are associated with a condensation process followed by an evaporation (see also Parlar et al., 1990). The temperature profile is also consistent with this interpretation. The temperature decreases while condensation occurs and flattens when evaporation takes place (see Figure 5b). The pressure profile shown in Figure 5c follows the trend of the temperature profile since both steam and water phases are flowing under saturated conditions.

Water saturation profiles obtained for five different steam quality values ($X_s = 0.0005, 0.05, 0.25, 0.50$ and 0.75) are shown in Figure 6. As steam quality increases greater displacement of water takes place therefore the average water saturation value within the flat region decreases. Figure 6 shows that the flat saturation value is about 0.40 for X_s=0.75 while it is about 0.74 for X_s=0.0005. As steam quality decreases the flat saturation region becomes narrower.

The effect of total injection rate is shown in Figure 7. Total flow rate has increased from 0.5 kg/D to 10 kg/D while steam quality has been kept as 0.25. The results shown are as expected. The region where oulet end effects are dominant becomes narrower as total flow rate increases since macroscopic capillary number also increases. Finally, we investigated the effect of the core length on saturation profiles. The simulation results suggested that a minimum core length of 38.10 cm would be required to avoid the end effects for typical experimental conditions.

CONCLUSIONS

Preliminary experimental and numerical efforts were made towards the final goal of determining steam-water relative permeability and capillary pressure functions in geothermal rocks. Experiments with nitrogen and water were carried out as a first step. Porosity and saturation distributions were calculated by using high resolution X-ray computer tomography (CT) equipment. Results indicated strong end effects, suggesting either use of a longer core or operation at higher total flow rates.

Numerical simulations were also carried out by using a commercial thermal simulator to study the problem of simultenous steam-water injection into a porous medium under adiabatic conditions. Numerical simulation results suggested the minimum core length to maintain a flat saturation profile would be 38.10 cm for typical laboratory conditions. Effects of steam quality and total injection rate were investigated. The results obtained were as expected.

ACKNOWLEDGEMENTS

This work was supported by DOE contract DE-FG07-90ID12934, the contribution of which is gratefully acknowledged. The authors also would like to thank Aldo Rossi for his assistance. The thermal simulator (STARS) was made available by Computer Modelling Group, Calgary, Alberta.

REFERENCES

N. Arihara. 1974. A study of nonisothermal single and two-phase flow through consolidated sandstones. Ph. D. Thesis, Stanford University, Stanford, California.

K. K. Chen. 1976. Measurement of water content in porous media under geothermal fluid flow conditions. Ph. D. Thesis, Stanford University, Stanford, California.

J. R. Counsil. 1979. Steam-water relative permeability. Ph. D. Thesis, Stanford University, Stanford, California.

R. A. Johns, J. S. Steude, L. M. Castanier, and P. V. Roberts. 1993. Nondestructive measurements of fracture aperture in crystalline rock core using x ray computed tomography. *J. Geophys. Res,*, 98(B2):1889–1900.

A. Monsalve, R. S. Schechter, and W. H. Wade. 1984. Relative permeabilities of surfactant/steam/water systems. Paper SPE 12661 presented at the 1984 SPE Symposium on Enhanced Oil Recovery, Tulsa, April 15-18.

M. J. Oak, L. E. Baker, and D. C. Thomas. 1990. Three-phase relative permeability of berea sandstone. *J. Petroleum Tech.*, pages 1054–1061.

M. Parlar, M. Zeybek, and Y. C. Yortsos. 1990. Steady-state, vapor-liquid concurrent flow: relative permeabilities and end effects. Paper SPE 20054 presented at the SPE California Regional Meeting, Ventura, CA, April 4-6.

J. Piquemal. 1994. Saturated steam relative permeabilities of unconsolidated porous media. *Transport in Porous Media*, 17:105–120.

J. M. Sanchez. 1987. Surfactant effects on the two-phase flow of steam/water and nitrogen/water in an unconsolidated permeable medium. Ph. D. Thesis, University of Texas, Austin, Texas.

A. E. Trimble and D. E. Menzie. 1975. Steam mobility in porous media. Paper SPE 5571 presented at the 50th Annual Fall Meeting, SPE of AIME, Dallas, TX, Sept.

A. K. Verma. 1986. Effects of phase transformation on steam water relative permeability. Ph. D. Thesis, University of California, Berkeley, CA.

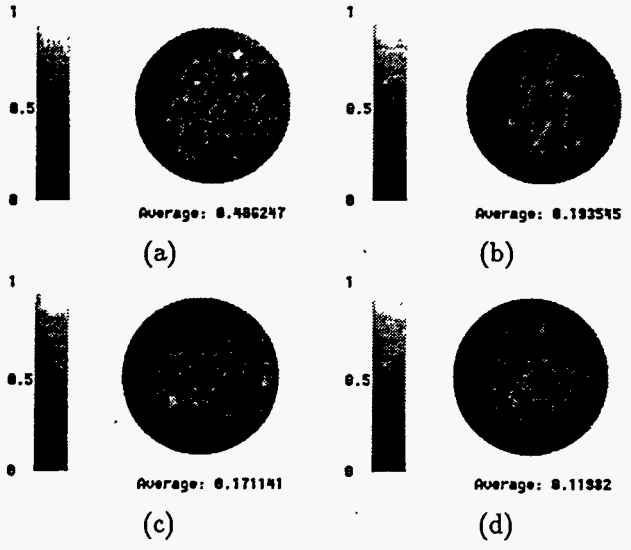

Figure 3: Nitrogen saturation distributions obtained from X-ray CT scanning at (a) 0.2 cm, (b) 8.2 cm, (c) 16.2 cm and (d) 25.2 cm from the inlet end of the core.

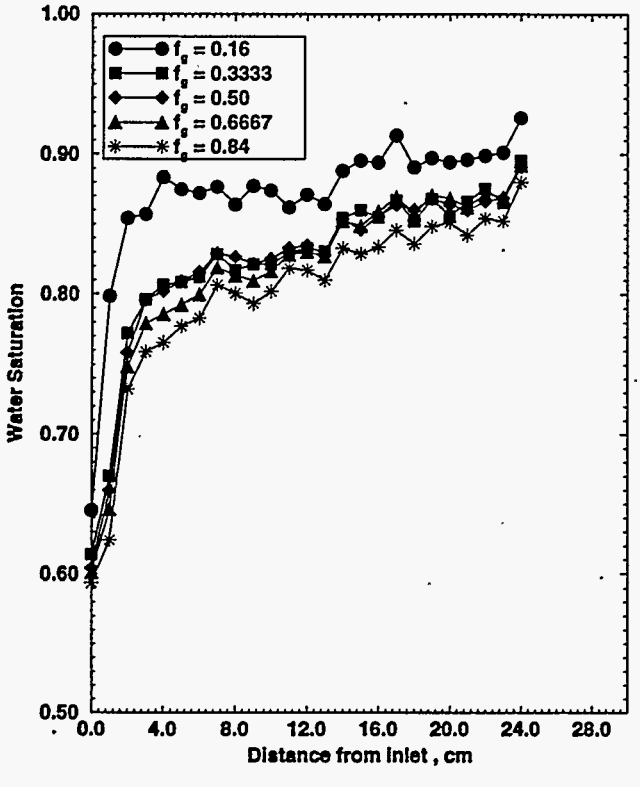

Figure 4: Water saturation distributions obtained in nitrogen-water steady-state experiments.

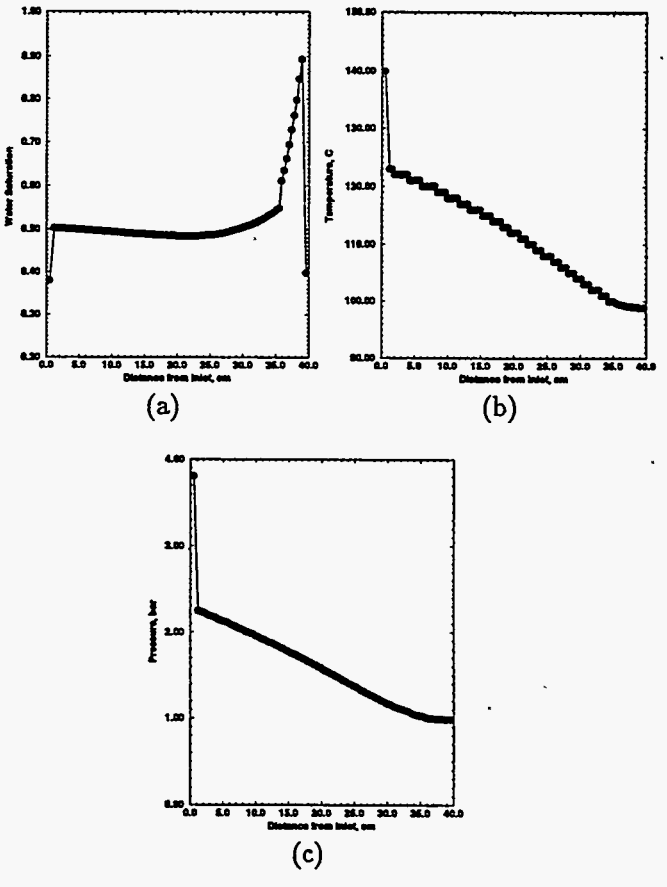

Figure 5: Steady-state steam-water simulation results (a) Saturation, (b) temperature and (c) pressure distributions.

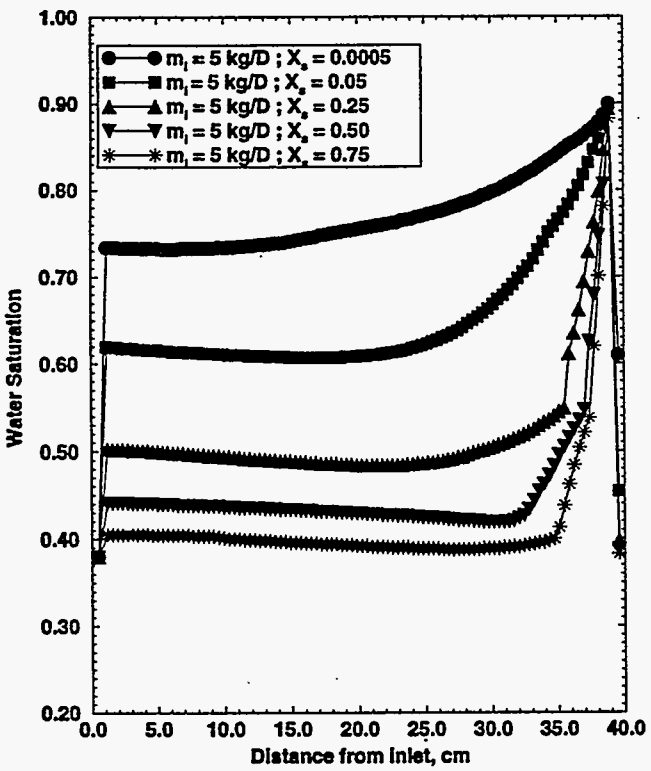

Figure 6: Water saturation distributions obtained in steam-water steady-state simulations at five different steam quality values.

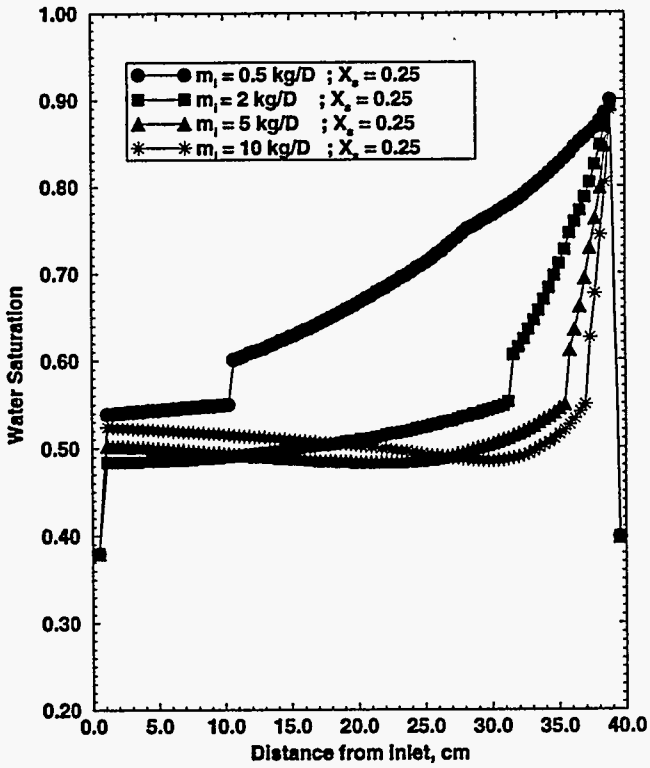

Figure 7: Water saturation distributions obtained in steam-water steady-state simulations at four different total injection rates.

1.2 CT Imaging of Two Phase Flow in Fractured Porous Media
(R. Hughes, W. Brigham and L. Castanier)

1.2.1 SUMMARY

The paper presented at the 21st Annual Workshop on Geothermal Reservoir Engineering, Stanford (January 22 - 24, 1995), is a short summary of this work. The technical report is completed and ready for publication.

CT IMAGING OF TWO PHASE FLOW IN FRACTURED POROUS MEDIA

Richard G. Hughes, William E. Brigham, and Louis M. Castanier

Stanford University
Stanford, CA 94305-2220

ABSTRACT

This paper describes the design, construction, and preliminary results of an experiment that studies imbibition displacement in two fracture blocks. Three core configurations were constructed. The configurations are a compact core, a two-block system with a 1 mm spacer between the blocks, and a two-block system with no spacer. The blocks are sealed in epoxy so that saturation measurements can be made throughout the displacement experiments using a Computed Tomography (CT) scanner.

Preliminary results are presented from a water/air experiment. These results suggest that it is incorrect to assume negligible capillary continuity between matrix blocks as is often done.

INTRODUCTION

The simulation of flow in naturally fractured reservoirs commonly divides the reservoir into two continua – the matrix system and the fracture system. Flow equations are written presuming that the primary flow between grid blocks occurs through the fracture system and that the primary fluid storage is in the matrix system. The dual porosity formulation of the equations assumes that there is no flow between matrix blocks while the dual permeability formulation allows fluid movement between matrix blocks. Since most of the fluid storage is contained in the matrix, recovery is dominated by the transfer of fluid from the matrix to the high conductivity fractures. The physical mechanisms influencing this transfer have been evaluated primarily through numerical studies. Relatively few experimental studies have investigated the transfer mechanisms. Early studies focused on the prediction of reservoir recoveries from the results of scaled experiments on single reservoir blocks. Recent experiments have investigated some of the mechanisms that are dominant in gravity drainage situations and in small block imbibition displacements. Hughes (1995) discusses these experiments in detail. One of the primary drawbacks to many of these experiments is the lack of understanding of the saturation distributions in the rock matrices. Other recent work has emphasized understanding flow through a single fracture with no transfer from the matrix (Persoff, et al (1991), Persoff and Pruess (1993), Fourar, et al (1993), Persoff and Pruess (1995)).

Guzman and Aziz (1993) initiated a study of two-phase flow in fractured porous media. The initial purpose for this work was to attempt to measure relative permeabilities in the fracture. An experiment was designed to measure saturation distribution in two cores of identical material. One core would be a control while the other would be cut in half and propped open with inert material to simulate a fracture. Oil and water would be injected into the cores at varying rates. Saturations would be measured by CT scanning the core at various stages of the injection process. Fine grid simulations would then be used to history match the experimental results.

Fine grid simulations were performed to help in the design of the experimental procedure (Guzman and Aziz, 1992). An experiment was built but, unfortunately, problems developed during single phase injection testing precluded obtaining results. The work reported here is a modification

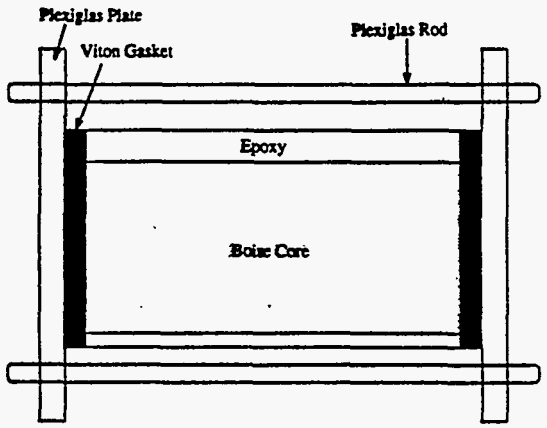

Figure 1: The core holder.

and extension of the Guzman and Aziz (1993) study. The focus will be on obtaining both qualitative and quantitative data on the movement of fluids in fractured blocks.

EXPERIMENTAL APPARATUS

Three rectangular blocks of Boise sandstone were prepared for use in this work. The first is a compact (solid) core measuring 3 1/8 × 3 1/16 × 11 inches. The second and third cores consist of two 2 15/16 × 1 1/2 × 11 inch blocks. The second core system has a 1 mm thick spacer fastened in place with Epoxy 907 to provide a separation between the blocks to simulate a fracture. The third core system is constructed similarly but has no spacer between the blocks.

Due to the rectangular shape and the desire to measure in-situ saturations through the use of the CT scanner, conventional core holders could not be used. A core holder similar to the original design by Guzman and Aziz (1993) was developed for each of the cores. It consists of an epoxy resin surrounding the core. The resin system used was Tap Plastics Marine Grade Resin #314 with Tap Plastics #143 Hardener. Plexiglas end plates were constructed for the core holders with a piece of 3/8 inch Viton acting as a gasket between the core and the Plexiglas end plates. The Viton gaskets were held in place with automotive gasket material and Plexiglas rods as shown in Figure 1.

The original design had six pressure taps all on the top of the core holder. The new design has two pressure taps on the top and two on the bottom. In addition, a Plexiglas plate that was epoxied to the top surface of the core was removed in the new design. The plate was found to be unnecessary and a potential source for leaks.

Several different epoxy systems were tested in addition to the system chosen. Among these were Tap Plastics 'One to One' General Purpose Epoxy, Tap Plastics 'Super Hard' Four to One Epoxy, and Evercoat Laminating Resin. All of these epoxies were extremely exothermic when reacting to become solid. The Tap Plastics Marine Grade Epoxy system selected uses the #314 resin in combination with various hardeners to provide different cure times with similar chemical resistances and strengths. The #143 Hardener was chosen because it provides a slower cure, yet retains its chemical resistance properties. This system is slightly less viscous so penetration is a bit deeper into the core than it was for some of the other systems we observed; however, for this experiment the added control the slow cure time provided was deemed to be a more important issue than penetration depth.

In addition to using a slower curing epoxy system, an aluminum mold was constructed to allow better heat dissipation. The mold was built so that there would be a 1/2 inch border of epoxy around the bottom and sides of the core. It had an open top with sides which were six inches taller than the estimated top of the epoxy. This allowed the heat to radiate out of the mold and helped to prevent cracking of the epoxy.

To construct the core holders, Plexiglas end plates were attached to both ends of a 12 inch long core with GE White RTV 102 Silicon Rubber Adhesive Sealant and held in place with clamps. Epoxy was layered on with a paintbrush and allowed to set for one hour. The core was then placed into the mold. The mold was tilted at a 45 degree angle and the epoxy was poured in. Tilting the mold reduced the number of air bubbles which can form along the bottom of the core. Once the liquid resin covered the core, the mold was returned to horizontal and additional resin was added to reach the desired height. During the construction of the compact core holder, heat expansion of the air inside the core caused air bubbles to form and rise to the surface of the epoxy at one of the ends. For the two subsequent cores, holes were drilled in the Plexiglas end plates. This action alleviated the problem. Figure 2 shows an oblique view of the core holder after the epoxy has cured.

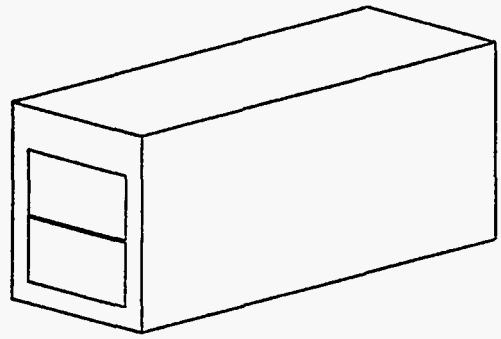

Figure 2: The core holder after curing.

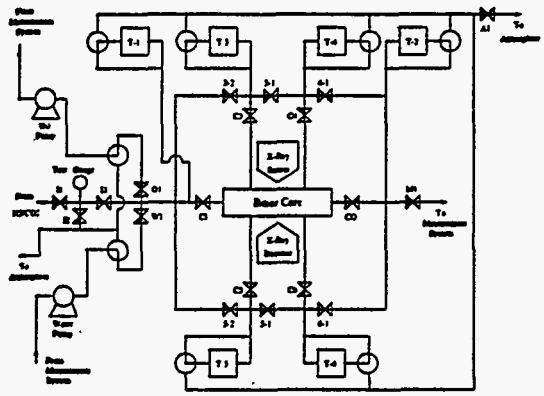

Figure 3: Experimental flow schematic.

Once the epoxy had cured, the cores were removed from the mold and the ends were trimmed with a water-cooled diamond circular saw to provide an 11 inch length. A piece of 3/8 inch Viton was then cut for each end face of the core holder. A hole was cut in the Viton so that the core face would be exposed. Automotive gasket material was then used to glue the Viton to the epoxy and the Viton to the Plexiglas end plates. Plexiglas rods were bolted into place through holes that had been drilled into each end plate. This provided added support and also allowed the gasket material/Viton to be compressed to eliminate leaks.

Figure 3 shows the flow schematic for this work. The injection system consists of two LDC Analytical, Inc. model constaMetric 3200 pumps. Each pump has the capability to deliver 0.01 to 9.99 cm^3/min in 0.01 cm^3/min increments. The pumps use a dual plunger system that has been designed to provide constant fluid discharge rates at outlet pressures from 100-6000 psi. To use the pumps the

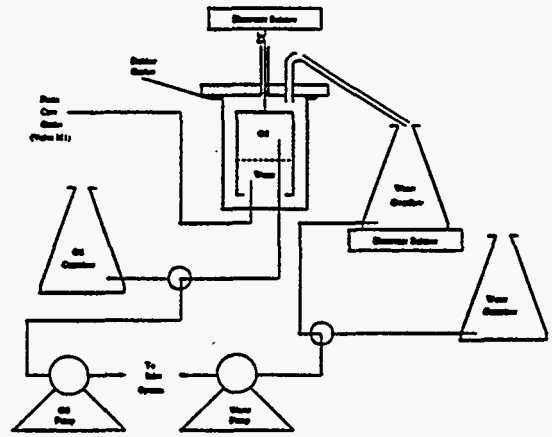

Figure 4: The production measurement system.

user sets the desired discharge rate, the minimum allowable pressure, and the maximum allowable pressure. Plumbing downstream of the pumps allows mixing of the fluids being discharged by each pump. This setup allows injection pressure to be monitored with a test gauge and recirculation to measure pump output rates. This configuration also is a convenient way to use nitrogen in the calibration of the pressure transducers, or to use CO_2 to help in the saturation of the core. Pump inlet can be from an extra "make up" container or from the measured fluids being discharged from the core.

All piping used for the experiment was Paraflex 1/8 inch diameter, 500 psi working pressure plastic tubing with stainless steel Swagelok fittings. The distribution of fluids throughout the experiment is controlled by Whitey B-43F2 ball valves. This system allows fluids to be directed to any port or combination of ports in the experiment. It can be directed to test the calibration of the pressure transducers, inject from one end and produce from the opposite end (the primary configuration), inject into one or more of the ports on the top and bottom of the core holder (which are normally used for monitoring pressures), or to bypass the core holder completely. The ability to direct fluids to any port in the experiment allows charging the core with fluids readily, testing various flow configurations, and cleaning the core more easily.

The production measurement system is an adaptation of a design first proposed by engineers at Conoco, Inc that was built by Ameri and Wang (1985) and modified by Qadeer (1994). Figure 4 shows the system.

The key element of the measurement system is the separator. It consists of two glass vessels, one inside the other. The inner vessel has an open bottom and a closed top. It hangs inside the outer vessel, suspended from an electronic balance by a hooked wire. Produced fluids enter this inner vessel and separate due to density differences. The lighter fluid (in this case, oil) rises and collects at the top of the inner vessel and the more dense fluid (water) exits from the bottom. The outer vessel is initially filled with water. When production begins, water from the inner vessel is displaced into the outer vessel and in turn, displaces water from the outer vessel through the glass tube at the top. The glass tube has a hole in the top to break any siphon effect. Total liquid production is calculated by the amount of water that is collected in a beaker which sits on an electronic balance. The electronic balance attached to the inner vessel measures the buoyant weight of the vessel. From the weight change measured on this balance, oil production is calculated.

Pressure measurement for the experiment is accomplished through the use of six Celesco DP31 differential pressure transducers. Two of the transducers are connected to ports on the top of the core holder and two on the bottom. The ports are approximately 8 cm from each end. Two other transducers are connected to the inlet and outlet ends of the core holder. The negative side of each transducer is open to the atmosphere. This differs from the original work by Guzman and Aziz (1993). In their study, only the outlet end port had the negative side of the transducer open to the atmosphere. The remaining ports had their negative sides connected to the core outlet end. All the stainless steel diaphragms for the transducers are the 5 psi type. The Celesco transducers work in combination with carrier demodulators, either Celesco model CD10A, CD10D, or CD25A demodulators. The demodulators take the output from the transducers and produce a DC signal in the range -10 to +10 volts.

Output signals for the carrier demodulators can be collected by a set of Soltec Transducer Products, Inc. 1243 Chart Recorders, or the signals can be fed into an HP3497A data logger. If the data logger is used, the digital signal from the data logger is sent to an IBM compatible personal computer (PC) through a HP-IB interface card in the PC. Output signals from the two electronic balances are sent directly to serial communication ports in the PC.

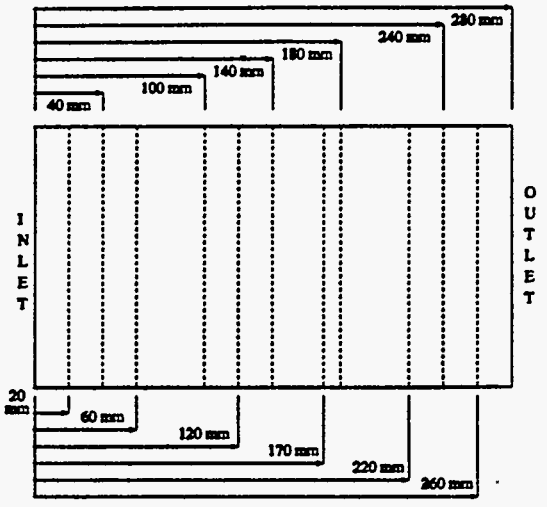

Figure 5: CT scan locations.

Saturation measurement for this experiment is through the use of a Picker 1200SX Dual Energy CT Scanner. This scanner is a fourth generation medical scanner that has been modified for laboratory use. The interested reader is referred to the Picker 1200SX Operators Guide (1983) for further specifications on the system.

PRELIMINARY RESULTS

Once the experiment had been designed and constructed, the equipment needed to be tested and evaluated for its ability to obtain meaningful results. Guzman and Aziz (1993) presented a figure in their work which showed how the CT scanner can indicate unsaturated conditions within the rock matrix.

For this study it was decided to evaluate how water imbibed into an unsaturated core. The first core that was used had the 1 mm fracture. Figure 5 shows the locations that were chosen for the CT scans. Two items prevented a regular sequence of scan locations. The first was that stainless steel fittings were used for the ports on the top and bottom of the core holder. These fittings caused artifacts and prevented scan locations from 70 mm to 85 mm and from 190 mm to 205 mm. These are distances measured from the inlet face. The second item that caused an irregular spacing of the scan locations was a large vug located 170 mm from the inlet face which we wanted to monitor throughout the experiment.

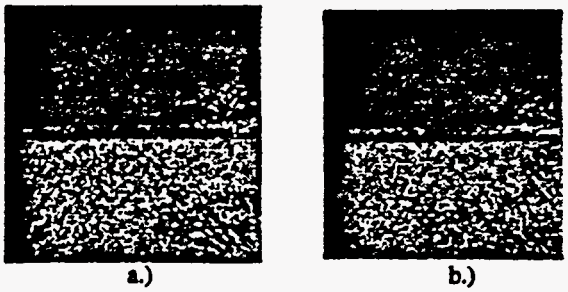

a.) b.)

Figure 6: CT scan at a.)+40 mm and b.)+60 mm from the inlet end at 0.09 PV injected. Lighter shades indicate higher water saturation.

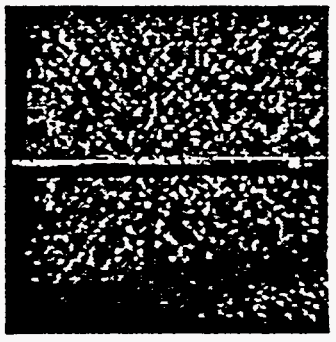

Figure 7: CT scan at +260 mm from the inlet end at breakthrough. Lighter shades indicate higher water saturation.

The core holder had a gap corresponding to the width of the Viton gasket at both the inlet and outlet face of the core. At an injection rate of 1 cm^3/min, the injected water simply dribbled down the inside of the Plexiglas inlet face plate and was imbibed into the bottom block. As the experiment progressed, the water began filling the gap between the Plexiglas plate and the core; however, it was very late in the experiment before the injection water got above the level of the fracture. The outlet condition was initially open to the atmosphere. After approximately 1.75 PV had been injected, the outlet was directed to the separation system and the injection rate was increased. Outlet pressure was 0.51 psi, while inlet pressure was 0.75 psi, at a flow rate of approximately 2 cm^3/min.

Migration of the water was monitored with the CT scanner. Initially, all water moved through the lower block only. When approximately 0.06 pore volumes (PV) had been injected, a slight amount of water was seen crossing the fracture to the top block at both the 40 mm location and the 60 mm location. Figure 6 shows CT scans taken at 40 mm and 60 mm from the inlet end when approximately 0.09 PV of water had been injected. These scans were chosen since they clearly show the water in the upper block. There appears to be at least one continuity across the fracture on the right edge of the blocks near these locations. The conclusion drawn from these and other CT scans is that the water crosses at these locations and then migrates towards the outlet face in the top and bottom blocks. The water also imbibes back towards the inlet face in the top block. Note also that water appears to be along the entire width of the fracture face on the top block in both scan locations, but that the fracture seems to be filled with air (except on the right edge as noted above).

As the injection process continues, water advances towards the outlet end in both the upper and lower blocks; however, since there is no water between the inlet face and where the water crosses the fracture, the advance in the upper block appears to lag behind that in the lower block. Once this space has been filled, water advance in the top block overtakes the advance in the bottom block.

Water breaks through and begins collecting on the bottom of the outlet face plate at approximately 0.47 PV injected. Figure 7 is the scan at 260 mm from the inlet face at the time of water breakthrough. It clearly shows areas in the bottom block where water has not contacted the rock pores. It also shows that the top block has a more uniform saturation distribution. Despite the fact that water was being injected only into the bottom block, capillary imbibition pulls the water across the continuity and through the top block such that the top block actually breaks through before the bottom block.

The experiment was run over the course of four days. Approximately 4.26 PV of water passed through the core. Once the experiment was terminated, the valves leading to the core were closed and the core was allowed to sit for three months. The core was then scanned again. The changes that occur between the scans at the end of injection and those three months later are most noticeable along the edges of blocks and the edges of the vug. These alterations could possibly be caused by positioning errors, since the core holder was removed from the scanning table during the three month wait. Figure 8 shows scans 170 mm from the inlet. Figure 8b has an increased saturation and appears more uniform than Figure 8a. The

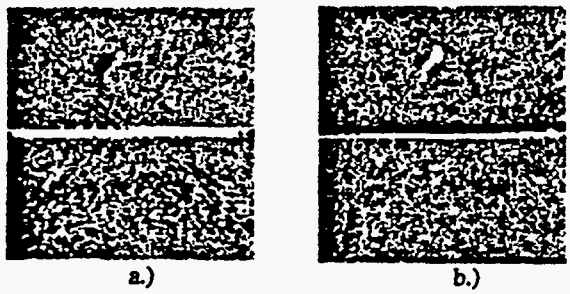

a.) b.)

Figure 8: CT scans at +170 mm from the inlet end a.) at the end of the displacement and b.) after a 3 month wait. Lighter shades indicate higher water saturation.

entire scan area has added water and a pocket of air has formed on the top of the fracture adjacent to the top block. Note that the vug has filled considerably with water but that there continues to be a small area in the upper left side of the vug that contains air. These results would suggest that, at least some of the changes seen are real, and are not positioning differences. This figure also emphasizes the slow nature of the approach to equilibrium in porous media.

One additional item on these experimental results is noteworthy. Withjack (1988) has shown that porosity can be calculated from the matrix of CT numbers obtained when scanning by using the equation:

$$\phi = \frac{CT_{cw} - CT_{cd}}{CT_w - CT_a} \qquad (1)$$

where: CT_{cw} is the CT number for a water saturated core at a matrix location, CT_{cd} is the CT number for a dry core at a matrix location, CT_w is the CT number for water, and CT_a is the CT number for air. The CT number for water is 0, while the CT number for air is -1000.

Despite passing more than 4 PV of water through the core, the average value for "porosity" calculated from the scans at the end of the displacement experiment using Eq. 1 was 14.35%. This differs from the average porosity measurements of 25.4% obtained by Guzman and Aziz (1993) and 29.3% obtained by Sumnu (1995) for rock samples obtained from the same part of the quarry that the samples used in this study were from. Sanyal (1971) also worked with Boise sandstone in his studies and obtained an average porosity value of 32% for his samples.

Attempts to saturate the core by the addition of CO_2 and injecting water into the pressure measurement ports raised the value calculated to an average of 20%. There continue to be areas (mainly in the lower block) that either have lower porosity or that have difficulty being saturated at the rates and pressures used in the experiment.

SUMMARY

The experiments conducted thus far have shown that the constructed system can obtain meaningful results in the effort to understand the physics of flow in fractured media. Flow in the experiment is across the blocks with gravity segregation possible at low rates. Thus, experiments can be run which mimic flow between wells (across the block) with water rising from below on one side. The flow configuration can be easily altered to accommodate other possible boundary conditions. Filter paper or fine grained sand could be used to fill the space between the Plexiglas plate and the core if a more even distribution inlet or outlet condition is desired. A tubing configuration could be devised similar to that described in a study by Kazemi and Merrill (1979) if injection is to be limited to the fracture space. Experimental pressures have been as high as 16 psi and flow rates up to 10 cm^3/min have been recorded. The preliminary experiments have also shown areas in the rock which have lower permeability. These areas will need special attention when charging the core with oil, during displacement experiments, and also during cleaning operations. We would not have been aware of these problems if we had not had the useful additional information provided by the CT scanner.

To use the CT scanner to monitor the migration of fluids when the core is being charged with oil, or when the core is being cleaned, the stainless steel Swagelok fittings should be replaced with equivalent plastic fittings. Artifacts in the CT numbers will still occur due to the fittings, but these would be minor and would allow observation of saturation changes near the injection ports. Such observations are not possible with stainless steel fittings.

Several authors (Kazemi and Merrill (1979), Beckner (1990), Gilman, et al (1994)) have assumed that fracture capillary pressures are negligible. Others have shown experimentally that capillary continuity becomes important when gravity provides a driving force (Horie et al (1988), Firoozabadi and Hauge (1990), Labastie (1990), Firooz-

abadi and Markeset (1992a, 1992b)). Kazemi (1990) states his belief that capillary continuity is prevalent in the vertical direction and has suggested that, to reduce the number of equations to solve, fractured reservoir simulations should use the dual permeability formulation for the z direction, and the dual porosity formulation for the x and y directions.

The CT scans shown in this report confirm that capillary continuity can occur in the vertical direction. This continuity pulls fluid in the opposite direction of gravity. The continuity works in any direction depending on the relative strengths of the capillary and Darcy terms in the flow equations. Thus, the simulation engineer should evaluate the forces present in the system being simulated to decide which directions should be evaluated by dual permeability equations and which by dual porosity.

It should be noted that it remains unclear as to what has caused the continuity between blocks in this experiment. The most likely explanation is that fine grained material from cutting the end pieces may not have been thoroughly cleaned from the fracture. Some fine grained material was observed in the space between the rock and the Plexiglas end plates once the core had been filled with water. A repeat of this experiment should reveal whether this material caused the continuity across the fracture, or if there is some other mechanism.

ACKNOWLEDGEMENTS

Financial support during the course of this work was provided by the Department of Energy through the Stanford University Petroleum Research Institute, under Contract No. De-FG-22-93BC14899, and the SUPRI-A Industrial Affiliates. This support is gratefully acknowledged.

References

[1] Ameri, H. and Wang, J.: "Effect of Temperature on Oil-Water Relative Permeability," SUPRI Heavy Oil Research Program, Eighth Annual Report, SUPRI TR–47, (April 1985), 11–24.

[2] Beckner, B.L.: *Improved Modeling of Imbibition Matrix/Fracture Fluid Transfer in Double Porosity Simulators*, PhD dissertation, Stanford University (July 1990).

[3] Firoozabadi, A. and Hauge, J.: "Capillary Pressure in Fractured Porous Media," *JPT* (June 1990) 784–791.

[4] Firoozabadi, A. and Markeset, T.: "An Experimental Study of Capillary and Gravity Crossflow in Fractured Porous Media," *SPE* 24918, presented at the 67th SPE Annual Technical Conference and Exhibition, Washington, D.C., October 4–7, 1992.

[5] Firoozabadi, A. and Markeset, T.: "An Experimental Study of Gas-Liquid Transmissibility in Fractured Porous Media," *SPE* 24919, presented at the 67th SPE Annual Technical Conference and Exhibition, Washington, D.C., October 4–7, 1992.

[6] Fourar, M., Bories, S., Lenormand, R. and Persoff, P.: "Two-Phase Flow in Smooth and Rough Fractures: Measurement and Correlation by Porous-Medium and Pipe Flow Models," *Water Resources Research* (November 1993), 3699–3708.

[7] Gilman, J.R., Bowzer, J.L. and Rothkopf, B.W.: "Application of Short-Radius Horizontal Boreholes in the Naturally Fractured Yates Field," *SPE* 28568, presented at the 69th SPE Annual Technical Conference and Exhibition, New Orleans, LA, September 25–28, 1994.

[8] Guzman, R. E. and Aziz, K.: *Design and Construction of an Experiment For Two-Phase Flow in Fractured Porous Media*, SUPRI TR–95, Stanford Petroleum Research Institute, Stanford, CA, (June 1993).

[9] Guzman, R. E. and Aziz, K.: "Fine Grid Simulation of Two-Phase Flow in Fractured Porous Media," *SPE* 24916, presented at the 67th SPE Annual Technical Conference and Exhibition, Washington, D.C., October 4–7, 1992.

[10] Horie, T., Firoozabadi, A. and Ishimoto, K.: "Capillary Continuity in Fractured Reservoirs," *SPE* 18282, presented at the 63rd SPE Annual Technical Conference and Exhibition, Houston, TX, October 2–5, 1988.

[11] Hughes, R.G.: *CT Measurements of Two-Phase Flow in Fractured Porous Media*, Masters Report, Stanford University (December 1995).

[12] Kazemi, H. and Merrill, L. S.: "Numerical Simulation of Water Imbibition in Fractured Cores," *SPEJ* (June 1979) 175–182.

[13] Kazemi, H.: *Naturally Fractured Reservoirs*, Third International Forum on Reservoir Simulation, Baden, Austria (1990).

[14] Labastie, A.: "Capillary Continuity Between Blocks of a Fractured Reservoir," *SPE* 20515 presented at the 65th SPE Annual Technical Conference and Exhibition, New Orleans, LA, September 23–26, 1990.

[15] Persoff, P. and Pruess, K.: "Flow Visualization and Relative Permeability Measurement in Rough-Walled Fractures," in *High Level Radioactive Waste Management: Proceedings of the Fourth International Conference, Las Vegas, NV, April 26–28, 1993*, vol. 2, 2033–2041, American Society of Civil Engineers, New York, 1993.

[16] Persoff, P. and Pruess, K.: "Two-Phase Flow Visualization and Relative Permeability Measurement in Natural Rough-Walled Rock Fractures," *Water Resources Research* (May 1995), 1175–1186.

[17] Persoff, P., Pruess, K. and Myer, L.: "Two-Phase Flow Visualization and Relative Permeability Measurement in Transparent Replicas of Rough-Walled Fractures," in Proceedings, Sixteenth Workshop on Geothermal Reservoir Engineering, Stanford University, Stanford, CA, January 23–25, 1991, 203–210.

[18] *Operator's Guide, Synerview 600s/1200SX, C850:F, REV1*, Picker International (January 1983).

[19] Qadeer, S.: *Techniques to Handle Limitations in Dynamic Relative Permeability Measurements*, PhD dissertation, Stanford University (in progress).

[20] Sanyal, S.K.: *The Effect of Temperature on Electrical Resistivity and Capillary Pressure Behavior of Porous Media*, PhD dissertation, Stanford University (December 1971).

[21] Sumnu, M.D.: *A Study of Steam Injection in Fractured Media*, PhD dissertation, Stanford University (November 1995).

[22] Withjack, E.M.: "Computed Tomography for Rock-Property Determination and Fluid-Flow Visualization," *SPEFE* (December 1988) 696–704.

1.3 Three-Phase Flow Observations in Micromodels

(T. Lolomari and M. Blunt)

1.3.1 ABSTRACT

This work is concerned with the description of fluid distribution and pore-scale displacement mechanisms for three phase flow (air, oil and water) and foam using silicon micromodels. The micromodels are an exact replica of a Berea sandstone and overcome most of the limitations of previous micromodels. Previous research on three phase flow using micromodels was reviewed. Also, details of a new micromodel design and experimental set-up are provided.

1.3.2 INTRODUCTION

The equations governing the multiphase flow of fluids requires information relating the rock and the constituent fluids. These relationships describing multiphase flow are capillary pressure - saturation and relative permeability - saturation (macroscopic) laws [1] and are usually obtained measured in the laboratory. This procedure is fairly straight forward for two phase systems. Empirical approaches [2],[3] and scaling methods [4] for describing two phase flow are also widely used. Examples of two phase systems are water injection into an undersaturated oil reservoir, an active aquifer in a gas field.

The addition of a third phase into a porous medium serves to complicate the multiphase flow description of the fluids. Three phase flow conditions arise during gravity drainage, gas or steam injection into an oil reservoir and water injection below the bubble point in an oil reservoir. Obtaining laboratory measurements of three-fluid systems is difficult, time consuming and expensive and few studies have been done with this approach [5]-[18]. A more common (empirical) approach for estimating constitutive relationships for three-fluid systems is by a combination of two-fluid measurements [19], [20], [4] or matching numerically limited experimental and field data [21],[22],[23].

These empirically obtained three phase relative permeabilities do not account for the physics of the flow and have very restrictive assumptions regarding the characteristics of the solid, fluids and solid-fluid interactions (for example, all the three phase flow relations assume that the capillary pressure and relative permeabilities are unique functions of saturation and fluid property independent; this assumption is very inaccurate especially at low oil saturation's). Comparisons of the empirical models to experimental data show that they generally failed to predict the measured relative permeabilities [21], [24], [18].

A recent computational approach for incorporating the physics of flow for calculating three-phase relative permeabilities is pore network modeling. The idea is to code the pore level displacement mechanisms for the flow into a numerical model and predict the capillary pressures and relative permeabilities [25],[26],[27], [28]. These network models require a better understanding of the physical mechanisms involved in the various fluid-fluid, fluid-rock interactions before significant progress can be made in

their accuracy. A better understanding of these pore scale displacement mechanisms can be obtained through the use of micromodel visualization techniques. The next section is a review of these visualization techniques for three phase flow.

1.3.3 LITERATURE REVIEW

Much experimental work has been done for two-phase systems using micromodels and the basic physical mechanisms involved are well understood [29], [30]. In contrast, there have been very few micromodel visualization studies on three-phase systems. The earliest works [31],[32] had only two of the three fluids mobile at any given time. More recent studies have been conducted by Soll *et al.* [33] and Oren and Pinczewski [34], [35]. One shortcoming of these studies is that the micromodels used had pore sizes (300-600 mm) which were not representative of real porous media (typically, at least one order of magnitude less) . This leads to different capillary and Peclet numbers from real porous media. Most recently, Keller et al. [36] used a micromodel that had realistic pore dimensions, geometry, and representative capillary numbers.

1.3.4 DISPLACEMENT MECHANISMS

Three phase displacement mechanisms involve one fluid displacing another which further displaces a third fluid. Hence they are termed double displacements. There are two main types of double displacements in three phase flow: (1) double drainage and (2) double imbibition. These double displacements can arise during gravity drainage in a reservoir, in a solution gas drive reservoir below the bubble point, or during the lowering of a gas-oil contact due to a gas cap or coning.

Double drainage occurs when gas displaces oil, which then displaces water or gas→oil→water (where the arrow is read as "displaced by"). The gas and water phases must be continuous in the pore space for double drainage to occur. Oren and Pinczewski [35] and Keller *et al.* [36] have observed several double drainage mechanisms in their micromodels. Double imbibition occurs when water→oil→gas. Again, the gas and water phases must be continuous for double imbibition to occur. Keller *et al.* [36] observed few double imbibition processes in the micromodel (the very high speeds of this event makes it very difficult to capture), though the majority of the displacements were two phase imbibitions. Using air, decane and water, they also observed DDI and IDI, bringing their total of observed displacements to four out of a possible six. These observed displacement mechanisms can subsequently be used to calculate three phase relative permeabilities and capillary pressures from a pore network model.

A total of six double displacements mechanisms are possible [28] and are summarized on the following page:

Table 1: Summary of three phase, double displacement mechanisms

MECHANISM	NAME	NOTES
Drainage		
Gas→Oil→Water	Double Drainage, DD	Mobilizes Residual Oil
Gas→Water→Oil	Drainage Imbibition with Overall Drainage, DDI	Oil Must be Continuous
Oil→Gas→Water	Drainage Imbibition, DID	Mobilizes Residual Gas
Imbibition		
Water→Oil→Gas	Double Imbibition, II	Mobilizes Residual Oil
Oil→Water→Gas	Drainage Imbibition with Overall Imbibition, IDI	Gas Must be Continuous
Water→Gas→Oil	Imbibition Drainage, IID	Mobilizes Residual Gas

1.3.5 ROLE OF OIL FILMS

It has been shown in previous studies [34],[35],[36] that residual oil displaced by a double drainage mechanism (gas→oil→→water) leads to the reconnection of the oil ganglia and subsequent oil production at the effluent. Oren and Pinczewski [35] show that the recovery efficiency in water-wet systems depends on the sign of the oil-water spreading coefficient. Higher oil recoveries were obtained for positive spreading systems which can be ascribed to the oil being able to flow through thin, continuous films thereby reconnecting and mobilizing the residual oil blobs. Lower recoveries for for a negative system was due to the absence of these films.

The oil spreading coefficient is defined for a flat surface as:

$$S_{po} = \sigma_{wg} - \sigma_{go} - \sigma_{ow} \qquad (1)$$

where S_{po} is the oil spreading coefficient, σ is the interfacial tension, and the subscripts, o, w, g represent the oil, water and gas phases respectively. A positive spreading coefficient indicates spreading which means the oil spreads and forms a film between water and gas, e.g. light hydrocarbons. Negative spreading coefficients are also possible e.g. for C_{10+}. The transport of fluid through these films is the most important process that must be accounted for in a capillary dominated model.

Until very recently, it was thought that only spreading oils could form layers in a porous medium. Dong *et al.* [37] did calculations to show that a nonspreading oil could form films over water layers present in the pore edges of a water-wet porous medium. The controlling parameters included the pore geometry, the interfacial properties and the water content in the pore edges. Their calculations have been supported by micromodel visualization experiments [36].

1.3.6 CHANGES TO EXPERIMENTAL SET-UP

A novel design for the micromodels has been developed. These new micromodels have several design enhancements over the previous models used by Keller *et al.* [37]:

1. Deeper etch depths (25-35 mm) which will give the new micromodels a higher permeability, whereas the old micromodels had a 15 mm etch depth. The advantages of a higher permeability model include lower entry pressures for the injected fluids and the ability to use higher surfactant concentrations in foam studies. Previous foam studies that used the old micromodels [38] were limited to the a concentration of about 0.0 1% surfactant (by active weight) which corresponded to the maximum pressure drops across the micromodels before gas breakthrough.

2. A deep (circa 200 mm) etch along two sides of the silicon wafer that connect to the inlet ports. These provide a larger area for the introduction of fluids into the porous medium and to capture the various displacement processes.

In addition, a new set up has been designed which addresses a weakness of the Keller's [36] experimental set-up. The photochemical etching procedure in the micromodel construction renders the silicon surfaces mixed wettability. It is preferable for the silica surface be strongly water-wet (contact angle close to zero). This was done by injection of a weak acidic solution, the acidity being limited by the epoxy-resin used to connect the ports to the glass of the micromodel. The new set-up overcomes this limitation by employing a tough plastic that is more resistant to acid for the connections.

1.3.7 FUTURE WORK

1. Investigate wettability and contact angles: Keller *et al.*'s experiments [36] were conducted in a weakly water wet micromodel which resulted in some oil/water contact angles being significantly greater than zero. The new experimental set-up allows for the use of stronger acids to render the surfaces of the micromodels completely water wet (oil/water contact angle of zero). The subsequent observations could then be used to corroborate theories of oil film stability [27].

2. The use of wide range of oils with different spreading properties: The oils that will be used are hexane, octane and decane (in decreasing order of spreading tendency) and the focus will be to investigate how spreading coefficients affect film formation. We expect to see a gradation in the film formation tendency (hexane most likely, decane least likely).

3. Foam interactions with oil: Spreading coefficient dependence on oil stability in the presence of foam. The new set-up enables better control of the wettability of the micromodels.

1.3.8 REFERENCES

[1] Brooks, R. H., and Corey, A.T.: "Properties of Porous Media Affecting Fluid Flow", J. Irrig. Drain. Div Am. Soc. Civ. Eng., **92**, 61-88 (1966).

[2] van Genuchten, M. A.: "A Closed-form Equation For Predicting The Hydraulic Conductivity Of Unsaturated Soils", Soil Sci. Soc Am. J., **44**, 892-898 (1980).

[3] Parker, J.C., Lenhard, R.J., Kuppusamy, T.: "Modeling Multiphase Contaminant Transport In Groundwater And Vadose Zones", presented at Petroleum Hydrocarbons and Organic Chemicals in Groundwater, Natl. Water Well Assco., Houston TX. (Nov. 12-14, 1986).

[4] Leverett, M.C and Lewis, W. B.: "Steady Flow Of Gas-Oil-Water Mixtures Through Unconsolidated Sand", Trans. Am. Inst. Min. Metall. Pet. Eng., **142**, 107-116 (1941).

[5] Caudle, B.H, Slobod, R.L, and Brownscombe, E.R.: "Further Developments In The Laboratory Determination Of Relative Permeability", Trans., AIME **192**, 145-150 (1951).

[6] Reid, S.: "The Flow Of Three Immiscible Fluids In Porous Media", PhD dissertation, U. Of Birmingham, U.K (1956).

[7] Corey, A.T. *et al.*: "Three-Phase Relative Permeability", Trans., AIME **207**, 349-351 (1956).

[8] Snell, R.W.: "Three-Phase Relative Permeability In An Unconsolidated Sand", J. Inst. Pet. **48**, 80-88 (March 1962).

[9] Snell, R.W.: "The Saturation History Dependence Of Three Phase Oil Relative Permeability", J. Inst. Pet. **48**, 81-84 (March, 1963).

[10] Sarem, A.M.: "Three-Phase Relative Permeability Measurements by Unsteady State Method", SPEJ (Sept. 1966).

[11] Donaldson, E.C. and Dean, G.W. "Two And Three-Phase Relative Permeability Studies", RI6826, USBM (1966).

[12] Saraf, D.N. and Fatt, I.: "Three-Phase Relative Permeability Measurement Using A Nuclear Magnetic Resonance Technique For Estimating Fluid Saturation", SPEJ (Sept. 1967).

[13] Guckert, L.G.: "Gammy-ray adsorption method of measuring gas saturation and its application to Three-Phase Relative Permeability Studies", PhD dissertation, Texas A&M U., TX (1968).

[14] Donaldson, E.C. and Kayser, M.B. : "Three phase fluid flow in porous media", Contract No. DOE/BETC/IC-80/4. US. DOE (April, 1981).

[15] Saraf, D.N. *et al.*: "An Experimental Investigation Of Three-Phase Flow Of Water/Oil/Gas Mixtures Through Water-Wet Sandstone's", SPE #10761 presented at the SPE California Regional Meeting, San Francisco (March, 24-26, 1982).

[16] van Spronsen, E.: "Three-Phase Relative Permeability Measurements Using The Centrifuge Method", SPE #10688 presented at the SPE/DOE Symposium on EOR, Tulsa (April 4-7, 1982).

[17] Oak, M.J., Baker, L.E., and Thomas D.C.: "Three-Phase Relative Permeability Of Berea Sandstone", JPT. 1054-1061 (August, 1990).

[18] Stone, H. L.:"Probability Model For Estimating Three-Phase Relative Permeability", JPT. **22**, 214-218 (1970).

[19] Stone, H.L. : "Estimation Of Three-Phase Relative Permeability", J. Can. Pet. Tech. 21(3), 21-27 (1973).

[20] Baker, L.E.: "Three-Phase Relative Permeability Correlation's", Proceedings Of SPE/DOE EOR Symposium, Tulsa (1988).

[21] Fayers, F.J. "Extension Of Stone's Method 1 And Conditions For Real Characteristics in Three Phase Flow", SPERE **4**, 436-445 (1989).

[22] Parker, J.C., and Lenhard, R.J.: "Determining Three-Phase Relative Permeability-Saturation-Pressure Relations From Two Phase System Measurements", J. Pet. Sci. Eng., **4**, 57-65 (1990).

[23] Delshad, M., and Pope, G.A.. "Comparison Of The Three-Phase Oil Relative Permeability Models", Transport in porous media, **4**, 59-83 (1989).

[24] Heiba, A.A., Sahimi, M., Sciven, L.E. : "StatisticalNetwork Theory Of Three-Phase Relative Permeabilities", SPE #12690 presented at the 4th DOE/SPE Symposium on EOR, Tulsa (April, 1984).

[25] Soll, W.E. and Celia, M.A.: "a Modified Percolation Approach To Simulating Three-Fluid Capillary Pressure-Saturation Relationships", Advances In Water Resources, **16**, No. 2, 107-126 (1993).

[26] Oren, P.E., Billiote, J., and Pinczewski, W.V.:" Pore-scale Network Modeling of Waterflood Residual Oil by Gas Flooding", SPE #27814 presented at the Improved Oil Recovery Symposium, Tulsa, OK (April, 1994).

[27] Fenwick, D.H. and Blunt, M.J. : "Pore Level Modeling of Three Phase Flow in Porous Media". 8th European Symposium on Improved Oil Recovery, Vienna, Austria (May, 1995).

[28] Lenormand, R. and Zarcone, C.: "The Role of Roughness and Edges During Imbibition In Square Capillaries", SPE #13264 presented at the SPE Annual Technical Conference and Exhibition, Houston, TX (September, 1984).

[29] Chen, J.D., and Koplik, J.: "Immiscible Fluid Displacement in Small Networks", J. Colloid Interface Sci., **108**, 304-330 (1985).

[30] Wardlaw, N.C. and Li, Y.: " Fluid Topology, Pore Size And Aspect Ratio During Imbibition", Trans. Porous Media **3**, 17-34 (1988).

[31] Campbell, B.T. and Orr, F.M. : "Flow Visualization For CO_2 Crude-Oil Displacements", SPEJ, **25(5)**, 665-678 (1985).

[32] Wilson, J. L., Conrad, S.H., Mason, W.R., Peplinski, W., and Hagan, E.: "Laboratory Investigation of Residual Liquid Organics From Spills, Leaks, and Disposal Of Hazardous Wastes In Groundwater", Rep. EPA/600/6-90/004, Environ. Prot. Agency, Washington, D.C (April, 1990).

[33] Soll, W.E., Celia, M.A., and Wilson, J.L.: "Micromodel Studies Of Three-Fluid Porous Media Systems: Pore-Scale Processes Relating Capillary Pressure-Saturation Relationships", Water Resources Research, **29(9)**, 2963-2974 (September, 1993).

[34] Oren, P.E., Billiote, J., and Pinczewski, W.V.: "The Effect of Wettability and Spreading Coefficients on the Recovery of Waterflood Residual Oil", SPE #24881 presented at the SPE 67^{th} Annual Technical Conference and Exhibition, Washington, D.C (October, 1992).

[35] Oren, P.E., Billiote, J., and Pinczewski, W.V.: "Fluid Distribution and Pore-Scale Displacement Mechanisms in Three Phase Flow", Transport in Porous Media, **20**, 105-133 (1995).

[36] Keller, A.A., Blunt, M.J., and Roberts, R.V.: "Micromodel Observation of the Role of Oil Layers in Three Phase Flow", submitted to Transport in Porous Media (1996).

[37] Dong, M., Francis, A.. Dullien, L., and Chatzis, I.: "Imbibition of Oil Film Form over Water Present in Edges of Capillaries with an Angular Cross Section, J. Colloid and Int. Sci. **172**, 21-36 (1995).

[38] Woody, F., Castanier, L., and Blunt, M.: "Pore Level Visualization of Foam Flow in a Silicon Micromodel", submitted. to Journal of Petroleum Science and Engineering, February 22 1996

1.4 Cat Scanner Status
(J. Burger)

During this year efforts have continued on hardware improvements and software development and testing.

1.4.1 HARDWARE IMPROVEMENTS

The positioning table was recovered from the EMI 5005 scanner and will be used to improve longitudinal accuracy. Various core holders have been built or purchased and are in the process of being tested. A design was made for a positioning system when vertical cores are scanned. A schematic of the system is shown on Fig.1. Implementation of this design is in progress. Minor building modifications are already done. Completion is expected by June 1996. A faster personal computer is going to be purchased to improve the speed of data analysis and display.

1.4.2 SOFTWARE

Software support is provided by Mr. Bill Wahlberg. Images from the CT scanner can be transferred on an optical disk. From there they are processed by a personal computer that transforms them in a readable format. Calculations can be made at this stage to find parameters such as porosity, density, atomic numbers and saturations. The calculations use scripts attached as modules to the main program.

The final results can be displayed as pictures or as matrices of numbers. The effort is now in validating the program and improving the menu by adding calculation modules. Spot checking of the results in terms of CT numbers is in progress. An error analysis is being made on various calculation modules.

VERTICAL POSITIONING SYSTEM

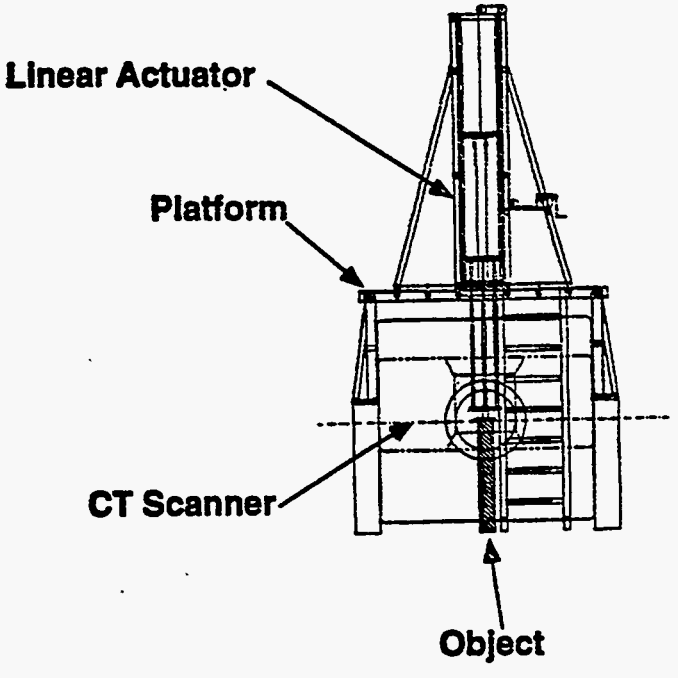

Figure 1

PROJECT 2: IN-SITU COMBUSTION

To evaluate the effect of different reservoir parameters on the in-situ combustion process. This project includes the study of the kinetics of the reactions.

2.1 A Study of In-situ Combustion on Saudi Tar

(V. Agrawal and S. Abu-Khamsin)

2.1.1 ABSTRACT

The technical report is completed and ready for publication.

Six in-situ combustion tube runs were made using Saudi tar and a matrix of sand and clay. Four of the runs contained iron nitrate while two were control runs without additive. The concentration of iron nitrate was 1%, 5% 10% and 20% by weight of iron nitrate dissolved in the connate water.

The two control runs and the run with 1% nitrate failed to ignite properly. The front of combustion never propagated along the tube after the first two hours. The runs containing over 10% iron nitrate burned steadily with the front propagating along the tube. The run with 5 % nitrate burned also but not quite as well. Front temperatures showed little variations and the front velocity did not show any change with iron nitrate concentration. The average fuel concentration was the same in all successful runs. In the failed runs, fuel concentration measured at the location where the front died correspond to about 8% oil saturation.

The results confirm that iron nitrate is an effective catalyst for the Saudi tar. More work should be done on additive transport and studies of other metals as possible catalysts.

2.2 Modifying In-situ Combustion with Metallic Additives

(L. Castanier and W. Brigham)

2.2.1 SUMMARY

The paper, accepted for publication in In-situ in 1996, is a review of our research program on in-situ combustion with additives.

MODIFYING IN-SITU COMBUSTION WITH METALLIC ADDITIVES

L.M. Castanier and W.E. Brigham
Petroleum Research Institute
Stanford University
Stanford, California 94305

ABSTRACT

In-situ combustion is the most energy efficient of thermal enhanced oil recovery methods. In light oil reservoirs, too little fuel may be deposited and in very heavy oil reservoirs too much fuel may be deposited. A research program has been ongoing to try to solve these problems. We chose to test water soluble additives to attempt to modify the fuel deposition reactions. In the first stage, kinetics experiments were run on Huntington Beach (18.5° API) and Hamaca, Venezuela (10.5° API) oils in the presence of aqueous solutions of metallic salts. The results were compared with control runs with no metal present. While copper, nickel and cadmium salts had little or no effect; iron, tin, zinc and aluminum increased fuel laydown for Huntington Beach oil. The results were similar for the heavier Hamaca oil. As no reduction in fuel was noticed with any of the metallic additives, ketals were mixed with Hamaca oil in an attempt to reduce fuel. No effect was observed when the ketals were used.

Twenty-one combustion tube runs were made in the second stage of the study. They included runs with the oils previously tested in the kinetics apparatus plus two California oils (Cymric light and Cymric heavy) as well as Saudi "tar"(19.7° API). Iron, tin and zinc salts improved the combustion efficiency in all cases. As a result of the additives, the front velocities were increased. Changes were also observed in the H/C ratios of the fuel, heats of combustion, air requirements and density of the crude produced.

The amount of fuel deposited varied among the oils. For Huntington Beach oil, the amount of fuel increased in the order: zinc, control, tin and iron; while for the Hamaca crude the order was: control, iron and tin. Cymric heavy oil shows the order: control, zinc and iron. Cymric light oil and the Saudi tar were only tested with iron additive. In the last case the effect of additive concentration was also investigated. We found that for this specific case a minimum near 5% by weight of hydrated ferrous nitrate in the connate water was needed to improve the combustion.

To date we have not been able to find a suitable additive to reduce fuel deposition. Iron and tin salts seem suitable agents to increase fuel when that is needed.

INTRODUCTION

One of the methods used to recover heavy or medium gravity crude oils is in-situ combustion. During an in-situ combustion field project, air or oxygen is injected into the reservoir to burn part of the oil in place, which generates a heat front propagating through the reservoir (Fig. 1). Heat is conducted forwards by conduction, convection of the combustion gases and condensation of the steam and the light hydrocarbons. The oil ahead of the combustion front is displaced by gas drive from the combustion gases, by hot water and steam drive as well as by miscible drive provided by the condensed light ends. The process is controlled by the kinetics of the combustion reactions as well as the deposition of the heavy portions of the crude on the rock matrix. The "fuel" burnt is the unrecoverable carbon rich residue deposited as a result of distillation, thermal cracking and some catalytic cracking.

An important parameter for the economics of the process is the amount of air needed to recover a given volume of oil (air/oil ratio). This, in turn, depends of the nature and amount of fuel deposited. Two limits in the amount of fuel can exist:

- For very heavy crudes, too much fuel may exist, causing excessive air requirements.
- For light crudes, the deposited fuel may not be enough to sustain the combustion front.

The literature on the effect of metals on the in-situ combustion process reports observations of increased air requirements and increased fuel deposited in metal rich reservoirs (Hardy and Sheppard, 1972; Burger and Sahuquet, 1974). Laboratory research includes mostly kinetics studies (Burger and Sahuquet, 1974; Fassihi, 1981; Racz, 1985), and the process of application of additives has been successfully tested in the field (Racz, 1985). Despite all this work, no consistent trends can be found in the literature.

The objectives of this work are to investigate means to modify the nature and the amount of fuel burned by adding water soluble additives to the system. General screening was performed by kinetics experiments , then some of the most promising products were tested in our combustion tube.

KINETICS EXPERIMENTS

The oxidation of oil during in-situ combustion involves numerous competing reactions occurring over different temperature ranges. A common procedure involves subjecting a mixture of oil, water and reservoir rock to a linear heating schedule. The effluent gases produced when passing air through the mixture are analyzed for oxygen and carbon oxides. Numerous studies such as Bousaid and Ramey, 1968; Burger and Sahuquet, 1972 and Fassihi *et al.*, 1984, established that the reactions may be grouped in three classes of competing reactions occurring over different temperature ranges. The three classes are:

- Low temperature oxidations, producing no carbon oxides. These are heterogeneous gas-liquid reactions.
- Medium temperature, fuel formation reactions that are homogeneous in the gas phase.
- Heterogeneous high temperature fuel combustion reactions.

The rates of the three classes of oxidation reactions are considered to be functions of the oxygen partial pressure and of the fuel concentration.

Although a recent study has showed that this model can be improved (Mamora *et al.*, 1994), we will use the three reaction model outlined above for the analysis of such experiments.

Metals have long been recognized for their catalytic potential in both hydrocarbon cracking and oxidation reactions. In addition two methods to reduce fuel laydown have been suggested in the literature (Shallcross *et al.*, 1989). The first one involves injection of a ketone acetal (ketal). The second would use a surfactant to increase the oil displacement by the water bank ahead of the front. We tested only the first case because of worries about the thermal stability of surfactants at combustion temperatures.

Experimental Apparatus and Procedure

A cell is charged with a mixture of sand and oil, plus water or an aqueous solution of the additive to be tested. The cell is heated at a constant rate of temperature increase while air is passed through the sample at controlled rate and pressure. The effluent gases are analyzed for oxygen, carbon monoxide and carbon dioxide. Spot checks of nitrogen concentration are made to verify the gas material balance. The experimental apparatus and procedure are similar to the ones used by Fassihi *et al.* (1984). The procedure is also discussed in detail by Shallcross et al. (1989). The main components of the equipment are shown in Fig. 2. The analysis of the data was performed using the method developed by Fassihi *et al.* (1984) and modified by Shallcross *et al.* (1989). The results are expressed in terms of classic kinetics parameters such as Arrhenius constants and order of reaction for the partial pressure of oxygen. Table 1 gives some properties of the crudes tested and describes the additives used in the experimental program. One may notice that the hydrogen plus carbon of the oils do not total 100 percent. this is caused by the presence of other elements such as sulfur which will not be discussed here.

Results and Discussion

This section is only a short summary because of space limitations. More details can be found in De Los Rios *et al.* (1988) and Shallcross *et al.* (1989). Table 2 shows the kinetic parameters obtained for Huntington Beach oil for the low medium and high temperature reactions. Figures 3-5 show the experimental data for selected additives. The presence of stannous chloride or ferrous chloride showed as solid lines (Fig. 3, for example) increased the level of oxygen consumed in all three reactions. The reactions also occurred at lower temperatures than for the control runs shown as dashed lines. Oxygen consumption and carbon oxides production started at lower temperatures and increased in magnitude when the additives were present.

Table 2 shows that changes in reaction order, activation energy and pre-Arrhenius constant were also observed for these two additives . Cuprous sulfate did not seem to affect the results, nor did nickel or cadmium. Aluminum chloride merely shifted the temperature peak to a slightly lower temperature (Fig. 4). Manganese has a similar effect. Zinc, chromium and magnesium increased oxygen consumption at lower temperature but decreased it over the higher temperature region (Fig. 5). From Table 2

it can be seen that the order of the low temperature reactions is relatively insensitive to the additives, while a slight increase was observed in the order of the middle temperature reactions with additives. Iron and tin significantly increased the order of the high temperature reactions.

For the heavier Venezuelan oil (Fig. 6), the high temperature combustion peak is more pronounced; this observation supports the conclusion that more fuel is laid down by the Hamaca oil than by the Huntington Beach oil.

We had hoped to be able to decrease fuel deposition by adding a ketal to the mixture for one run performed with Hamaca oil. If anything the fuel deposition increased slightly. A recent study on Australian light oils (Kisler and Shallcross, 1995) seems to offer hopes for the use of lithium, cobalt or magnesium as a way to decrease the amount of fuel deposited. However, these results need to be confirmed by combustion tube runs, for it is difficult to quantitatively interpret kinetics experiments.

COMBUSTION TUBE RUNS

The kinetics experiments showed that the metallic additives caused changes in the reactions of combustion. To obtain quantitative information on the amount and nature of the fuel formed and the air required to propagate a combustion front, it is necessary to experimentally simulate the in-situ combustion process via tube runs. The tube mimics the system shown in Fig. 1 with a region at reservoir temperature, followed by a region where the temperature increases due to heat transfer ahead of the steam plateau. Next is the steam plateau where the temperature is constant. Since all of our runs were performed at the same pressure, the steam plateau temperature ranged from 129°C to 132°C. Behind this, the temperature rapidly increases until peak temperature is reached at the combustion front. The region behind the front shows decreasing temperatures caused by heat losses and cooling by the injected air.

Experimental Apparatus

The equipment is similar to that used by a number of researchers at Stanford University and elsewhere. The following outlines the main features of the apparatus.

Further detail is given by Baena *et al.* (1989). A schematic or the equipment is shown on Fig 7.

The combustion tube is 1 m long and 7.6 cm O.D. with 0.041 cm wall thickness made of 316 stainless steel. A thermowell is placed along its center, allowing temperature measurements anywhere along the axis of the tube. Two electrical heaters located 10 cm from the top of the tube are used as ignitors. The tube is placed vertically in a thermally insulated pressure shell. Air injection is controlled by a mass flowmeter. The produced fluids are collected via a separator and condenser. The produced gases are continuously monitored for oxygen, carbon monoxide and carbon dioxide. A gas chromatograph is used to spot-check for other gases. All the measurement sensors are connected to a microcomputer for storage and display of the data.

Procedure and Experimental Program

A mix or 20-30 mesh Ottawa sand, fire clay, oil and water containing the desired amount and type of additive is packed into the tube. The clay content is 5% by weight of the sand. Porosity of the pack is about 35%, oil saturation around 35% and water saturation about 25%. The tube is preheated to a reservoir temperature of 60°C by external heaters, nitrogen is injected and the igniter is turned on. When the temperature at the ignitor reaches 350°C, air at a rate or 3.0 std l/min. is injected and nitrogen shut off. The start of combustion is indicated by the gas composition at the outlet. The ignitor is shut off when the combustion is stable and the front begins to propagate downwards. At the end of the run the combustion is quenched by switching injection from air to nitrogen. This is typically done at 90 cm from the top to avoid damage to the bottom flange.

Four runs were performed using California, Huntington Beach oil of 22° API gravity. The first one had no additive while the next three had ferrous chloride, stannic chloride and zinc chloride at 1.0 mole percent concentration dissolved in the connate water Four runs were done using Hamaca oil (10° API gravity) from Venezuela. Two control runs with no additive were followed by runs with iron chloride and with stannic chloride at 1.0 percent mole concentration in the connate water Three runs were performed on Cymric heavy crude (12° API gravity) from California. One was a control run while the other two included ferrous and zinc nitrates at 1.0 mole percent

concentration. Four runs were made with Cymric light oil (34° API), two control runs and two including ferrous nitrate at 1 mole percent concentration. Finally five runs were made on a Saudi "tar" (19.7°API) at various concentrations of hydrated ferrous nitrate. All of the above runs were performed at air fluxes or 3 std l/min and 100 psig (7 bars) back pressure.

Oxygen Utilization and Produced Gases

The main feature of the behavior of the produced gases during the control runs was the poor oxygen utilization with average oxygen produced ranging from 2 to 5 mole percent. In addition, fluctuations were observed in the oxygen and carbon dioxide produced. The carbon dioxide shows a lower level in the control run with concentration fluctuations which are reversed in time compared to the oxygen fluctuations. Figure 8 is an example of a typical control run. It is for the Cymric heavy oil. The fluctuations could possibly have been caused by improper packing of the combustion tube, however, repeat control runs with different packing methods still showed the same fluctuations. An examination of the cores by Cat scanning showed no pack defect or porosity fluctuations.

When ferrous nitrate was introduced as an additive, a marked change was observed. The produced oxygen concentration went down to almost zero and the gas production curves were essentially flat with time, showing a much more uniform and more efficient combustion. Figure 9 is an example of this kind of result, again on Cymric heavy oil.

The stanous chloride had an effect similar to ferrous nitrate on the gas production curves while the zinc chloride runs exhibited a behavior intermediate between iron and the control runs.

In the control runs for Huntington Beach and Hamaca oils, an average of 4 to 5% unreacted oxygen was produced from the outlet end of the tube. This amount was reduced to 1.3% by addition of ferrous nitrate in the Huntington Beach oil case and decreased to almost zero when using stanous chloride and also when using ferrous nitrate with Hamaca oil. For Cymric heavy oil, the control run and the run with zinc

chloride were similar with about 2% oxygen produced while ferrous nitrate decreased this concentration to less than 0.5%.

Conversely, the $C0_2$ produced increased in the following order: control, zinc, tin and iron; while the CO concentration produced increased in the order: iron, control and tin. The front temperatures for the control runs for Huntington Beach oil averaged 500°C. For stannous chloride they were around 535°C, while for ferrous nitrate and zinc chloride they were slightly lower than for the control runs. The Cymric heavy oil temperatures increased from 502°C to 518°C with zinc chloride and 539°C with ferrous nitrate. Temperature behavior was similar for the Hamaca oil.

The last two oils (Cymric light and the Saudi tar) could not burn during the control experiments but sustained combustion was achieved with the additives. This result has been commonly seen for light oils but it is an interesting and important observation that the heavy Saudi tar would not burn without a metallic additive.

One must notice that the combustion front velocities increased with the presence of metallic additives. This also shows better combustion. Despite that increase in velocity, the air utilization was better and the air/oil ratio improved with the metallic additives in all cases.

The $C0_2$/CO ratio (m) increased for both Huntington Beach and Hamaca oils in the order: control, tin and iron; ranging from 2.2 to 3.7. The H/C ratio (n) of the fuel burnt can be calculated from the produced gases (Alexander *et al.*, 1962). The three oils tested exhibited different behaviors. While for the 18.5° API Huntington Beach oil, n increased in the order control, iron and tin; ranging from slightly over 0 to 0.9, the ratio n for the 10.5° API Hamaca oil increased in the order tin, iron and control, and ranged from 1.2 to 1.8. The Cymric heavy oil went from 2.8 in the control run to 1.7 with zinc and 0.8 with iron. We cannot explain the n ratio results at this stage.

Economic Parameters

The economic parameters were calculated based on the gas produced. The amount of fuel burned per unit volume of reservoir is estimated from the front velocities and a material balance on the oxygen consumed. Although a detailed analysis

of the results is outside the scope of this paper and can be found in Baena (1990), Holt (1992), Agrawal (1995) and Tavares (1990), some comments can be made at this stage.

The heat of combustion of the fuel, which depends of its composition increased with the metallic additives for the Huntington Beach oil, but slightly decreased for the heavy Hamaca oil. It also decreased for the Cymric heavy oil.

The air required by a unit mass of fuel burned followed the same trends. The amount of fuel burned per unit volume of reservoir was not changed for Huntington Beach oil, but increased in the order: control, iron and tin, for the heavier Hamaca oil. It also increased in the order: control, zinc and iron, for the Cymric heavy oil. Air/oil ratios for all the oils tested decreased in the order: control, zinc, tin and iron, ranging from 14.3 to 11.5. These results show that the additives modify the nature of the fuel burned as well as its amount. This fact explains that for a more efficient combustion, such as the ones obtained with the additives, less air needs to be injected than for the control runs.

Effect of Additive Concentration

Six runs were performed using the Saudi tar of 19.7°API gravity. Two runs were control runs with no additive, and during these runs the combustion could not be sustained. Hydrated ferrous nitrate $Fe(No_3)^2(H_2O)^6$ was added in concentrations of 1%, 5%, 10% and 20% by weight in the connate water for the four remaining runs. Concentrations of 5% and over promoted combustion and stable fronts were obtained. At 1% concentration the combustion front died after about 2 hours. In all successful runs, the fuel concentration was constant at around 0.042 g/cc. The front temperature was also constant at around 510°C. The front velocities were also the same independent of the iron nitrate concentration.

CONCLUSIONS

The metallic additives cause changes in the nature and the amount of fuel formed during an in-situ combustion process. These changes appear to depend on the

type of oil used. Different crude oils may be affected differently by different additives. No trend has yet been detected because of our small data base.

The rock matrix in these experiments was sand and clay. It would be useful to repeat those types of tests using representative reservoir materials.

The efficiency of various metals as additives does not follow the usually cited order for cracking reactions of coke $Cu < V < Fe < Cr = Zn < Ni$. For the cases studied, iron and tin seem to be the additives which best increased fuel deposition and promoted combustion.

Based on the data for the Saudi tar, it appears that a minimum concentration of additive is needed to improve the combustion. Above that threshold, no effect of increased concentration was found.

In general, metallic additives increase the amount of fuel deposited and seem to be applicable to light oil projects where the fuel deposited is not enough to sustain combustion.

In heavy oil reservoirs, the presence of metals may also allow combustion in reservoirs where poor burning or no burning would occur without the additives . The improved air/oil ratios could make a significant difference in the economics of the process. To date no additive has been found to decrease the fuel burned.

REFERENCES

Agrawal, V., Abu Khamsin, S., and Brigham,W.E., "A Study of In Situ Combustion of Saudi Tar," SUPRI Technical Report, to be published by U.S. Dept. of Energy (1996).

Alexander, J.D., Martin, W.L. and Dew, J.N., "Factors Affecting Fuel Availability and Composition During In-situ Combustion," JPT, 14, 1154-1162 (1962).

Bardon, C. and Gadelle, C., "Essai de Laboratoire Pour L'Etude de la Combustion In Situ," Institut Francais du Petrole, Paris (1977).

Baena, C.J., "Effect of Metallic Additives on In-situ Combustion of Huntington Beach Crude," SUPRI TR 78, U.S. Dept. of Energy, DE-FGl9 87BC14126 (1990).

Bousaid, I.S. and Ramey H.J., Jr., "Oxidation of Crude Oil in Porous Media" SPEJ., 8, 137-148 (1968).

Burger, J.G. and Sahuquet, B.C., "Chemical Aspects of In-situ Combustion," SPEJ., 12, 410-422 (1972).

Castanier, L.M., Baena ,C.J., Holt, R.J. and Brigham, W.E., "In Situ Combustion with Metallic Additives," SPE 23708, Proceedings 2nd LAPEC Conference, Caracas, Venezuela, (March 8-11, 1992).

de los Rios, C.F., Brigham, W.E. and Castanier, L.M., "The Effect of Metallic Additives on the Kinetics of Oil Oxidation Reactions in In-situ Combustion," SUPRI TR 63, US Dept. of Energy, DOE/BC/14126-4 (1988).

Dew, J.N. and Martin, W.L., "Air Requirement for Forward Combustion," Pet.Eng.J., 82 (1964) and 82-85 (1965).

Emery, L.W., "In-Situ Combustion Process Using a surfactant, U.S. Patent No. 3,11S,929 (1963).

Fassihi, M.R., Brigham, W.E. and Ramey, H.J.,Jr., "Reaction Kinetics of In situ Combustion," SPEJ,. 24, 399-416 (1984).

Gilehrist, RE., "Reduction of Coke Formation During In-Situ Combustion," U.S. Patent No. 3,363,686 (1968).

Gureyev, A.A. and Sablena, Z.A., "The Role of Metals in Oxidation of Hydrocarbon Fuels in the Liquid Phase," Scientific Research Institute of Fuel and Lubricating Materials, Pergamon Press (1965).

Hardy, W.C. and Shepard, I.C., "In Situ Combustion Method" U.S. Patent No. 3,4S2,816 (1969).

Holt, R.J., "In-Situ Combustion with Metallic Additives," SUPRI TR 87, Dept. of Energy, DOE/BC/14600-29 (1992).

Kisler, J.P. and Shallcross, D.C., "Effect of Metallic Catalysts on Light Crude Oil Oxidation," to be published by In-situ Journal; also Ph.D. Thesis, University of Melbourne, Australia (1995).

Mamora D., Ramey, H.J., Jr., Brigham, W.E and Castanier, L.M., "Kinetics of In-Situ Combustion," SUPRI TR 91, Dept. of Energy, FG22-90BC14600 (1993).

Racz, D., "Development and Application of a Thermocatalytic In-situ Combustion Process in Hungary," Proceedings 1985 European Meeting on Improved Oil Recovery, Rome (1985).

Satman, A., "In-situ Combustion Models for the Steam Plateau and for Fieldwide Oil Recovery," Ph.D. Thesis, Stanford University (1982).

Severin, D., Glinzer, O., Kiklesriter, H. and Neumann H.J., "The Quiet Oxidation of a Crude Oil and the Effect on its Viscosity," *Erdol Kohle Erdgas 36(3)* 127-130 (1983).

Shallcross, D.C., de los Rios, C.F., Castanier, L.M. and Brigham, W.E., "Modifying In-situ Combustion Performance by the use of Water Soluble Additives," SPE 19485 Asia Pacific Conference, Sydney, Australia (September 13-15, 1989).

Shalp, D.W.A. "Miall's Dictionary of Chemistry," 5th ed., Longman, Essex, UK. (1981)

Tavares C., "Effect of Metallic Additives on Hamaca Crude Oil Combustion," SUPRI TR 80, Dept. of Energy, DE- BC /14600-14 (1991).

ACKNOWLEDGEMENTS

This work was supported by the United States department of Energy under contracts DE-FG19-87BC14126 and FG22-90BC14600. Additional support was provided by the Stanford University Petroleum Research Institute industrial committee. C.F. De Los Rios, Dr. D.C. Shallcross, C. Baena, P.A. Pettit , C. Tavares, R.J. Holt, Dr. S. Abu Khamsin and V. Agrawal performed the experiments. They also wrote the detailed reports that can be found in the bibliography.

LIST OF FIGURES

Table 1
Crude Oil Properties and Kinetics Program

Crude Properties		
Source	Huntington Beach	Venezuela
Gravity (°API)	18.5	10.5
%C	84.50	82.61
%H	11.53	10.47
Atomic H/C Ratio	1.64	1.52

Kinetics Program		
Additive	Molar Concentration of Additive (mole %)	Pressure (psig)
None	--	80
None	--	43
$FeCl_2 \cdot 4H_2O$	1.99	79
$FeCl_2 \cdot 4H_2O$	1.99	43
$SnCl_2 \cdot 2H_2O$	2.02	82
$SnCl_2 \cdot 2H_2O$	2.02	39
$CuSO_4 \cdot 5H_2O$	1.01	81
$CuSO_4 \cdot 5H_2O$	1.01	40
$ZnCl_2$	1.90	83
$MgCl_2 \cdot 6H_2$	1.98	83
$K_2Cr_2O_7$	2.02	80
$AlCl_3 \cdot 6H_2O$	2.00	82
$MnCl_2 \cdot 4H_2O$	2.00	80
$Ni(NO_3)_2 \cdot 6H_2O$	2.00	40
$3CdSO_4 \cdot 8H_2O$	2.00	40

Table 2
Kinetic Parameters for Temperature Oxidation

Additive	Pressure (psig)	n_{II}	E_{II}/R ($°K \times 10^{-3}$)	β_{II}
High				
None	80	0.8	12.4	3.8×10^5
None	43	0.7	12.7	6.1×10^5
$FeCl_2$	79	1.2	18.4	2.5×10^8
$FeCl_2$	43	0.9	15.5	2.1×10^7
$SnCl_2$	82	1.0	14.0	1.3×10^6
$SnCl_2$	39	0.8	15.5	2.6×10^7
$CuSO_4$	81	0.7	11.9	4.9×10^5
$CuSO_4$	40	0.8	14.3	6.4×10^6
$ZnCl_2$	83	0.8	11.0	3.2×10^4
$MgCl_2$	83	0.9	12.4	2.1×10^5
$K_2Cr_2O_7$	80	0.9	11.5	6.7×10^4
$AlCl_3$	82	0.8	12.5	3.2×10^5
$MnCl_2$	80	0.8	12.6	3.2×10^5
$Ni(NO_3)_2$	40	0.8	14.5	7.3×10^6
$CdSO_4$	40	0.8	15.4	2.1×10^7
Medium				
None	80	0.9	8.67	6.3×10^3
None	43	0.9	8.65	4.4×10^3
$FeCl_2$	79	1.0	7.62	2.0×10^2
$FeCl_2$	43	0.9	8.37	4.5×10^3
$SnCl_2$	82	1.1	9.03	3.9×10^3
$SnCl_2$	39	1.3	10.1	3.1×10^3
$CuSO_4$	81	0.8	8.22	4.5×10^3
$CuSO_4$	40	1.0	8.17	8.3×10^2
$ZnCl_2$	83	1.1	10.3	4.0×10^4
$MgCl_2$	83	1.2	10.7	2.7×10^4
$K_2Cr_2O_7$	80	1.2	10.5	2.8×10^4
$AlCl_3$	82	1.0	8.52	2.9×10^3
$MnCl_2$	80	1.0	9.11	1.0×10^4
$Ni(NO_3)_2$	40	1.2	10.5	1.6×10^4
$CdSO_4$	40	1.3	10.3	5.9×10^3
Low				
None	80	0.9	8.15	9.6×10^3
None	43	0.9	8.17	5.6×10^3
$FeCl_2$	79	0.8	6.24	5.8×10^2
$FeCl_2$	43	0.8	5.90	2.4×10^2
$SnCl_2$	82	0.8	7.33	3.5×10^3
$SnCl_2$	39	0.7	6.11	3.8×10^2
$CuSO_4$	81	0.8	8.41	3.2×10^4
$CuSO_4$	40	0.7	8.47	2.7×10^4
$ZnCl_2$	83	0.8	7.51	5.5×10^3
$MgCl_2$	83	0.8	6.70	8.8×10^2
$K_2Cr_2O_7$	80	0.7	5.87	4.0×10^2
$AlCl_3$	82	0.8	6.64	1.0×10^3
$MnCl_2$	80	0.7	6.48	1.1×10^3
$Ni(NO_3)_2$	40	0.7	6.98	2.1×10^3
$CdSO_4$	40	0.7	6.22	5.3×10^2

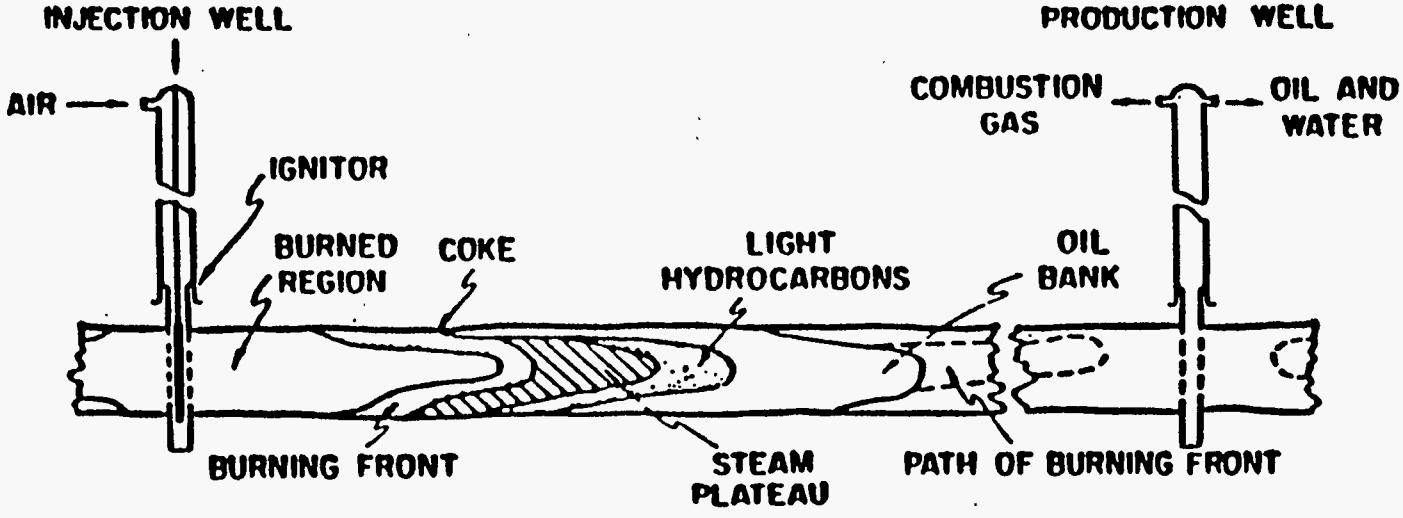

TEMPERATURE DISTRIBUTION

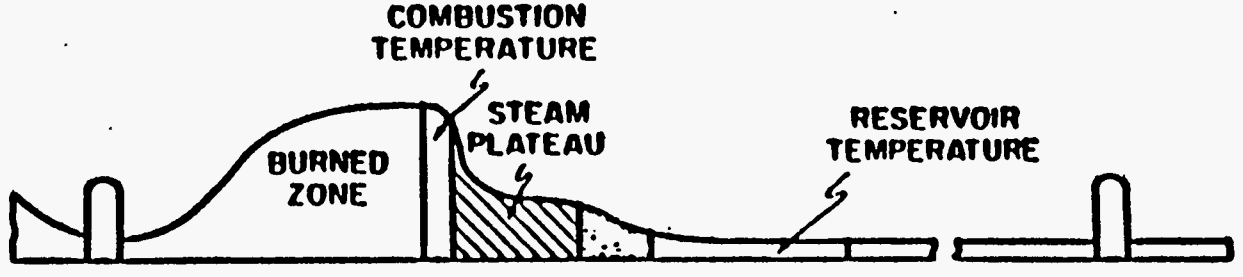

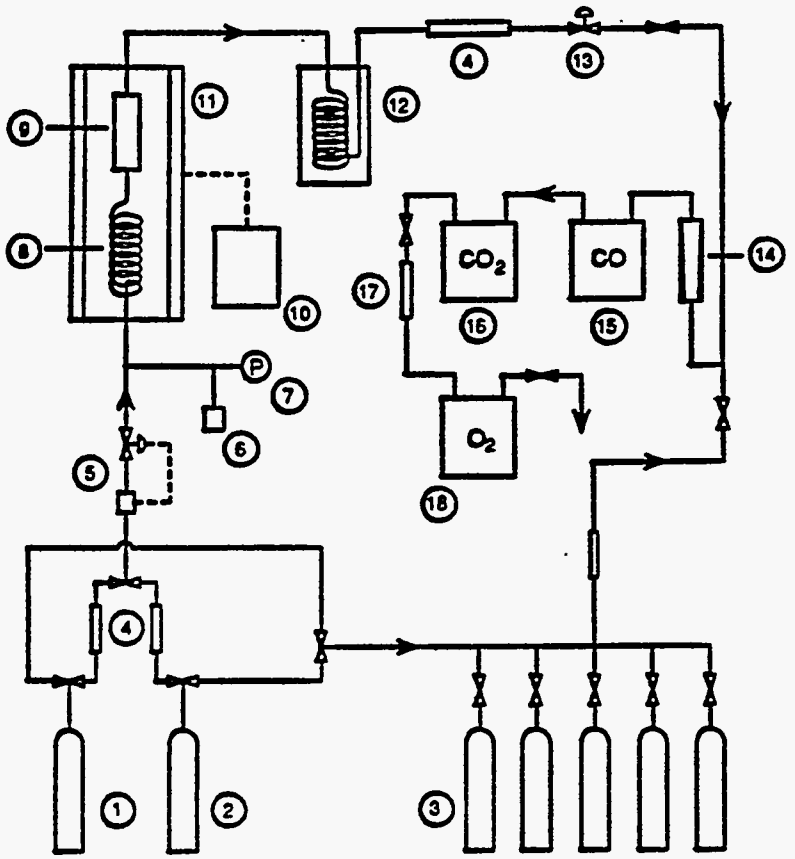

1 Air supply
2 Nitrogen supply
3 Analyzer calibration gases
4 Dryer
5 Mass flowrate controller
6 Pressure transducer
7 Pressure gauge
8 Preheating coil
9 Combustion cell
10 Oven temperature controller
11 Oven
12 Production gas condenser
13 Backpressure regulator
14 Rotameter
15 Carbon monoxide analyzer
16 Carbon dioxide analyzer
17 Acid gas scrubber
18 Oxygen analyzer

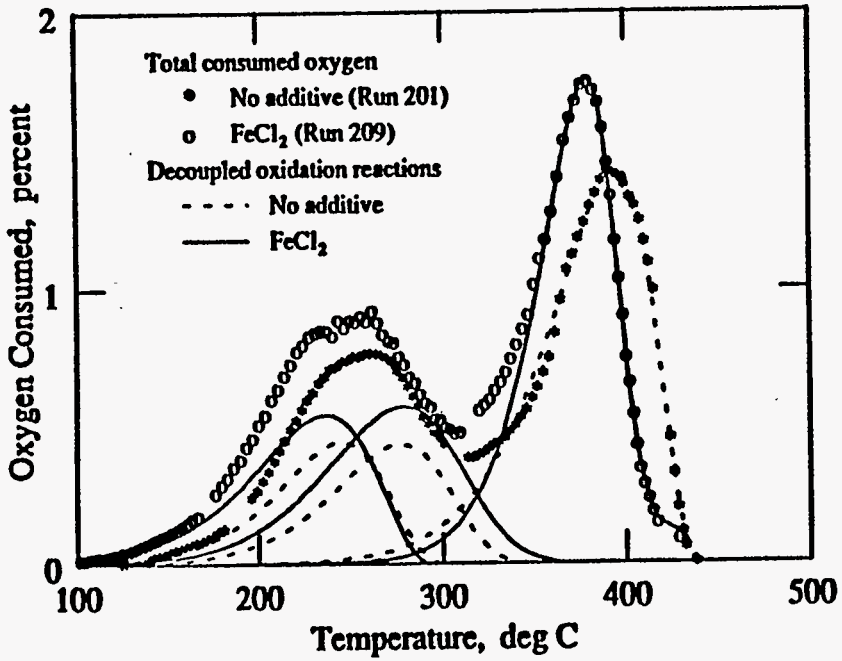
Total consumed oxygen
No additive (Run 201)
FeCl2 (Run 209)
Decoupled oxidation reactions
No additive
FeCl2
Oxygen Consumed, percent
Temperature, deg C
0
1
2
100
200
300
400
500

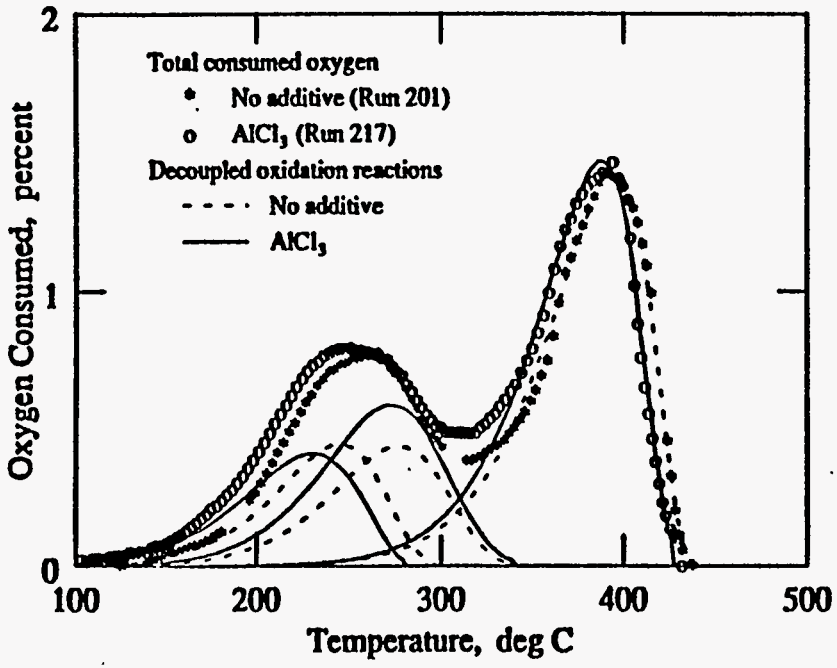
Total consumed oxygen
No additive (Run 201)
AlCl3 (Run 217)
Decoupled oxidation reactions
No additive
AlCl3
Oxygen Consumed, percent
Temperature, deg C
0
1
2
100
200
300
400
500

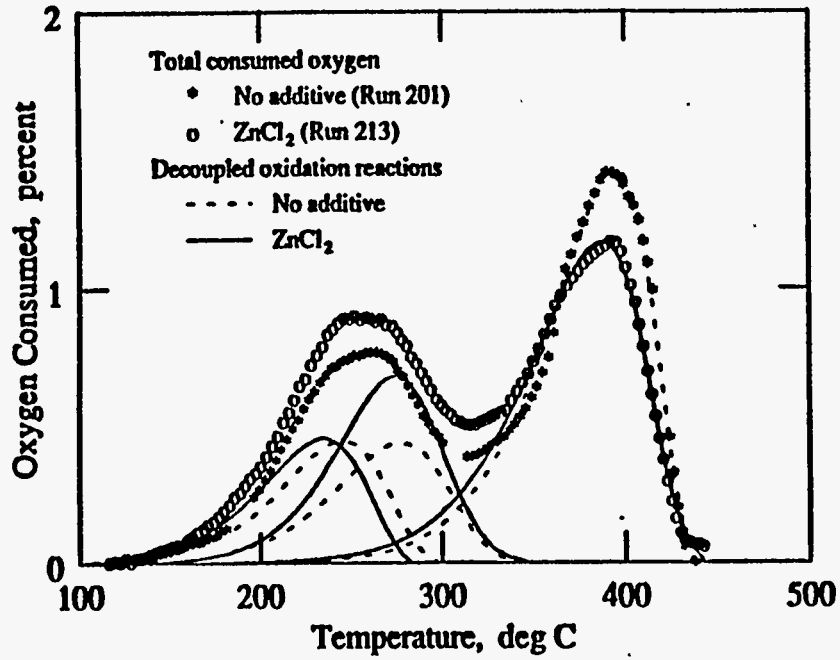
Total consumed oxygen
No additive (Run 201)
ZnCl2 (Run 213)
Decoupled oxidation reactions
No additive
ZnCl2
Oxygen Consumed, percent
Temperature, deg C
0
1
2
100
200
300
400
500

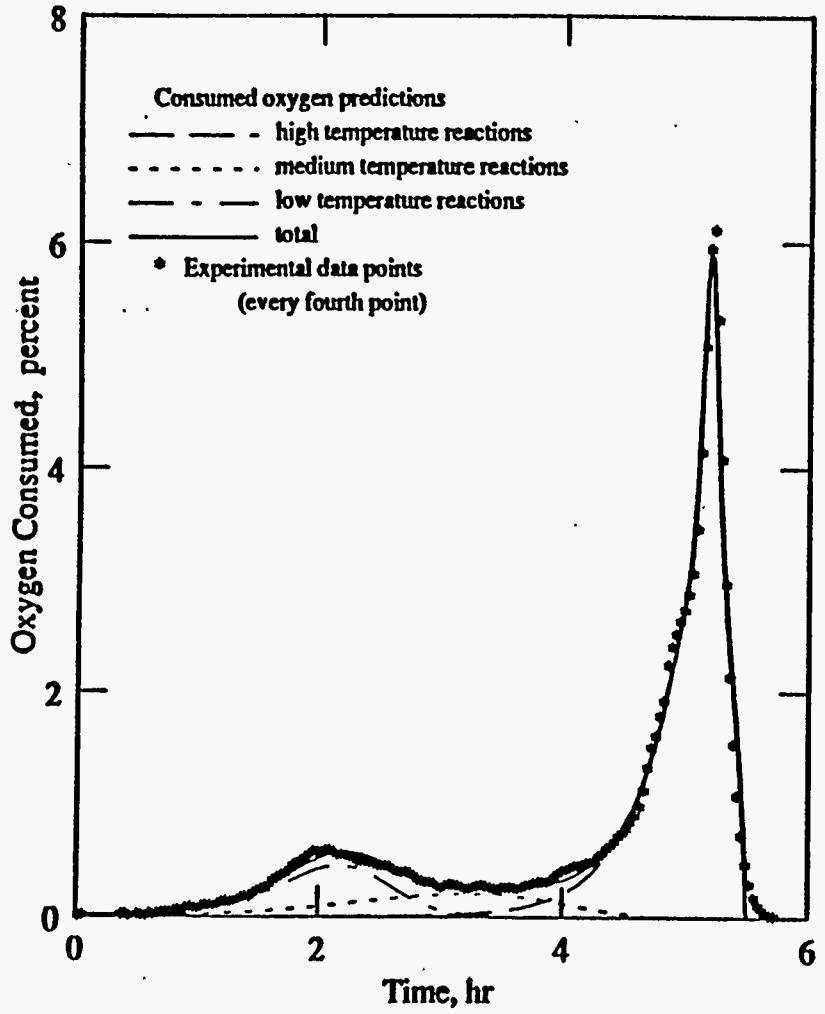
Consumed oxygen predictions
high temperature reactions
medium temperature reactions
low temperature reactions
total
Experimental data points
(every fourth point)
Oxygen Consumed, percent
Time, hr
0
2
4
6
8

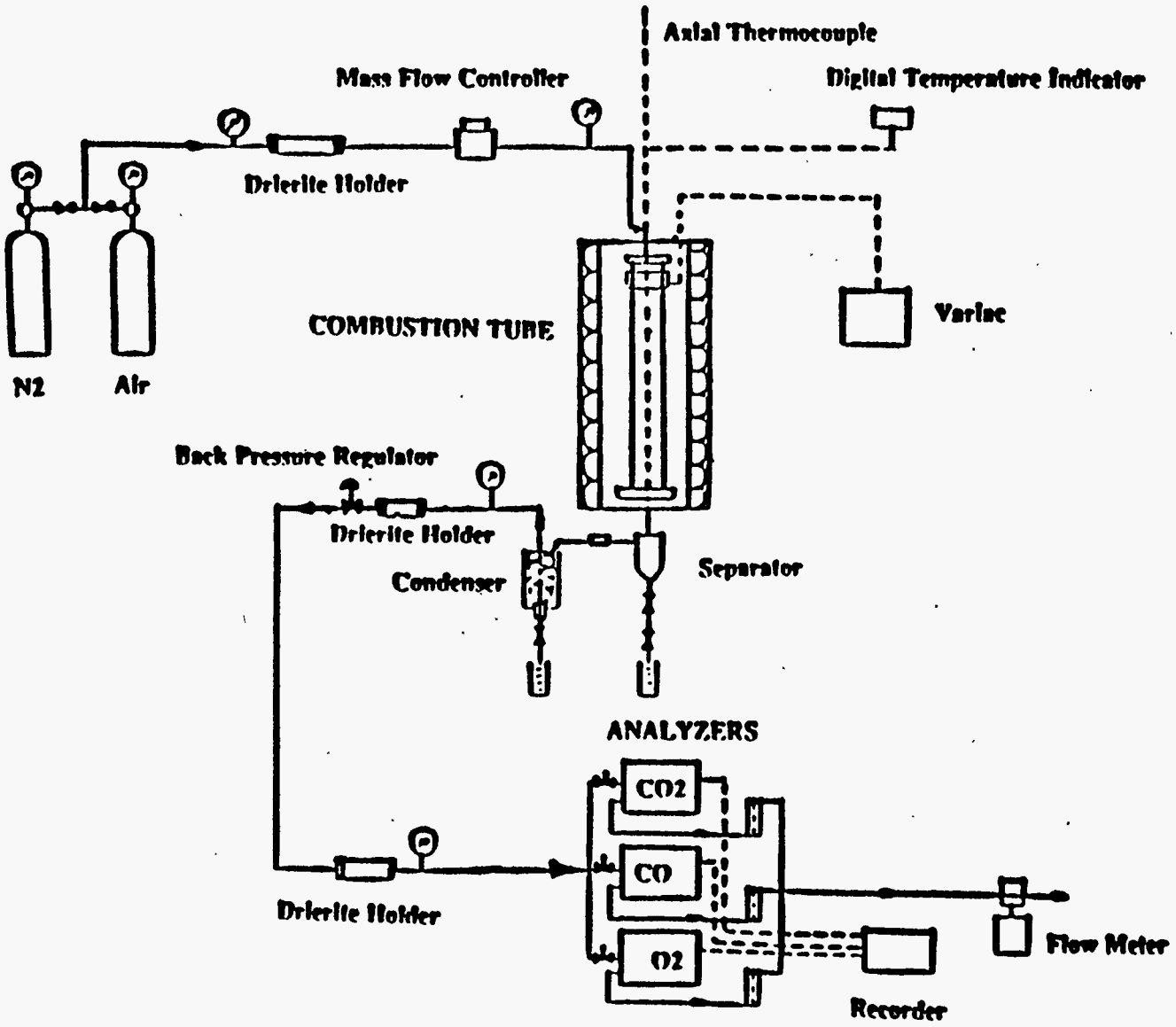
Axial Thermocouple
Mass Flow Controller
Digital Temperature Indicator
Drierite Holder
COMBUSTION TUBE
Variac
N2
Air
Back Pressure Regulator
Drierite Holder
Condenser
Separator
ANALYZERS
CO2
CO
O2
Drierite Holder
Flow Meter
Recorder

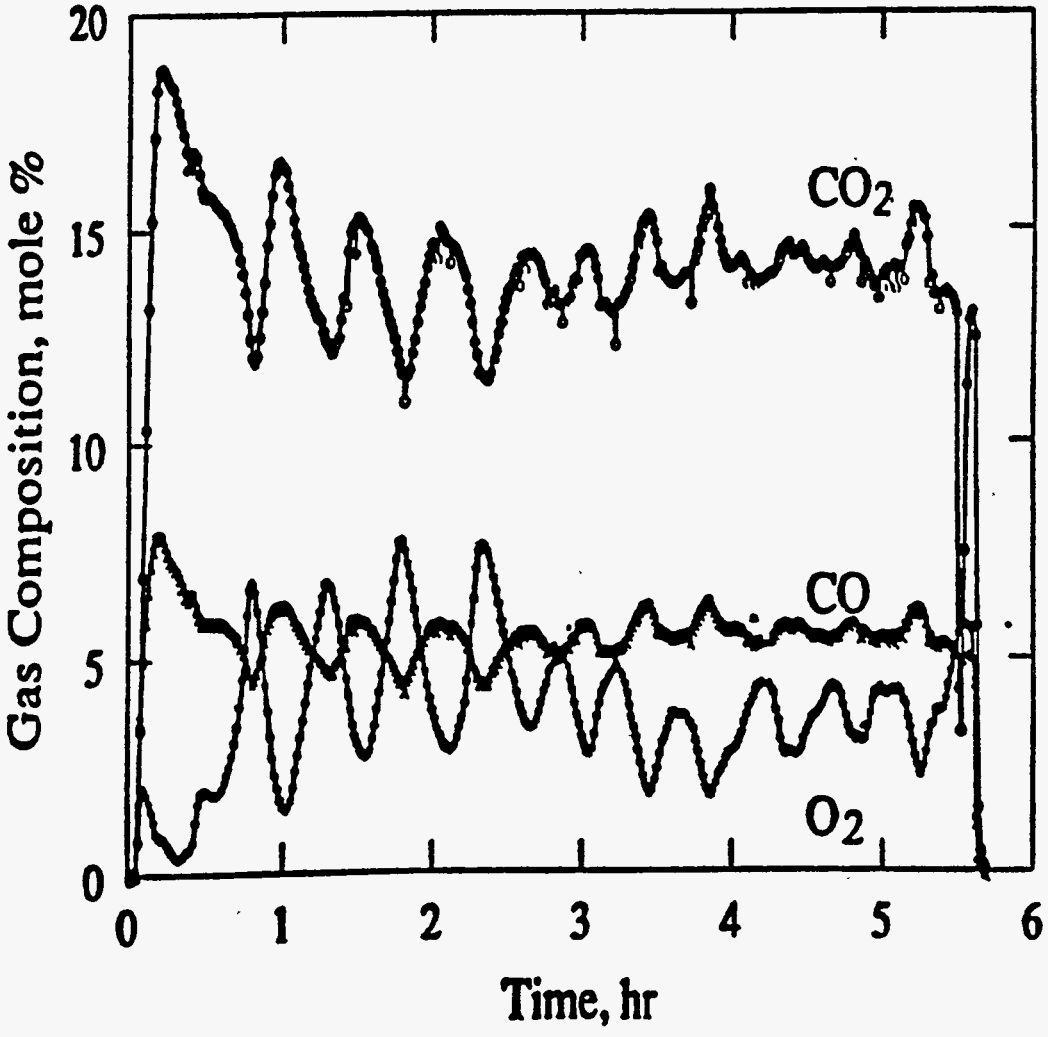
20
15
10
5
0
Gas Composition, mole %
CO2
CO
O2
0
1
2
3
4
5
6
Time, hr

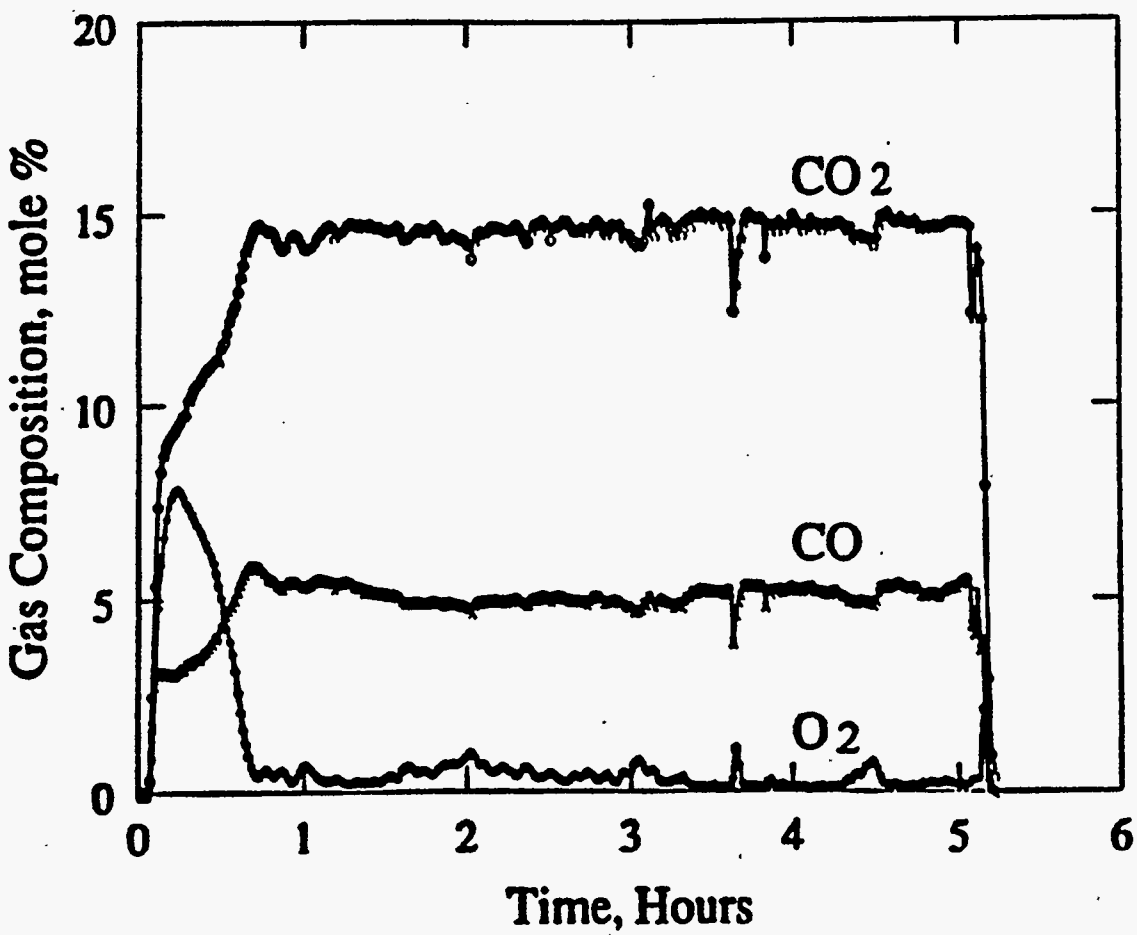
20
15
10
5
0
Gas Composition, mole %
CO2
CO
O2
0
1
2
3
4
5
6
Time, Hours

2.3 The Effect of Low Temperature Oxidation on Fuel and Produced Oil During In-situ Combustion

(D. Mamora and W. Brigham)

2.3.1. SUMMARY

The paper, published in In Situ Journal, is included, as a summary of the work done by Mamora on this topic. His SUPRI report has already been sent to DOE and the Industrial Affiliates..

THE EFFECT OF LOW-TEMPERATURE OXIDATION ON THE FUEL AND PRODUCED OIL DURING IN-SITU COMBUSTION

D. D. Mamora
Department of Petroleum Engineering
Texas A&M University
College Station, Texas 77843-3116

W. E. Brigham
Department of Petroleum Engineering
Stanford University
Stanford, California 94305-2220

ABSTRACT

Combustion tube experiments clearly showed the cause and effect of low-temperature oxidation (LTO) and high-temperature oxidation (HTO). LTO occurred due to the low fuel concentration which resulted in: (i) a reaction front temperature of only 350°C (662°F), compared to 500°C (932°F) for HTO, and (ii) oxygen moving ahead of the reaction front and oxidizing the crude oil. Consequently, an oxygenated hydrocarbon fuel was formed, while the produced oil viscosity and specific gravity increased. A method was derived to estimate the heats of reaction for oxygenated hydrocarbon fuels. During HTO, practically all of the oxygen injected was consumed, so that the fuel was not oxygenated. As a result of distillation, viscosity and specific gravity of the produced oil during HTO decreased significantly.

INTRODUCTION

Dry, forward in-situ combustion may be described by a simple chain reaction consisting of two competitive steps: fuel deposition and fuel combustion.[1-3] A third reaction, low-temperature oxidation (LTO), may occur, if oxygen is present downstream of the combustion front.

Fuel Deposition

Fuel deposition is the process of leaving fuel on the reservoir matrix. The amount of fuel deposited, or fuel concentration, is an important parameter in in-situ combustion project design. The maximum oil recovery is the difference between the initial oil-in-place and the amount of fuel consumed. A high fuel concentration will reduce the combustion front velocity and increase air requirements, which will result in higher air compression costs. On the other hand, if the fuel concentration is too low, combustion heat generated may be insufficient to propagate a self-sustaining combustion.

Analyses of core samples from South Belridge indicated reservoir lithology to be an important parameter for fuel deposition.[4] Based on kinetic experiments, Bousaid and Ramey[1] showed that the amount of fuel deposited increased with the addition of clay to the sample of oil and sand.

Alexander *et al.*[5] performed flood-pot experiments, and found that the amount of fuel deposited increased with initial oil saturation, oil viscosity and the Conradson residue, and decreased with increasing atomic hydrogen-carbon ratio and API gravity of the oil. Showalter[6] carried out combustion tube experiments, and found results similar to those of Alexander *et al.*, and that the amount of fuel deposited increased with decreasing API gravity of the oil.

Thermogravimetric studies were performed by Bae[7] for a wide range of crude oil gravities (6°-38°API). One of the conclusions of the study is that the main mechanism for fuel deposition is distillation.

Poettmann *et al.*[8] concluded from their studies that the specific area of the porous medium is an important parameter for fuel deposition, particularly for high-gravity, paraffin base crude oils. Results of combustion tube experiments performed by Vossoughi *et al.*[9] indicate that clay particles increase the amount of fuel deposited.

Fuel Combustion

The hydrocarbon fuel, CH_x, deposited at the combustion zone reacts with injected oxygen to generate heat for the combustion process. Based on the experimental studies of Benham and Poettmann,[10] the stochiometry of hydrocarbon fuel combustion may be described by Eq. 1.

$$CH_x+\left(1-\frac{m}{2}+\frac{x}{4}\right)O_2 \rightarrow (1-m)CO_2+mCO+\frac{x}{2}H_2O \qquad (1)$$

where x is the atomic hydrogen-carbon (H/C) ratio of the fuel, and m is the m-ratio (fraction of carbon oxidized to carbon monoxide).

Several researchers studied the effect of fuel concentration, C_f, and the rate of oxygen consumption on the combustion front velocity, V_F.[10-14] The results may be described by Eq. 2.[12]

$$V_F = \frac{U}{C_f R_{af}} \tag{2}$$

where U is the air flux at the combustion front, and R_{af} is the air-fuel ratio.

In combustion and kinetic tube experiments, the atomic hydrogen-carbon and m-ratios of the fuel may be determined from analysis of the effluent gas. If CO_2 and CO are the mole percent of carbon dioxide and carbon monoxide respectively in the produced gas, the m-ratio is given by Eq. 3.

$$m = \frac{CO}{(CO + CO_2)} \tag{3}$$

Let O_{2p} and N_2 denote the mole percent of oxygen and nitrogen respectively in the effluent gas. The mole percent of oxygen consumed, O_{2c}, may be obtained from a nitrogen material balance and is given by Eq. 4.

$$O_{2c} = 0.2682 N_2 - O_{2p} \tag{4}$$

Based on an oxygen material balance, and using Eq. 4, the apparent atomic hydrogen-carbon ratio, x, can be calculated:

$$x = 4\frac{\left[0.2682 N_2 - \left(O_{2p} + CO_2 + 0.5CO\right)\right]}{(CO_2 + CO)} \tag{5}$$

Low-Temperature Oxidation

Low-temperature oxidation (LTO) of crude oil occurs at temperatures less than about 650°F (345°C). The reaction is exothermic and is characterized by the production of little or no carbon oxides. The main products of LTO are oxygenated compounds such as carboxylic acids, aldehydes, ketones, alcohols and hyperoxides.[15]

To investigate the effect of LTO on fuel formation, Alexander *et al.*[5] subjected a sample of oil and sand to a continuous injection of air and a heating schedule. A coke-like residue was deposited on the sand matrix as a result of prolonged LTO reactions. For a 21.8°API crude oil, the amount of residue increased to a maximum at about 425°F (218°C) and decreased sharply to zero at about 650°F (345°C). The apparent atomic hydrogen-carbon ratio decreased from about 50 at 250°F (121°C) to about 1 at 650°F

1. Air filter
2. Mass flow controller
3. Pressure transducer
4. Kinetic cell
5. Electric furnace
6. Combustion tube
7. Pressure jacket
8. Separator
9. Water pump
10. Condenser
11. Separator
12. Drierite tube
13. Micro filter
14. Gas flow meter
15. Back-pressure regulator
16. Rotameter
17. Pressure relief valve
18. Acid scrubber
19. Gas auto-sampler
20. Gas chromatograph
21. Carbon dioxide analyzer
22. Carbon monoxide analyzer
23. Oxygen analyzer
24. Vent manifold

⊕ Valve

2-way valve

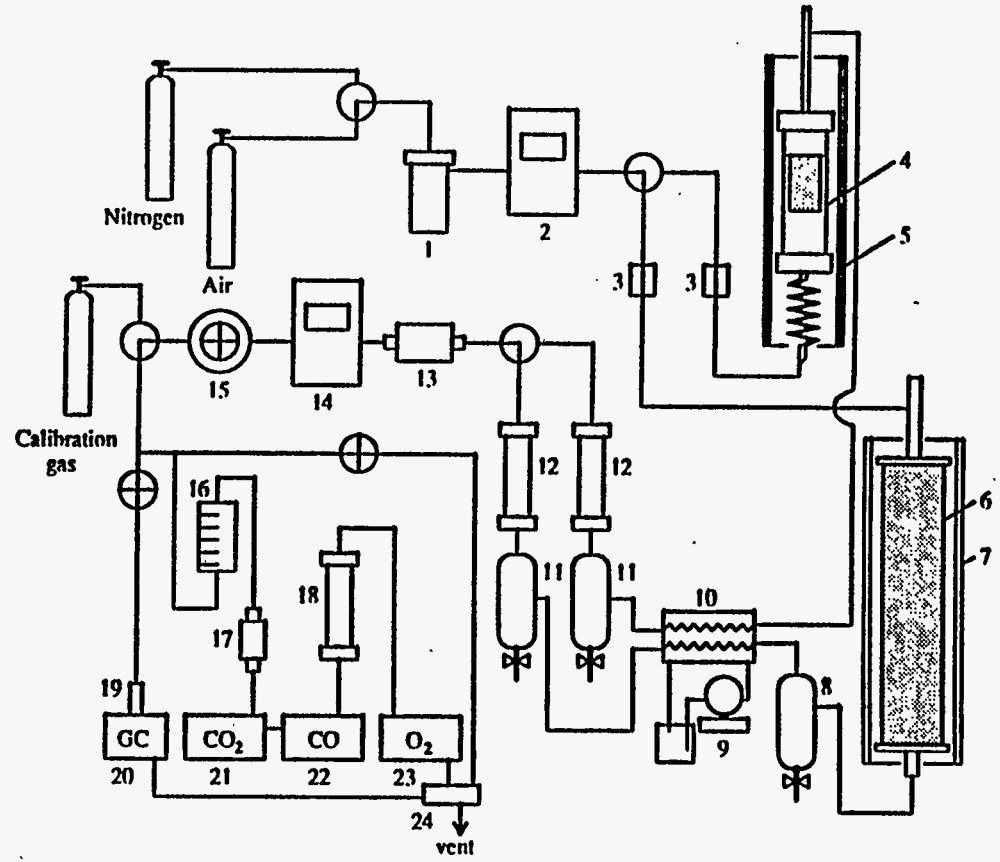

FIG. 1 - Schematic diagram of kinetic and combustion tube apparatus.

(345°C). The large apparent atomic hydrogen-carbon ratio is a result of oxygen being consumed in LTO reactions which do not produce carbon oxides. The viscosity and boiling range of the crude oil were increased due to LTO. Alexander *et al.* concluded that LTO reactions have a pronounced effect on fuel deposition and composition. Crude oils generally increase in total weight as a result of LTO.[7]

Crawford[16] found that aldehydes promote LTO reactions. Certain metallic additives and soils have a catalytic effect on LTO reactions.[1,9,16,17] The LTO reaction rate was found to be proportional to the matrix specific area raised to a power between 0 and 1.[15,18] Dabbous and Fulton concluded that during LTO, oxygen diffusion into the oil phase is greater than the oxidation reaction rate, so that oxygen is dissolved throughout the oil phase during LTO.

Several investigators have used the heat released during LTO to estimate the spontaneous ignition time for an in-situ combustion project.[4,19,20] Light crude oils were found to be more susceptible to LTO than heavy crude oils.[18]

This paper describes the combustion tube experiments which were carried out to investigate the factors that cause low-temperature oxidation and its effect on the combustion process and properties of the produced oil.

EXPERIMENTAL APPARATUS AND PROCEDURE

Figure 1 is a schematic diagram of the apparatus, which is set up to run either kinetic or combustion tube experiments. Major equipment, such as the gas analyzers, gas chromatograph, and the data acquisition unit, are shared between the two types of experiments, to minimize redundancy and cost of the apparatus.[21] A description of the apparatus and procedure for combustion tube experiments only will be given.

Air was supplied from pressurized gas cylinders and injected at the top of the combustion tube, which was placed in a vertical position. Air injection rate and pressure were kept constant by means of the mass flow controller and the back-pressure regulator. Produced fluids passed through a condenser coil in an ice-cooled water bath to cool and remove liquids from the produced stream. Further liquid removal was made in the separators. Water was removed from the produced gas by passing the gas through a trap containing Drierite (anhydrous calcium sulfate). A tube containing Purafil II Chemisorbant was placed at the inlet of the oxygen analyzer to remove any acid in the gas stream. The produced gas passed through three gas analyzers and a gas chromatograph, where the concentrations of carbon dioxide, carbon monoxide, oxygen and nitrogen were measured. The personal computer was programmed to record, at 30-sec intervals, the gas analyzer readings; injected gas rate and pressure; produced gas rate; and to compute and record nitrogen concentration data at six-minute intervals.

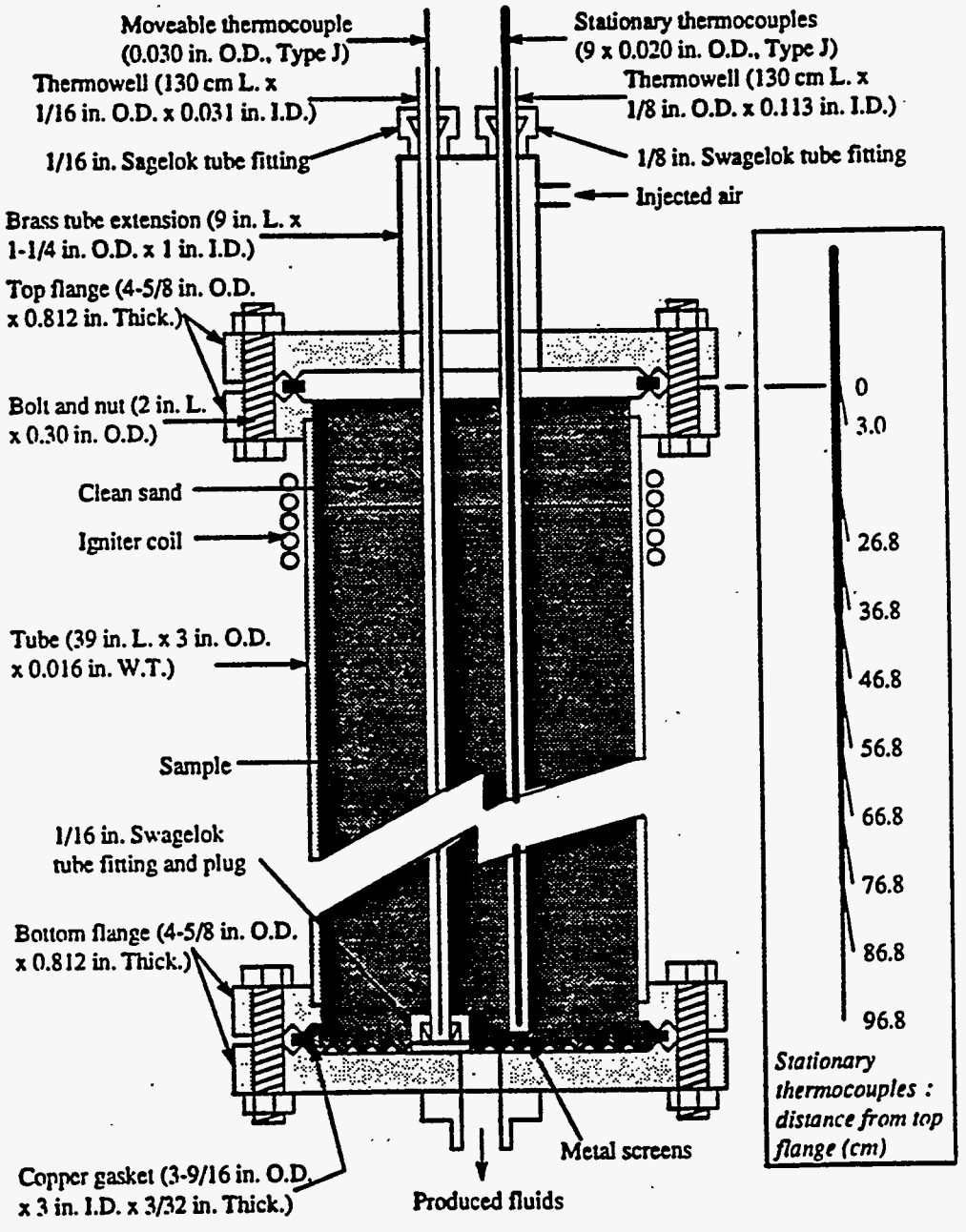

FIG. 2 - Schematic diagram of combustion tube.

The combustion tube consisted of a thin-walled stainless steel tube measuring 39 in. long × 3 in. O.D. × 0.016 in. wall thickness (Fig. 2). Knife-edge flanges were silver soldered to both ends of the tube. A 9 in. long × 1 in. I.D. brass tube was silver soldered to the top flange. A pair of 1/8 in. and 1/16 in. Swagelok tube fittings was silver soldered to the top of the brass tube, through which two thermowells passed and were secured. The thermowells consisted of a pair of 1/8 in. and a 1/16 in. stainless steel tubes about 94 cm long, silver soldered at several places along the length. A bundle of nine thermocouples (each of 0.020 in. I.D.) were silver soldered with the tips spaced at 10 cm intervals. This thermocouple bundle was inserted in the larger thermowell, and recorded temperatures at known positions in the tube. A thermocouple of 0.030 in. O.D. was placed in the smaller thermowell. This thermocouple could be moved freely to measure temperatures in small traverse increments. The combustion tube was sealed by a system of copper gaskets between the flanges, and Teflon twin ferrules at the thermowell-tube fitting connections. An electric igniter was wound around the tube about 10 cm from the top flange.

Three different matrix types were used in the experiments: (1) 20-30 mesh sand with 4.6 % by weight of clay, (2) 20-30 mesh sand, and (3) 20-30 mesh sand and 4.6 % by weight of 170-270 mesh sand fines (Table 1). For direct comparison of results of the tube runs, the same 10.2°API Hamaca (Venezuela) crude was used, and the air injection rate and pressure were kept at 3 L/min and 100 psig.

TABLE 1: Properties of Sand Packs

	Run No.		
	VEN5	VEN14	VEN21
Oil gravity (°API)	10.2	10.2	10.2
Oil viscosity at 50°C (cp)	14,000	14,000	14,000
Length (cm)	85.4	87.1	85.4
Weight (g)	7739	7461	7447
Oil (wt. %)	4.6	4.9	4.6
Water (wt. %)	4.1	4.3	4.1
20-30 mesh sand (wt. %)	86.8	90.8	86.8
Clay (wt. %)	4.6	0	0
170-270 mesh sand (wt. %)	0	0	4.6
S_o (fraction of pore vol.)	0.29	0.26	0.26
S_w (fraction of pore vol.)	0.27	0.23	0.24
S_g (fraction of pore vol.)	0.44	0.51	0.50
ϕ (fraction of bulk vol.)	0.31	0.35	0.33

TABLE 2: Combustion Tube Experimental Results

	Run No.		
	VEN5	VEN14	VEN21
Injection pressure (psig)	100	100	100
Injection rate (L/min)	3.00	3.00	3.00
Air flux (scf/hr-sq.ft.)	130.9	130.9	130.9
Comb. front temp. (°C)	500	350	500
Comb. front velocity (cm/hr)	10.5	7.7	11.1
Produced liquids:			
Oil gravity (°API)	14.0	9.8	11.2
Oil viscosity at 50°C (cp)	260	17,000	2600
Produced water vol. (ml)	353	285	271
Produced oil vol. (ml)	287	346	298
Oil recovery (wt. %)	78	94	88
Produced gas:			
Ave. prod. rate (L/min)	2.80	2.55	3.05
CO_2 (mole %)	11.6	4.3	9.7
CO (mole %)	4.9	2.0	4.3
O_2 (mole %)	1.1	10.1	3.8
N_2 (mole %)	81.4	82.8	81.2
Calculated results:			
m-ratio	0.298	0.312	0.308
Apparent H/C ratio	1.63	4.35	1.77
Residue after burn (g)	28.7	143.9	8.6
Fuel conc. (lb/ft^3 bulk vol.)	0.784	-	0.539
O_2 utilization efficiency (%)	95.0	54.5	82.6
Air-fuel ratio (scf/lb fuel)	167	-	169
Air req'ments (scf/ft^3)	139	-	112
Heat of comb. (Btu/lb fuel)	16,458	-	16,773

Almost from the start, water was produced, while oil was produced after about 4 to 5 hours. Produced liquids were collected in graduated sample bottles which were tightly sealed for subsequent analysis. The sand pack was burned to the bottom, so that the amount of fuel burned could be determined accurately. Each tube run took about 8 to 10 hours. After each run, the produced liquids were analyzed to determine the volumes of oil and water, the produced oil API gravity, and the produced oil viscosity as a function of temperature using a Brookfield viscometer.

DISCUSSION OF RESULTS

The results of the combustion tube runs are summarized in Table 2. A brief description of each tube run follows.

Run VEN5

The sample matrix consisted of sand and clay. Stable combustion was observed from the start of the run, as indicated by the stable produced gas composition readings (Fig. 3). Based on gas analysis, apparent H/C and *m*-ratios were calculated, as shown in Fig. 4. In the period 1-7.5 hours, the average H/C ratio is 1.63, compared to 1.65 for the original crude, as determined from elemental analysis. This result indicates the absence of low-temperature oxidation and the predominance of distillation as the fuel deposition mechanism. The average combustion temperature was 500°C (Fig. 5). Produced oil gravity at the end of the run was 3.8°API higher than that of the original crude (Fig. 6). The average combustion front velocity was 10.5 cm/hr (0.35 ft/hr). The viscosity of the produced oil decreased from the crude oil original value of 14,000 cp at 50°C to 260 cp (Fig. 7).

Run VEN14

The sample matrix consisted of sand only. The electric igniter was left on for two hours into the run to aid ignition. However, ignition was not obtained. This run was a low-temperature burn, as indicated by the temperature and gas analysis data. In the period 3-9 hours, the produced gas molar concentrations were: CO_2, 4.3 %; CO, 2.0 %; O_2, 10.1 % and N_2, 82.8 % (Fig. 8). The average apparent H/C and *m*-ratios were 4.35 and 0.312 (Fig. 9). The high apparent H/C ratio is a result of low-temperature oxidation, during which oxygen enters reactions which do not form carbon oxides. The average temperature at the reaction zone was 350°C (Fig. 10). Figure 11 indicates a reaction front velocity of 7.7 cm/hr (0.25 ft/hr), significantly lower than that in Run VEN5. Produced

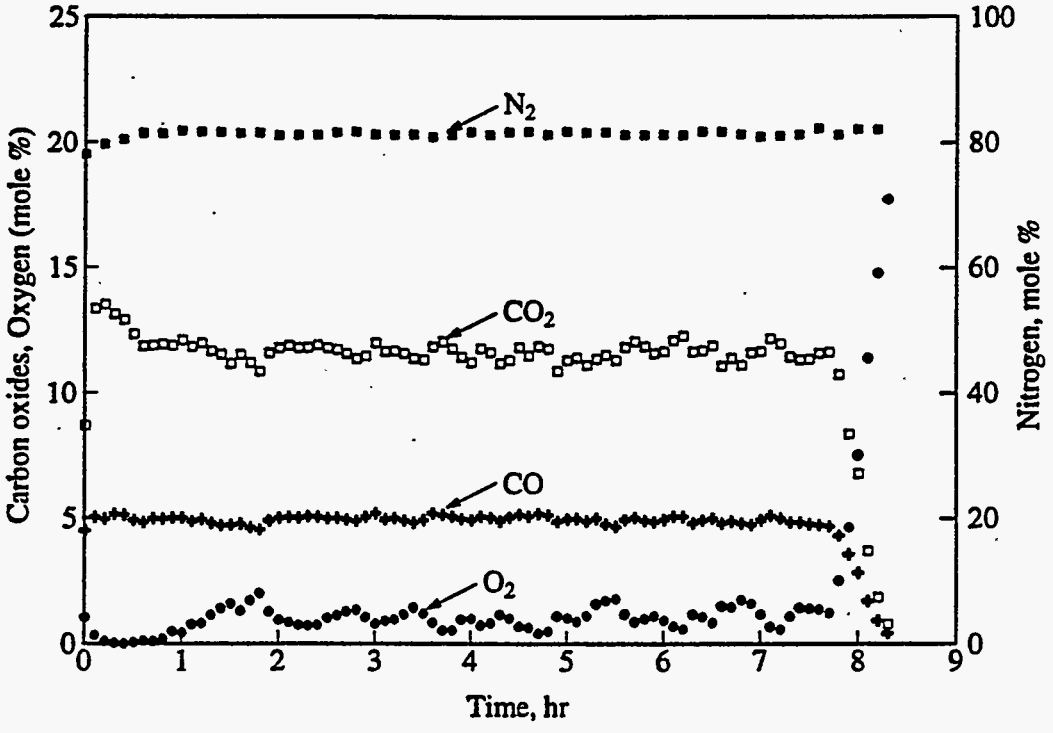

FIG. 3 - Produced gas composition versus temperature (run VEN5).

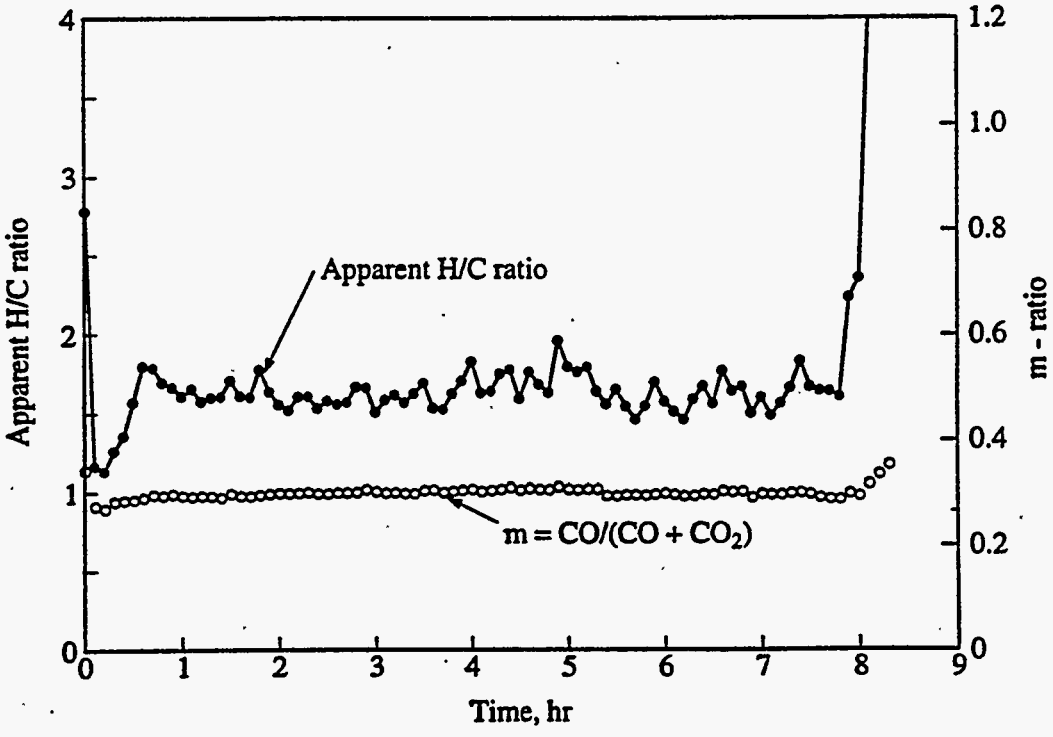

FIG. 4 - Apparent H/C and *m*-ratio versus time (run VEN5).

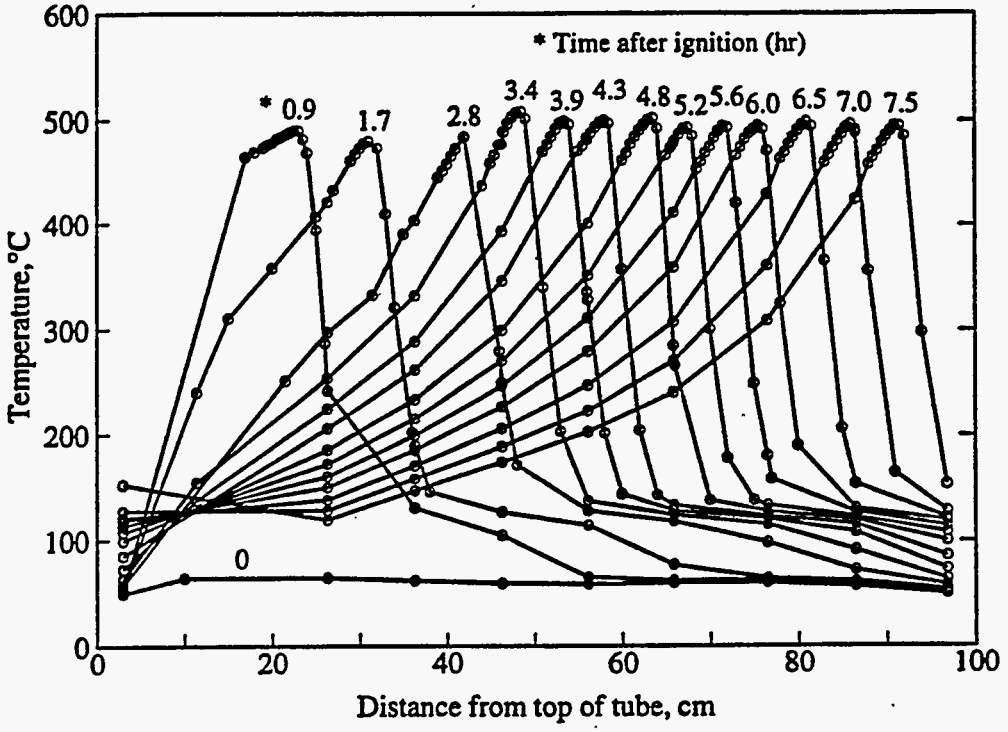

FIG. 5 - Temperature profiles (run VEN5).

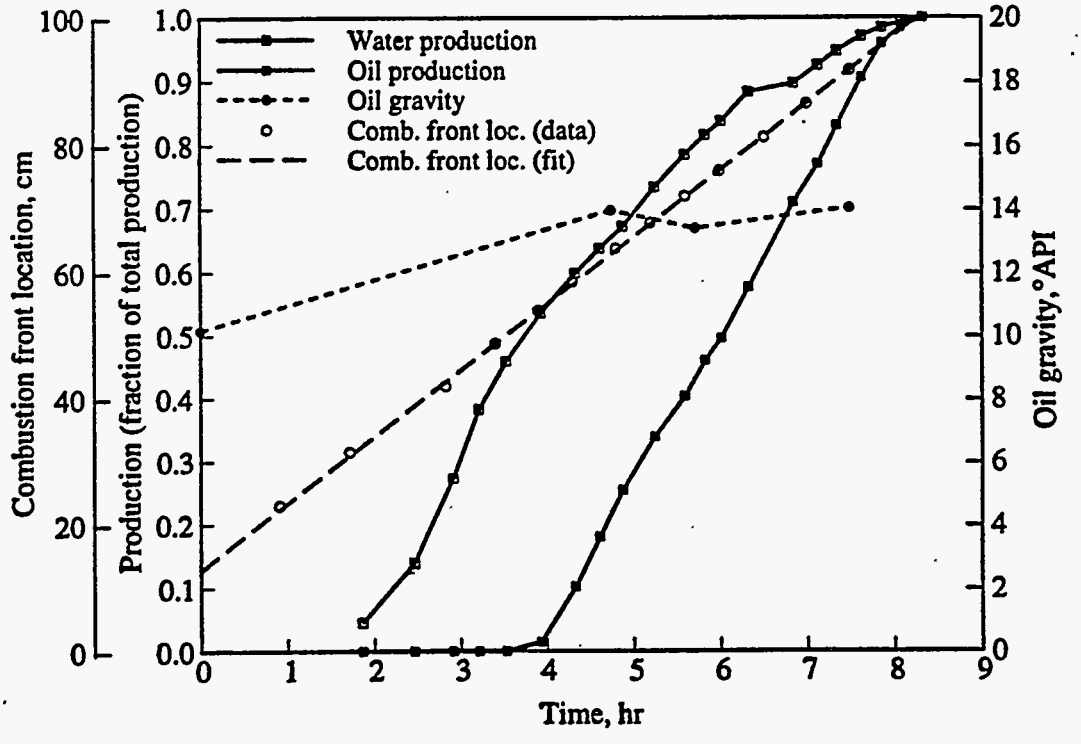

FIG. 6 - Production, oil gravity and comb. front location versus time (run VEN5).

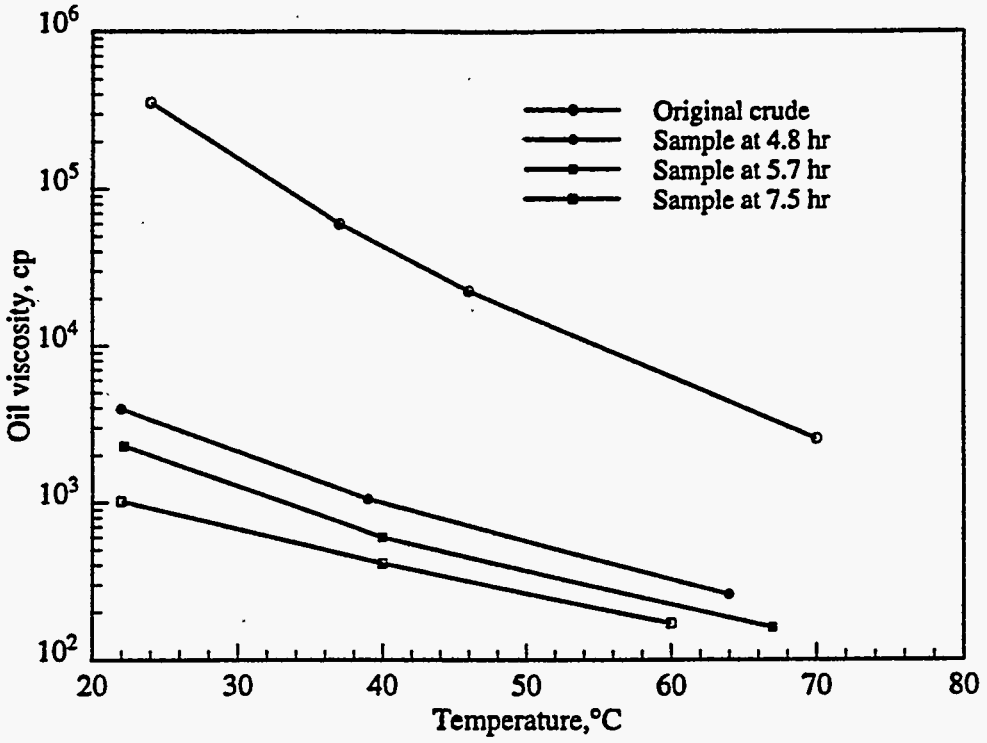

FIG. 7 - Oil viscosity versus temperature (run VEN5).

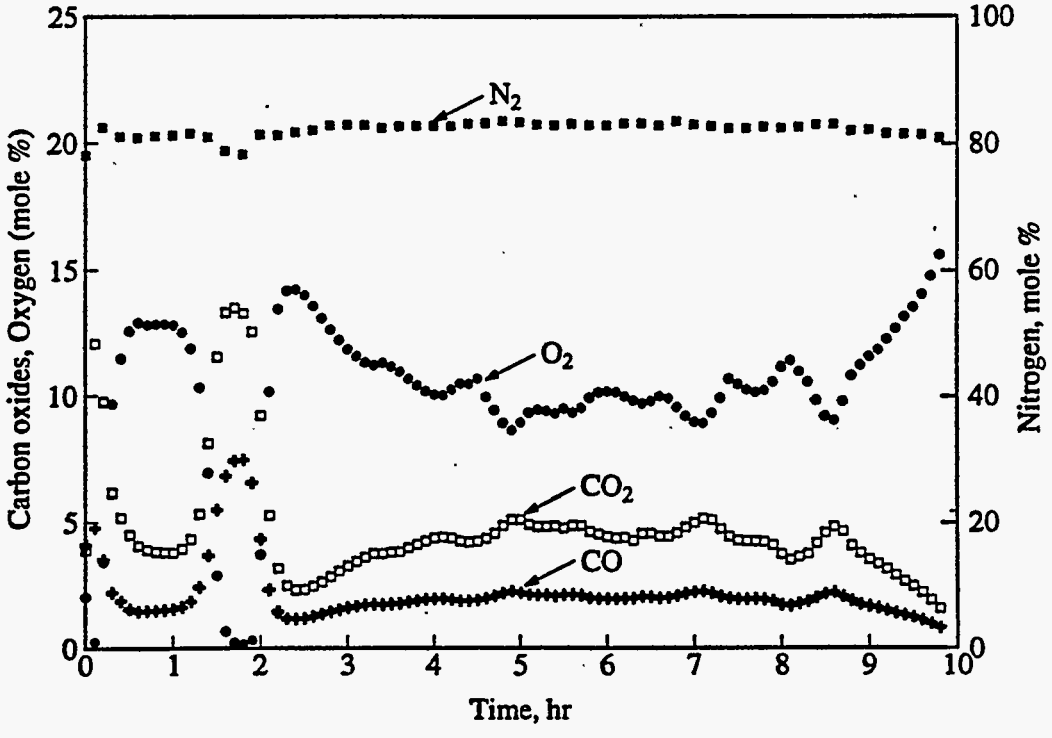

FIG. 8 - Produced gas composition versus temperature (run VEN14).

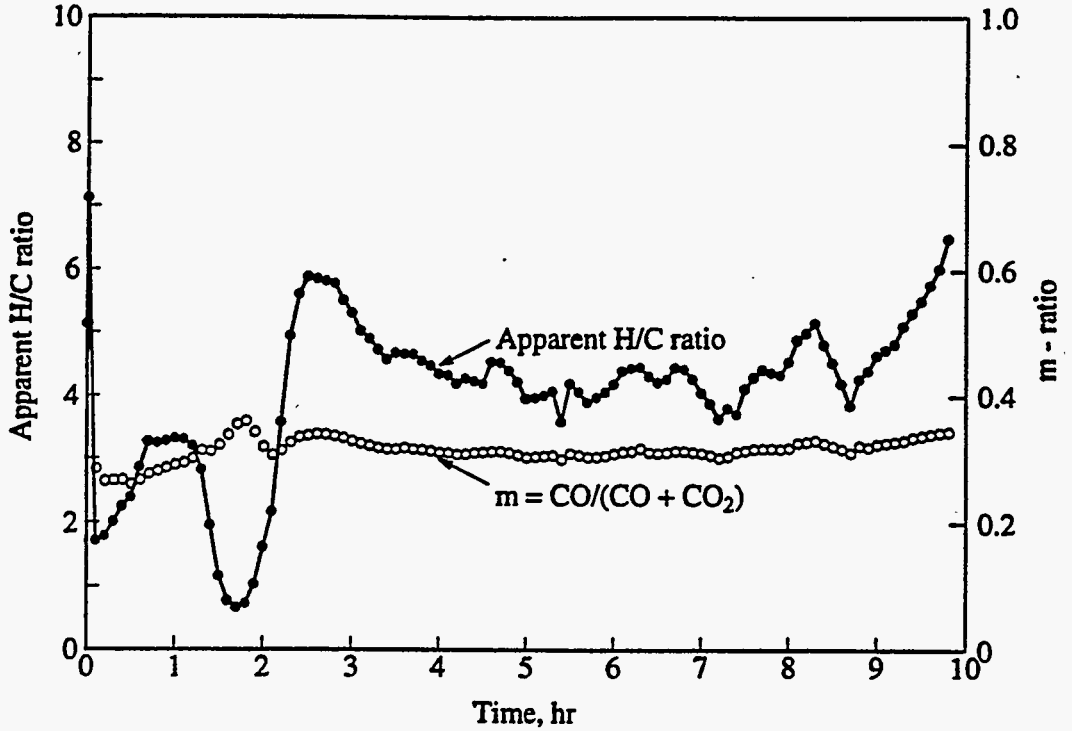

FIG. 9 - Apparent H/C and *m*-ratio versus time (run VEN14).

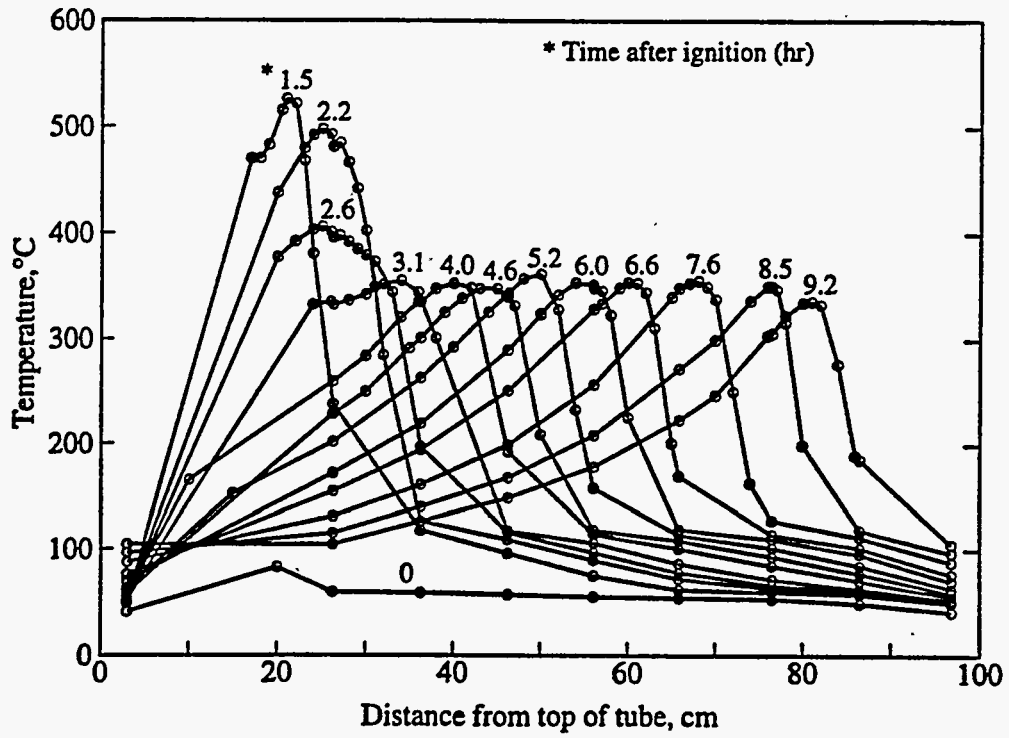

FIG. 10 - Temperature profiles (run VEN14).

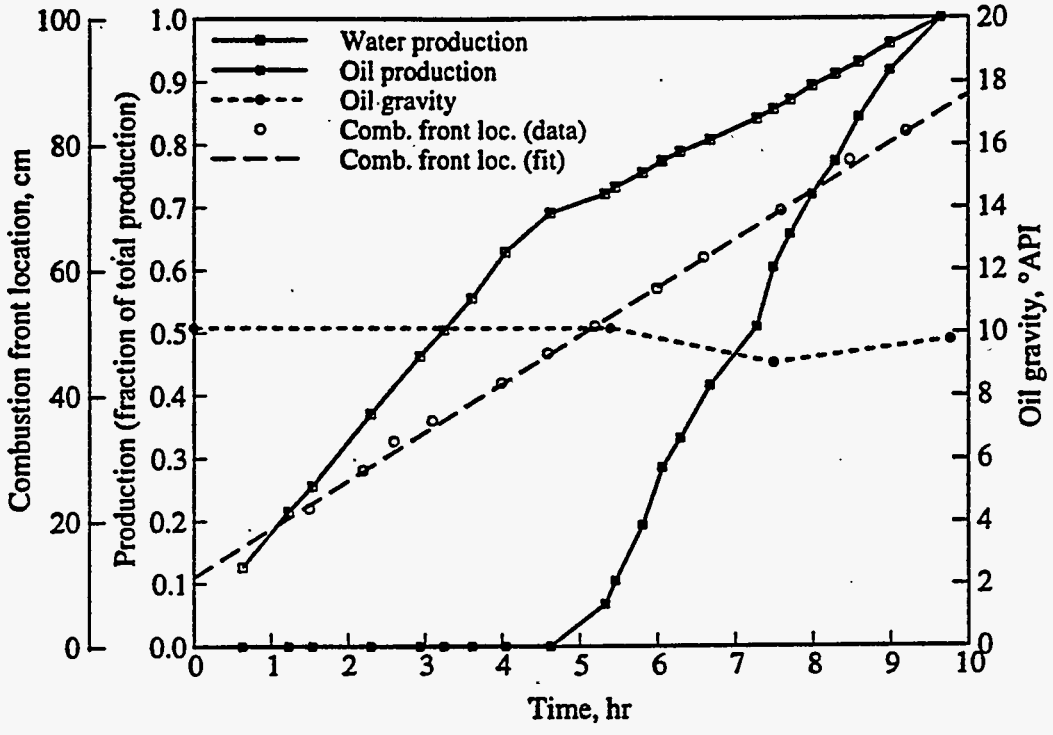

FIG. 11 - Production, oil gravity and comb. front location versus time (run VEN14).

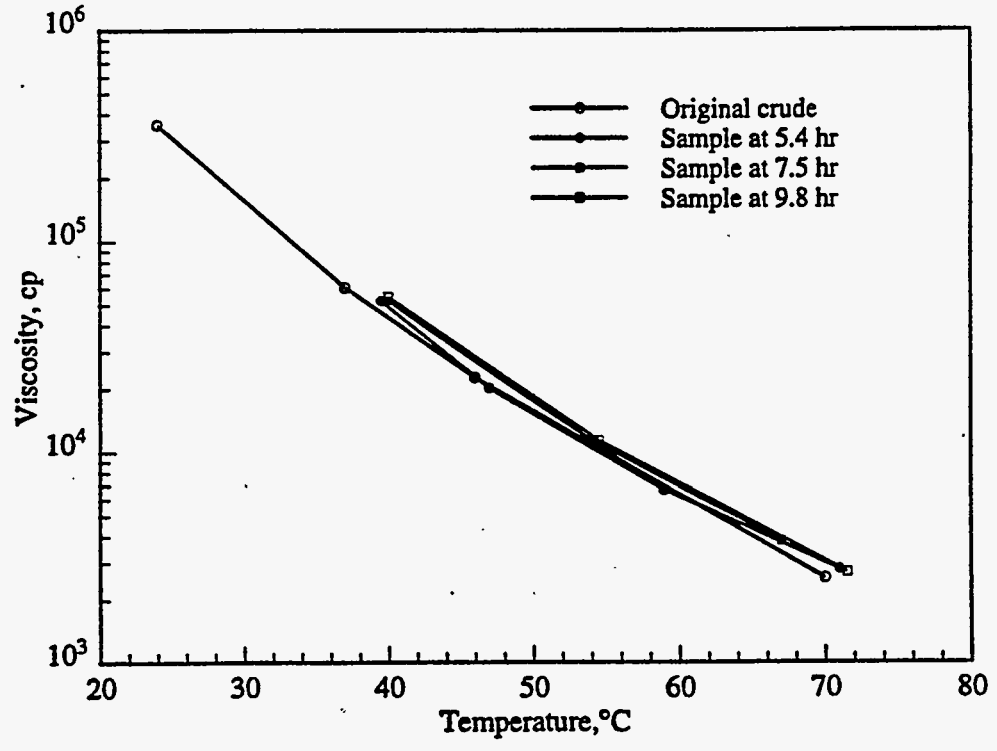

FIG. 12 - Oil viscosity versus temperature (run VEN14).

oil gravity and viscosity data are shown in Figs. 11 and 12 respectively. Produced oil gravity, 9.8°API, was slightly lower than that of the original crude oil, while the oil viscosity increased slightly to 17,000 cp at 50°C from the original crude oil value of 14,000 cp. The decrease in oil gravity and increase in oil viscosity were due to low-temperature oxidation. Alexander *et al.*[5] also found an increase in the viscosity of oil which had undergone low-temperature oxidation. Bae[7] also observed a decrease in the API gravity of oil subjected to low-temperature oxidation.

The percent of oxygen used in LTO may be estimated using Eq. 6.[22]

$$\text{Percent of oxygen in LTO} = \frac{100\left(x_{apparent} - x_{true}\right)\left(CO_2 + CO\right)}{4\left(0.2682N_2 - O_{2p}\right)} \qquad (6)$$

Based on Eq. 6, 35 % of oxygen injected went into LTO and 46 % of oxygen injected was produced and did not generate heat. Thus only 19 % entered into HTO reactions. A material balance on oil indicated 43 % was deposited as an immobile residue and 57 % was displaced with little or no improvement in quality. Elemental analysis of a produced oil sample from this run indicated an atomic oxygen-carbon ratio of 0.25.

Run VEN 21

The sample matrix was made up of sand and sand fines. Despite the absence of clay in the matrix, a fairly stable burn was obtained, although the produced gas readings were rather oscillatory. In the period 1-7 hours, the produced gas molar concentrations were: CO_2, 9.7 %: CO, 4.3 %; O_2, 3.8 % and N_2, 81.2 % (Fig. 13). Apparent H/C and *m*-ratios averaged 1.77 and 0.308 respectively (Fig. 14). The average combustion front temperature and velocity were 500°C and 11.1 cm/hr (0.36 ft/hr) respectively (Figs. 15 and 16). The gravity of the produced oil increased by 1°API (Fig. 16), while the oil viscosity decreased to 2,600 cp at 50°C from 14,000 cp for the original crude oil (Fig. 17).

The results of this run were very similar to that of Run VEN5 (in which clay was included in the sample), except for the oscillatory gas composition readings. Vossoughi *et al.*[9] inferred from combustion tube experiments that clay did not have a catalytic effect on combustion. A possible effect of clay and the sand fines is as follows. Both clay and the 170-270 mesh sand particles are smaller than those of 20-30 mesh sand. These smaller particles most likely increase oil entrapment and thereby increase fuel concentration. Oil entrapment may be caused by permeability reduction and the greater surface area of these particles. Similarly, fuel concentration is decreased when the sample does not contain clay or sand fines, which may lead to low-temperature oxidation, as observed in Run VEN14.

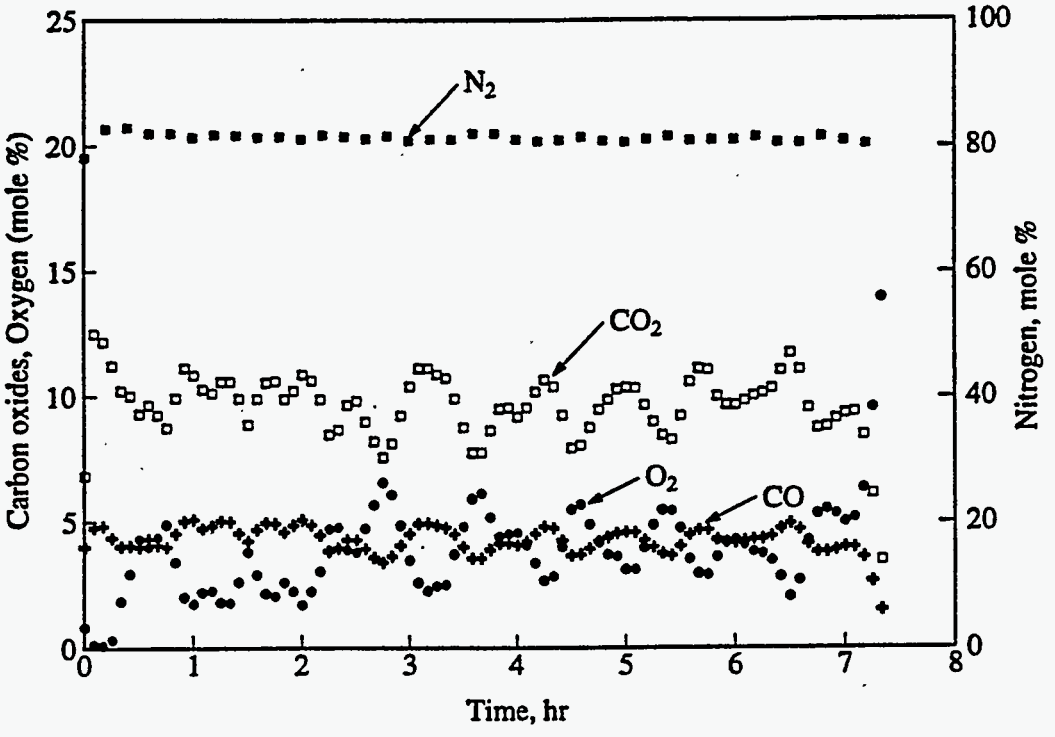

FIG. 13 - Produced gas composition versus temperature (run VEN21).

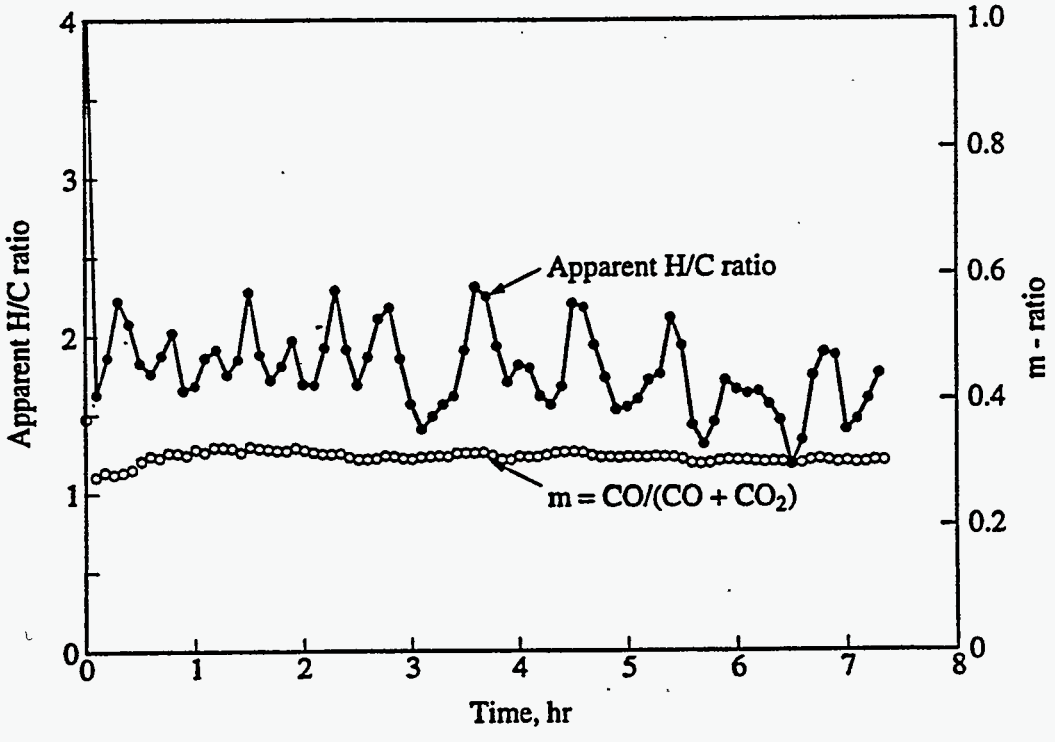

FIG. 14 - Apparent H/C and *m*-ratio versus time (run VEN21).

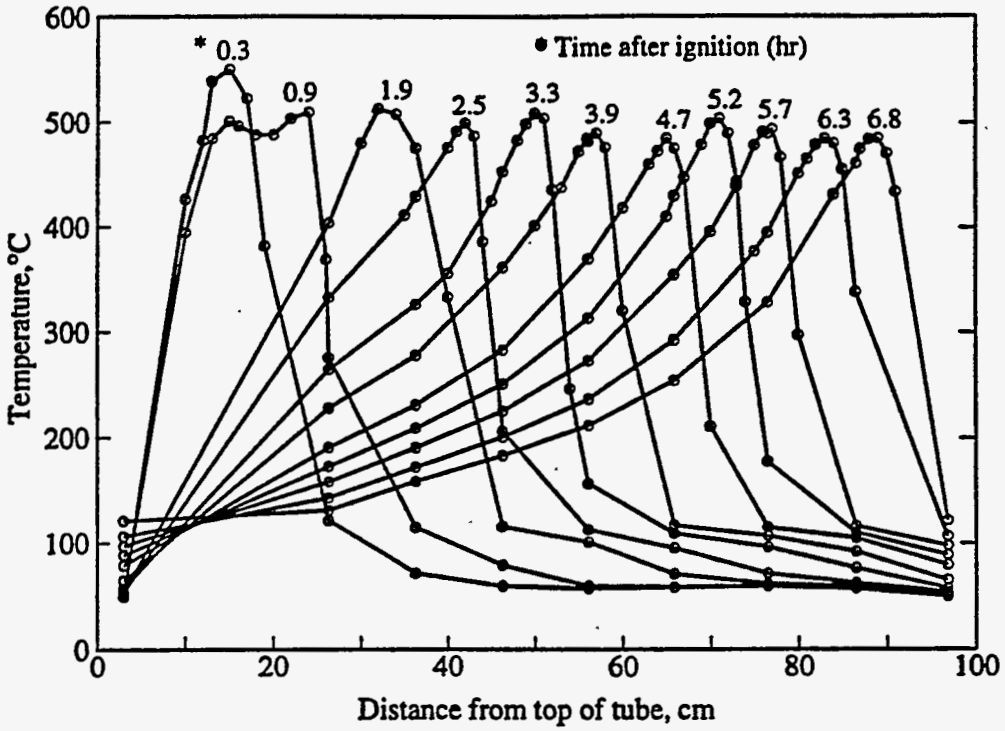

FIG. 15 - Temperature profiles (run VEN21).

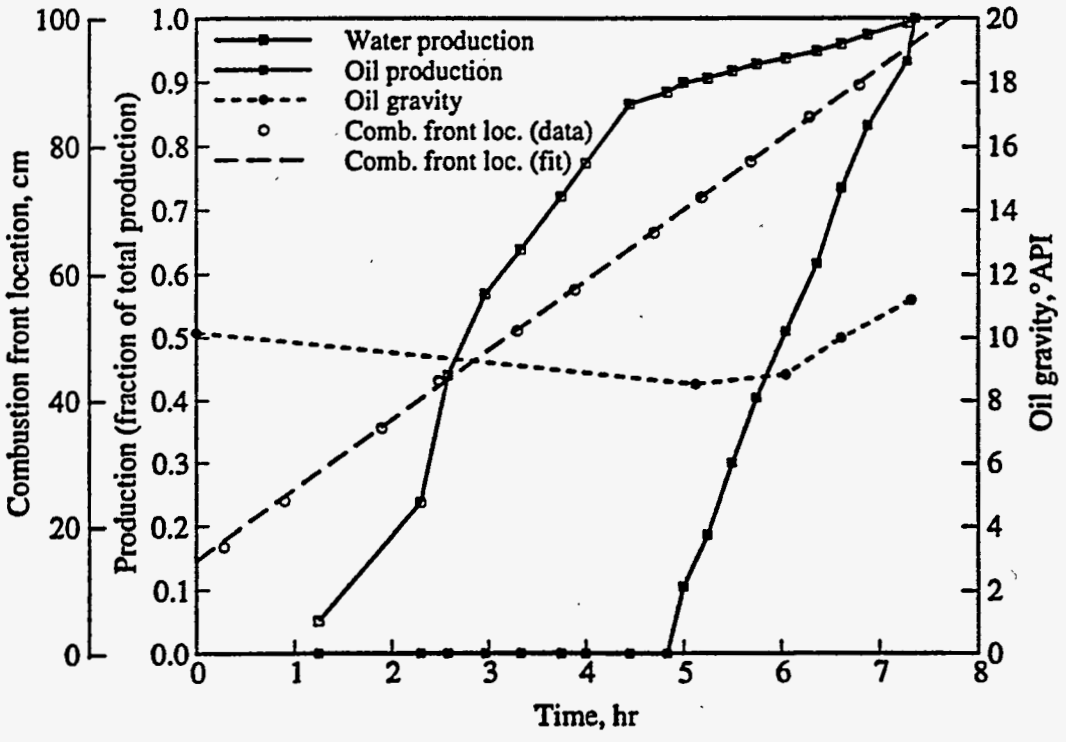

FIG. 16 - Production, oil gravity and comb. front location versus time (run VEN21).

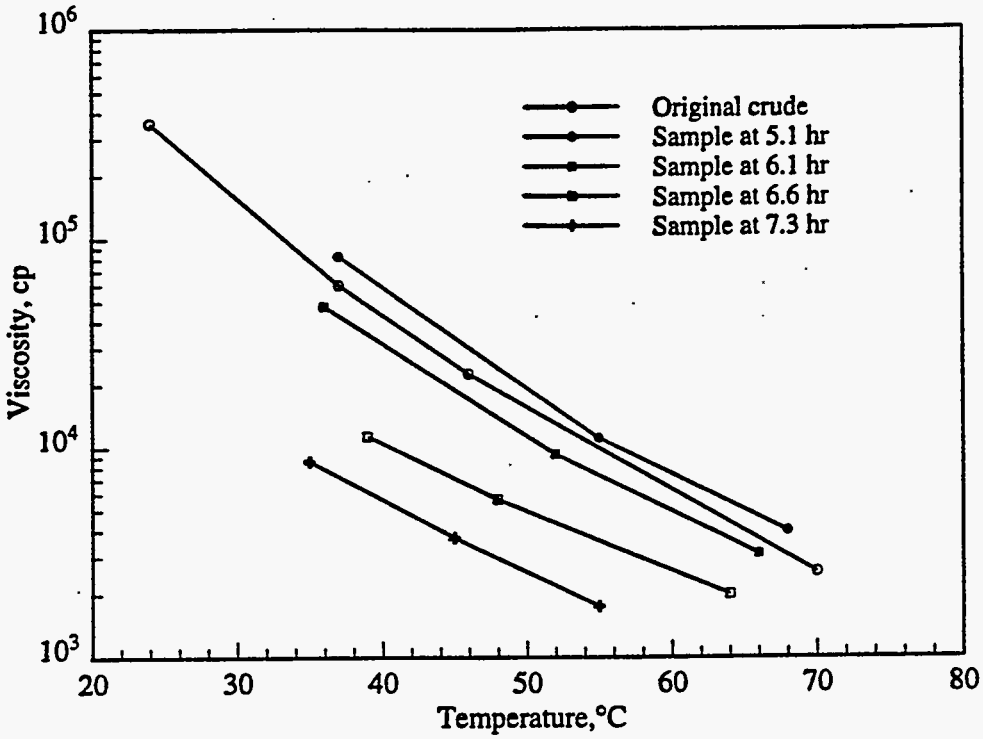

FIG. 17 - Oil viscosity versus temperature (run VEN21).

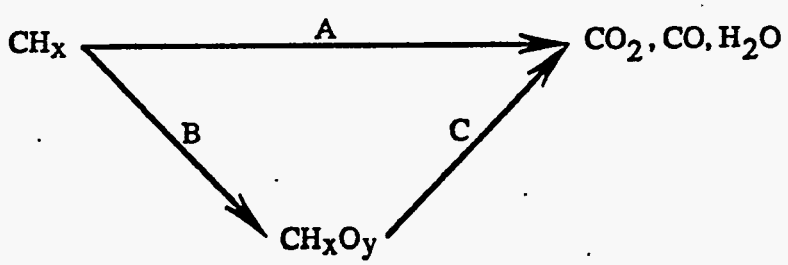

FIG. 18 - Fuel oxidation paths.

HEAT OF COMBUSTION OF OXYGENATED FUEL

For a hydrocarbon fuel, CH_x, which undergoes combustion according to the stochiometry given by Eq. 1, the heat of reaction, ΔH_x (Btu/lb of fuel), is estimated using Eq. 7.[15] It is assumed in Eq. 7 that the products of combustion are gaseous carbon dioxide and carbon monoxide and condensed water.

$$\Delta H_x = \frac{1800}{(12+x)}(94.0 - 67.9m + 31.2x) \tag{7}$$

For an oxygenated hydrocarbon fuel, CH_xO_y, where y is the atomic oxygen-carbon (O/C) ratio, the heat of combustion is considerably less than that for a hydrocarbon fuel, on a per unit mass basis, since an oxygenated fuel is partially oxidized and also its mass includes oxygen. The heat of combustion of an oxygenated hydrocarbon was estimated by considering the fuel oxidation paths as indicated in Fig.18. In Fig. 18, Path A is the oxidation of a hydrocarbon fuel to form carbon oxides and water. Path B represents the oxygenation of the fuel to form CH_xO_y, while Path C is the oxidation of the oxygenated fuel to form carbon oxides and water.

Let ΔH_A be the heat of reaction per mol of oxygen consumed for Path A, and ΔH_B and ΔH_C the heats of reaction for Paths B and C for the same mass of fuel as in Path A. ΔH_A (KJ/mol O_2) may be calculated from Eq. 8.[15]

$$\Delta H_A = \frac{786.4 - 567.6m + 260.9x}{2 - m + 0.5x} \tag{8}$$

The heats of reactions (KJ/mol O_2) for the main products of hydrocarbon oxygenation are as follows: carboxylic acid (430.8), aldehyde (363.1), ketone (375.7) and alcohol or phenol (306.6).[15] The averaged heat of reaction for these oxygenated products is 369.0 KJ/mol O_2. For one mole of oxygen consumed for Path A, the number of moles of oxygen consumed for Path B is $(y/2)(1 - m/2 + x/4)$. Therefore:

$$\Delta H_B = \frac{369.0y}{2(1 - 0.5m + 0.25x)} \tag{9}$$

From conservation of energy:

$$\Delta H_C = \Delta H_A - \Delta H_B \tag{10}$$

Using Eqs. 8, 9 and 10:

$$\frac{\Delta H_C}{\Delta H_A} = 1 - \frac{369.0y}{786.4 - 567.6m + 260.9x} \tag{11}$$

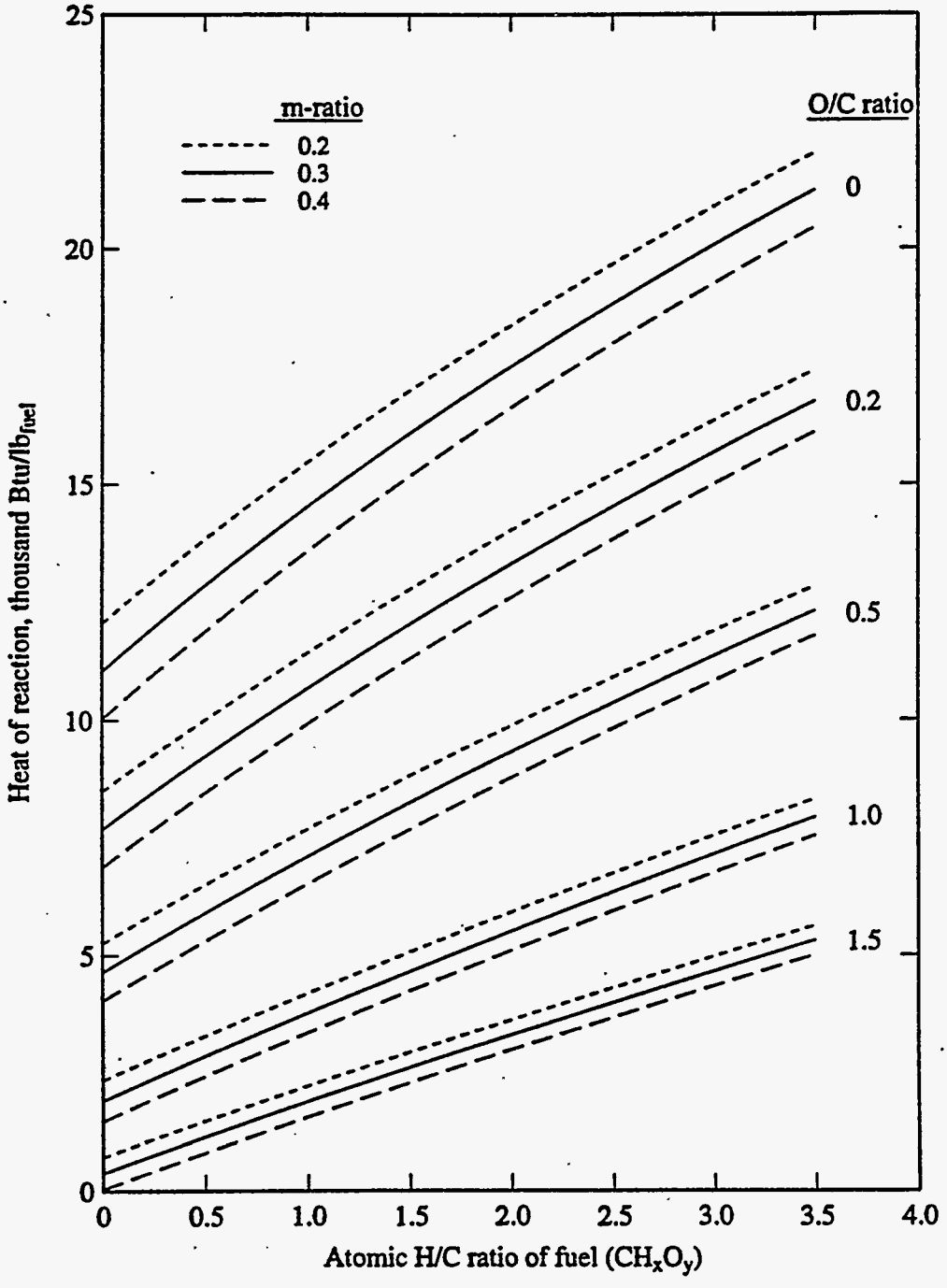

FIG. 19 - Heat of combustion versus atomic H/C, O/C and *m*-ratios.

Let R_m denote the molar mass ratio of CH_x to CH_xO_y:

$$R_m = \frac{12+x}{12+x+16y} \tag{12}$$

The heat of reaction for an oxygenated fuel, ΔH_{xy} (Btu/lb of oxygenated fuel), is proportional to ΔH_x but reduced by the heat of oxygenation and by the addition of oxygen to the fuel mass. That is:

$$\Delta H_{xy} = \frac{\Delta H_C}{\Delta H_A} R_m \Delta H_x \tag{13}$$

Substituting Eqs. 7, 11 and 12 into Eq. 13:

$$\Delta H_{xy} = \frac{1800(94.0-67.9m+31.2x)}{(12+x+16y)}\left[1-\frac{369.0y}{(786.4-567.6m+260.9x)}\right] \tag{14}$$

Using Eq. 14, the heat of combustion for an oxygenated hydrocarbon was computed as a function of atomic H/C, O/C and *m*-ratios. The results are presented in Fig. 19. The heat of combustion decreases significantly with increasing atomic O/C ratio, and also decreases slightly with increasing *m*-ratio for typical *m*-ratio ranges. For example, for a fuel with an atomic H/C ratio of 1.5 and *m*-ratio of 0.3, the heat of combustion decreases from 16,000 Btu/lb fuel, for an atomic O/C ratio of 0.0, down to 8,000 Btu/lb fuel for an atomic O/C ratio of 0.5. Therefore, if the fuel is oxygenated as a result of low-temperature oxidation, an inefficient combustion process will occur. For the same reason, oxygenated gasoline used in automobiles will give considerably lower mileage per gallon than non-oxygenated gasolines.

CONCLUSIONS

High combustion temperatures were obtained when clay or sand fines were present. These particles reduced the permeability of the sand pack and also provided a large reaction surface area. Consequently, the residual oil saturation, and therefore the fuel concentration, increased, resulting in high temperature burns. Practically all the injected oxygen was consumed at the combustion zone. Hence, hydrocarbons ahead of the combustion front did not undergo low-temperature oxidation. This resulted in atomic H/C ratios which were similar to those of the original crude oils. The viscosity of the produced oil was reduced significantly, while the produced oil gravity increased by 1°-4°API.

In contrast, low-temperature oxidation occurred when the sample matrix contained only 20-30 mesh sand. Ignition was not obtained due to the low fuel concentration, and a

significant amount of oxygen moved ahead of the combustion zone. This resulted in low-temperature oxidation of the crude oil to form an oxygenated hydrocarbon. Low-temperature oxidation was found to be a very inefficient process, both from the standpoint of oxygen usage and heat generated. In addition, the resulting oxygenated crude viscosity increased significantly.

Before starting a combustion project, it is essential to run combustion tube experiments, using oil and core samples and fluid saturations representative of the field, to ascertain that low-temperature oxidation will not occur.

ACKNOWLEDGMENT

This paper is dedicated to our co-worker and friend, the late Dr. Henry J. Ramey, Jr., whose contribution to this research is invaluable. It is our great privilege to have known and worked with such a tireless, devoted, and unselfish engineer.

NOMENCLATURE

C_f	fuel concentration, lb/ft^3
CO	concentration of carbon monoxide in produced gas, mole %
CO_2	concentration of carbon dioxide in produced gas, mole %
m	m-ratio as defined by Eq. 3, fraction
N_2	concentration of nitrogen in produced gas, mole %
O_{2c}	concentration of oxygen consumed during combustion, mole %
O_{2p}	concentration of oxygen in produced gas, mole %
R_{af}	air-fuel ratio, ft^3/lb
R_m	molar mass ratio of CH_x to CH_xO_y
U	air flux at combustion front, ft/day
V_F	combustion front velocity, ft/day
x	atomic hydrogen-carbon ratio, fraction
y	atomic oxygen-carbon ratio, fraction
ΔH_A	heat of reaction (Path A), KJ/mol oxygen consumed
ΔH_B	heat of reaction (Path B), KJ/mol oxygen consumed
ΔH_C	heat of reaction (Path C), KJ/mol oxygen consumed
ΔH_x	heat of reaction for a hydrocarbon fuel, Btu/lb of fuel
ΔH_{xy}	heat of reaction for an oxygenated hydrocarbon fuel, Btu/lb of oxygenated fuel

REFERENCES

1. Bousaid, I. S. and Ramey, H. J. Jr.: "Oxidation of Crude Oil in Porous Media," *Soc. of Pet. Eng. J.* (June 1968) 137-148.

2. Dabbous, M. K. and Fulton, P. F.: "Low-Temperature Oxidation Reaction Kinetics and Effects on the In-Situ Combustion Process," *Soc. of Pet. Eng. J.* (June 1974) 253-262.

3. Thomas, G. W., Buthod, A. P. and Allag, O.: "An Experimental Study of the Kinetics of Dry, Forward Combustion-Final Report," Report No. BETC-1820-1, distributed by Dept. of Energy (Feb. 1979).

4. Gates, G. F. and Ramey, H. J. Jr.: "A Method of Engineering In-Situ Combustion Oil-Recovery Projects," *J. Pet. Tech.* (Feb. 1980) 285-94.

5. Alexander, J. D., Martin, W. L. and Dew, J. N.: "Factors Affecting Fuel Availability and Composition During In-Situ Combustion," *J. Pet. Tech.* (Oct. 1962) 1154-1164.

6. Showalter, W. E.: "Combustion Drive Tests," *Soc. of Pet. Eng. J.* (March 1963) 53-58.

7. Bae, J. H.: "Characterization of Crude Oil for Fireflooding Using Thermal Analysis Methods," *Soc. of Pet. Eng. J.* (June 1977) 211-217.

8. Poettmann, F. H., Schilson, R. E. and Surkalo, H.: "Philosophy and Technology of In-Situ Combustion in Light Oil Reservoirs," Proc. of the Seventh World Pet. Congress, Mexico City (1967) III, 487.

9. Vossoughi, S., Willhite, G. P., Krikitos, W. P., Guvenir, I. M. and El Shoubary, Y.: "Automation of an In-Situ Combustion Tube and Study of the Effect of Clay on the In-Situ Combustion Process," *Soc. of Pet. Eng. J.* (Aug. 1982) 493-502.

10. Benham, A. L. and Poettmann, F. H.: "The Thermal Recovery Process-An Analysis of Laboratory Combustion Data," *Trans., AIME* (1958) 213, 406-408.

11. Martin, W. L., Alexander, J. D. and Dew, J. N.: "Process Variables of In-Situ Combustion," *Trans., AIME* (1958) 213, 28-35.

12. Penberthy, W. L. Jr. and Ramey, H. J. Jr.: "Design and Operation of Laboratory Combustion Tubes," *Soc. of Pet. Eng. J.* (June 1966) 183-198.

13. Moss, J. T., White, P. D. and McNeil, J. S. Jr.: "In-Situ Combustion Process - Results of a Five-Well Field Experiment in Southern Oklahoma," *J. Pet. Tech.* (April 1959) 55-64.

14. Wilson, L. A., Reed, R. L., Reed, D. W., Clay, R. R. and Harrison, N. H.: "Some Effects of Pressure on Forward and Reverse Combustion," *Soc. of Pet. Eng. J.* (Sept. 1963) 127-137.

15. Burger, J. G. and Sahuquet, B. C.: "Chemical Aspects of In-Situ Combustion - Heat of Combustion and Kinetics," *Soc. of Pet. Eng. J.* (Oct. 1972) 410-422.

16. Crawford, P. B.: "Water Technology - Underground Combustion of Hydrocarbons," *Producers' Monthly* (June 1968) p. 15.

17. Johnson, H. R. and Burwell, E. L.: "Carbon Deposition for Thermal Recovery of Petroleum - A Statistical Approach to Research," *Producers' Monthly* (July 1968) p. 8-15.

18. Dabbous, M. K. and Fulton, P. F.: "Low-Temperature Oxidation Reaction Kinetics and Effects on the In-Situ Combustion Process," *Soc. of Pet. Eng. J.* (June 1974) 253-262.

19. Tadema, H. J. and Weijdema, J.: "Spontaneous Ignition in Oil Sands," *Oil and Gas Journal* (Dec. 1970) 77-80.

20. Burger, J. G.: "Spontaneous Ignition in Oil Reservoirs," *Soc. of Pet. Eng. J.* (April 1976) 73-81.

21. Mamora, D. D.: "*Kinetics of In-Situ Combustion*," Ph.D. dissertation, Stanford University, Stanford, CA (May 1993).

22. Ramey, H. J. Jr., Stamp, V. W., Pebdani, F. N. and Mallinson, J. E.: "Case History of South Belridge, California, In-Situ Combustion Oil Recovery," paper SPE 24200 presented at the SPE/DOE Eight Symposium on Enhanced Oil Recovery, Tulsa, Oklahoma, April 21-24, 1992.

PROJECT 3: STEAM WITH ADDITIVES

To develop and understand the mechanisms of the process using commercially available surfactants for reduction of gravity override and channeling of steam.

3.1 A Study of Steam Injection in Fractured Media

(M.D. Sumnu-Dindoruk, K. Aziz, W. Brigham, and L. Castanier)

A copy of the abstract from the technical report is included; also the abstract that will be presented at the SPE/DOE Tenth Symposium on Improved Oil Recovery, Tulsa (April 21-14, 1996).

3.1.1 ABSTRACT FROM SUPRI TR 101

Steam injection is the most widely used thermal recovery technique for unfractured reservoirs containing heavy oil. There have been numerous studies on theoretical and experimental aspects of steam injection for such systems.

Fractured reservoirs contain a large fraction of the world supply of oil, and field tests indicate that steam injection is feasible for such reservoirs. Unfortunately there has been little laboratory work done on steam injection in such systems. The experimental system in this work was designed to understand the mechanisms involved in the transfer of fluids and heat between matrix rocks and fractures under steam injection.

Fine grid simulations, where both the fracture and the matrix systems were represented by grids, were used to study the effects of certain flow parameters. Among the fluid flow properties investigated, water-oil capillary pressure of the matrix and gas-oil capillary pressure of the fracture were found to have the strongest effect on oil recovery. Matrix gas-oil capillary pressure and fracture water-oil capillary pressure had little effect. Matrix and fracture relative permeabilities also had little effect on recovery.

Experimental design involved the use of both simulations and analytical heat transfer models. Steady state and transient heat transfer models were used to calculate heat losses to determine insulation thickness. Simulations were also used to determine thermocouple locations, maximum expected pressure in the system and injection rates.

Two-phase, continuous steam drive experiments were performed on systems containing water, at differing rates, injection temperatures and back pressures. Saturation distributions, temperature distributions and heat fluxes were measured. The saturations were measured in-situ, both in the fractures and the consolidated rock matrix, by a CT scanner. The results indicated that steam does not enter the matrix, and prefers to flow in the fracture. The matrix is heated by conduction. Cyclic steam injection experiments showed the same results; steam saturation did not develop in the matrix.

Numerical simulations were used to model both continuous and cyclic steam injection experiments. To model experimental heat losses, heat loss models in the simulator had to be adjusted, based on analytical models. The results from the solution using a variable temperature inner boundary condition, and a convective outer boundary condition, showed good agreement with the experiments and heat transfer coefficients were incorporated into the simulator. After this adjustment, the results from the simulations agreed well with the experiments. Complete matches were made to the heat losses, temperatures and saturations.

The same numerical simulator was used to simulate a case with no external heat losses from the fracture-matrix system. This mimics the process in the field. No steam saturation developed in the matrix. However, when pressure cycling was simulated with no heat losses, matrix steam saturation did develop. This justifies the application of cyclic steam injection in fractured reservoirs, and pinpoints the need to modify any future laboratory work to minimize heat losses from the fractures.

Finally, simulation runs were performed for the laboratory system with oil present. The results were similar to the steam-water experiments. Steam only flowed in the fracture. Oil recovery was found to be mainly due to water imbibition, and conduction was the dominant heat transfer mechanism. When cyclic steam injection was simulated with no external heat losses, steam saturation did develop in the matrix; however, the oil recovery was similar to the case with no cycling, showing that water imbibition was the dominant recovery mechanism.

3.1.2 ABSTRACT FROM SPE 35459

Fractured reservoirs contain a large fraction of the world supply of oil. For viscous crudes, steam is the most successful technique and field tests indicate that steam has the best potential to recover significant amounts of oil from fractured reservoirs. Unfortunately, there has been little laboratory work done on steam injection in such systems.

The experimental system discussed here was designed to understand the mechanisms involved in the transfer of fluids between the matrix rock and the fracture as a result of steam injection. Both continuous and cyclic steam injection experiments were performed on a fractured laboratory system. Saturations were measured in-situ both in the fracture and the consolidated matrix by a CT scanner. The results indicated that there was no steam saturation in the matrix, and that conduction was the dominant heat transfer mechanism.

Numerical simulations were used to model both continuous and cyclic steam injection experiments. To model heat losses, heat loss models in the simulator had to be adjusted based on the analysis of the heat losses from the laboratory system with analytical models. After this adjustment, the results from the simulations agreed well with the experiments.

When pressure cycling was applied in the simulations with no external heat losses, a considerable amount of steam saturation was observed in the matrix.

While the experiments were done with water and steam, simulation runs were also performed for the laboratory system with oil present. Again, steam only flowed in the fracture. Oil recovery was found to be mainly caused by water imbibition into the matrix and heat conduction.

Results of this work should be useful in modeling matrix/fracture transfer in dual porosity thermal models.

3.2 CT Imaging Techniques for Two-Phase and Three Phase In-situ Saturation Measurements

(B. Sharma, W.E. Brigham, L.M. Castanier)

3.2.1 ABSTRACT

The aim of this research is to use the SUPRI 3-D steam injection laboratory model to establish a reliable method for three-phase in-situ saturation measurements, and thereafter investigate the mechanism of steamflood at residual oil saturation.

Demiral *et al.* (1992) designed and constructed a three-dimensional laboratory model that can be used to measure temperature, pressure and heat loss data. The model is also designed so that its construction materials are not a limiting factor for CT scanning. We have used this model for our study. In this study, we saturated the model with mineral oil, and carried out a waterflood to residual oil saturation. Steamflood was then carried out. A leak appeared at the bottom of the model. Despite this problem, the saturation results, obtained by using two-phase and three-phase saturation equations for the Cat scanner, were compared with the saturations obtained from material balance. The errors thus obtained were compared with those obtained by an error analysis carried out on the saturation equations.

This report gives details of the experimental procedures, the data acquisition and data processing computer programs, and the analysis of a steamflood experiment carried out at residual oil saturation.

3.3 Pore Level Visualization of Foam Flow in a Silicon Micromodel

(F. Woody, M. Blunt and L. Castanier)

This report is completed. The abstract is as follows.

3.3.1 ABSTRACT

This paper is concerned with the behavior of foam in porous media at the pore level. Identical, heterogeneous silicon micromodels, two dimensionally etched to replicate flow in Berea Sandstone, were used. The models, already saturated with varying concentrations of surfactant and, at times, oil were invaded with air. Visual observations were made of these air displacement events in an effort to determine foam flow characteristics with varying surfactant concentrations, and differing surfactants in the presence of oil. These displacement events were recorded on video tape. These tapes are available at the Stanford University Petroleum Research Institute, Stanford, California.

The observed air flow characteristics can be broadly classified into two: continuous and discontinuous. Continuous air flow was observed in two phase runs when the micromodel contained no aqueous surfactant solution. Air followed a tortuous path to the outlet, splitting and reconnecting around grains, isolating water located in dead-end or circumvented pores, all without breaking and forming bubbles. No foam was created.

Discontinuous air flow occurred in runs containing surfactant -- with smaller bubble sizes appearing with higher surfactant concentrations. Air moved through the medium by way of modified bubble train flow where bubbles travel through pore throats and tend to reside more statically in larger pore bodies until enough force is applied to move them along. The lamellae were stable, and breaking and reforming events by liquid drainage and corner flow were observed in higher surfactant concentrations. However, the classic snap-off process, as described by Roof (1973) was not seen at all.

With oil, we saw coarser bubble texture along with stable water lenses between gas. Events consistent with the drainage of thin spreading oil layers, as well as the collapse of a water film between oil and gas were observed.

3.4 Oil-Foam Interactions in a Micromodel

(N. Sagar)

3.2.1 INTRODUCTION

There has been a considerable amount of work published regarding foam research. The literature provides valuable insight into the occurrence, properties, importance and propagation mechanisms of foams based on colloid science. Many laboratory investigations of foam flooding have been carried out in the absence of oil, and comparatively few have been carried out with oil present. An argument for not including oil was simply, that a need to understand the basic propagation mechanisms of foam dictated such a move. Any additional components would only serve to complicate matters. As research on foam and its propagation in porous media progressed, foam was seen as a fascinating fluid, both because of its unique microstructure, and because of its dramatic influence on the flow of gas and liquid.

When research began to include oil, it was seen that the effect of oil on foam stability was indeed complicated. Oil saturation could alter foam stability and its propagation mechanisms to a great extent. From a practical viewpoint for example, a field application where the residual oil saturation may vary from as low as 0% to as high as 40%, depending on the recovery method applied, any effect of oil on foam stability becomes a crucial matter. Also the nature of the foam, foam injection procedures, reservoir wettabilities and pore geometry were beginning to be seen as detrimental to the oil-foam interactions making it even more complicated.

Clearly as more work is required in this area, this need provides a basis for our study.

3.2.2 LITERATURE SURVEY

The production of oil from a petroleum reservoir involves first the primary and secondary production modes, which may recover less than half of the oil originally in place. To recover additional oil, it is necessary to apply enhanced oil recovery (EOR) techniques such as miscible or immiscible gas displacement. However major problems occur in these EOR methods because the displacing agent often has high mobility and low density compared with that of reservoir fluids. Fingering (channeling) and gravity override reduce the sweep efficiency, contribute to early breakthrough of injected fluid, and thus reduce the amount of oil recovered.

3.2.2.1 Early Work on Mobility and Propagation of Foam

The use of surfactant stabilized foams to counteract these kinds of problems was suggested several decades ago. Fried (1961) demonstrated that aqueous surfactant stabilized foam could dramatically reduce the mobility of gases in porous media. At that time foam was studied mainly from a phenomenological perspective. In the intervening 35

years, foam has been recognized as a fluid with unique rheological properties within porous media, and the scope of research has expanded to include local pore scale phenomena and local microstructure. Considerable work was published by Raza, Marsden, Bernard et al, Mast, Khan, Nahid in the 1960's and 70's regarding the behaviour of foam. Details of these are not covered in this literature survey as they have been exhaustively covered earlier.

However none of these proposed early mechanisms adequately accounted for all the observed properties of foam in porous media. The only general agreement was that foam generally hindered the flow of gas in porous media.

3.2.2.2 Recent Work on the Mobility and Propagation of Foam

Marsden (1986) reviewed previous findings, surmising that apparent gas viscosity was indeed a function of the gas flow rate, flow history and surfactant concentration, and that 'breaking and reforming' processes are a dominant mode of foam propagation in micromodels. Sanchez and Schechter (1986) suggested that gas permeability was a function of wetting phase film thickness.

Owete *et al.* (1986) suggested that air was propagated by displacement of lamellae in long bubbles flowing and extending across several pore lengths while the liquid flowed through the network of films. They also observed snap-off occurring at pore constrictions and the resultant bubble 'break and reform' process. Radke and Ransohoff (1986) categorized the various mechanisms of foam generation within glass bead packs as 'snap-off', 'lamella leave behind', and 'lamella division', with snap-off being the primary mechanism for strong foam propagation.

Roof (1970) and Mohanty *et al.* (1980) each studied and reported specific pore geometry necessary for snap-off mechanisms. Roof noted that the front is always at least seven pore radii from the throat of the constriction before snap-off can occur. Mohanty et al. calculated that snap-off occurs when the ratio of pore body radius to adjacent throat exceeds three. Falls *et al.* (1988) and Kovscek *et al.* (1994) proposed that the rate of generation of lamella must be equal to their collapse.

Castanier and Hanssen (1995) noticed the sliding of lamellae (bubble train flow) over liquid films covering the grains in silicon micromodels. Using atomic force microscopy between the liquid/solid interface, a thick layer of surfactant was found. This layer they state could explain the apparent bubble train effect observed.

3.2.2.3 Spreading and Entering Coefficient Theory for Oil-Foam Interactions

The spreading coefficient, S, for an oil-foam system is given by:

$$S = \gamma_f^o - \gamma_{of} - \gamma_o^o$$

where : γ_f^o = Foaming solution surface tension

γ_{of} = Initial foaming solution/oil interfacial tension

γ_o^o = Surface Tension of the oil

When oil spreads over the gas-aqueous interface, a certain amount of both gas-oil and aqueous-oil interface is created, and some gas-aqueous interface is eliminated. For a unit surface area, the Gibbs free energy change (ΔG) is given by '-S'. The spreading is predicted to be favored when ΔG is negative and S is positive. Rapid spreading of a drop of oil that has a low surface tension over the lamella can cause rupture by providing a weak spot. The spreading oil lowers the surface tension, increases the radius of curvature of the bubbles, alters the original surface elasticity, and also changes the surface viscosity. Thus the interfacial film loses its foam stabilizing capability. If S is negative, then the oil should not spread at the interface.

Another mechanism of rupture involves the drawing up of a droplet of defoamer into the lamella region between two adjacent bubbles so that it can bridge the two bubbles. The breaching of the aqueous-gas interface by the oil from within the lamellar liquid is termed 'entering'. The process is thermodynamically favorable if the 'Entering Coefficient' is positive (originally defined by Robins and Woods (1948) as a rupture coefficient, R). For a oil-foam system, the entering coefficient is given as :

$$E = \gamma_f^o + \gamma_{of} - \gamma_o^o$$

For unit surface area, the Gibbs free energy change is given by '-E'. The entering is predicted to be favored and spontaneous when ΔG is negative and E is positive.

3.2.2.4 Work on Effect of Oil on Foam Stability and Propagation

Oils such as Castor oil, are among the earliest chemicals to be used for foam inhibition and foam breaking. Literature by Harkins (1941), Robinson *et al.* (1948), Ross (1944) deals with it. Some theories for the mechanisms of anti-foaming action have emerged from this work. In general matters are not simple. Apparently foams can be destabilized by oils by several mechanisms, and more than one mechanism may be operating in a given case.

Some possibilities for the mechanisms of foam destabilization by a given oil phase include :

- Foam-forming surfactant may be absorbed by the oil, especially if there is emulsification , causing depletion in the aqueous phase and hence from the gas-liquid interface.

- Surfactants from the oil may be adsorbed by the foam lamellae, from either a mixed or replaced adsorption layer, and produce a less favorable state of foaming.

- Components from the oil may be adsorbed by the porous medium altering the wettability of the solid phase, and this alteration makes it more difficult for foam to be generated and regenerated.

- The oil may spread spontaneously on foam lamellae and displace the foam stabilizing interface.

- The oil may emulsify spontaneously and allow the drops to break and rupture the stabilizing interface.

Nikolov *et al.* (1986), when studying bulk oil-foam interactions, reported the possible occurrence of three distinct films during the process of three phase foam thinning. They are 'foam films', which are water films between air bubbles; 'emulsion films', which represent water films between oil droplets; and 'pseudo-emulsion films' where water films reside between air and oil droplets. Their findings said that pseudo-emulsion films, droplet size and droplet numbers may all contribute to foam destabilization.

Rendall *et al.* (1990) investigated the behavior of several commercial surfactant destabilized foams, in the presence of crude oil. On the basis of dynamic bulk foaming tests, gas mobility reduction factors measured in reservoir cores, and observations in a microvisual apparatus, it was found that all but one of the foams studied were destroyed when brought into contact with oil.

Similarly Kuhlman (1988) and Manlowe and Radke (1990) observed in micromodel studies that oils were capable of destroying foams. Work done by Novosad *et al.* (1989), Jensen and Friedmann (1987) and Holt (1991) suggested that foam sensitivity to oil is also manifested as an increased difficulty of forming and in propagating foams through porous media containing oil. Novosad and Ionescu (1987) found lower mobility reduction factors in foam floods conducted in cores containing residual oil compared to the same floods conducted in cores that were completely free of oil. The lower mobility reduction factors were interpreted to be due to some kind of foam destruction by the oil.

Lau and O'Brien (1988) provided further insight into the effects of oil saturation on foam propagation. Their work relies upon an understanding of oil spreading ability in which spreading is determined from 'spreading coefficients' or free surface energies. Through the use of sandpacks and both spreading and non-spreading oils, they were able to show an increase in foam generation time, a reduction in foam propagation rate, and an increased foam destruction rate with spreading oils. This finding is contrary to Manlowe and Radke's (1980) who argue that there is no correlation between oil spreading and foam stability. Instead, they state pseudo-emulsion film collapse is the general destabilization mechanism.

Hanssen *et al.* (1990), in a model system (glass bead pack) of a gas blocking foam in an oil reservoir, observed clear trends in the mobility reduction as measured in a gas-blockage test, with varying concentrations of oil and surfactant. They concluded that the change in interfacial tension between gas and the aqueous phase, upon equilibration with oil, appeared to be a good predictor of gas-blockage efficiency for the systems studied.

Oil interactions with foam have been studied by Dalland *et al.* (1993). On conducting experiments with flowing and gas blocking foams in porous media, using a set

of conventional and fluorinated surfactants and various oils, they found varying oil tolerance and sensitivities. In all cases it was found that the combination of non-spreading and non-entering oil created a strong gas-blocking foam or a low mobility flowing foam. The 'Lamella number', L, calculated from interfacial tensions was found to be of no predictive power. The results indicated that the mechanisms of oil-foam interactions are the same for gas blocking and for flowing foams in porous media.

From unpublished work by Castanier on oil-foam interactions using a fluorosurfactant foam and an AOS foam, the fluorosurfactant foam seems to give the oil tolerant behavior expected from its non-entering, non-tolerant characteristics. AOS foam by contrast, is seen to be controlled by formation of oil-water emulsions which appear to prevent the formation of strong foam until a large excess of foaming agent is present.

3.2.2.5 Work on Effect of Wettability of the Rock on Oil-Foam Interactions

Most of the research on foam sensitivity to oils in porous media, whether in microvisual apparatus or core-fluid tests, has been concerned with water wetted pore and throat surfaces. Because many petroleum reservoirs are of intermediate, mixed or oil wettability, some researchers have spread their work to include reservoir wettabilities.

Huh et al. (1988) found that micromodel wettability was altered to intermediate or oil-wet as a result of crude oil saturation. The effects of various phase affinities to grain surfaces was studied by Sanchez and Hazlett (1989) as well. An indication of surface reaction, from hydrophobic to hydrophilic, was detected after the addition of surfactant. This fact, along with a shift in liquid phase relative permeability of the oil-wet medium, suggested wettability alteration.

Kuhlman (1990) commented on similar results of his own, remarking that the deleterious effect of oil on foam was due, in part at least, to the high concentration of light hydrocarbons in the oil, and the oil wetness of the medium itself. Work by Hornbrook *et al.* (1992) noted that wettability alteration was due to the surfactant injection procedure. They found that with surfactant slug injection, oil appeared to be the wetting phase, and with foam injection, surfactant appeared to wet the medium.

Schramm and Mannhardt(1992) conducted oleophilic microvisual cell experiments with several foams. They found that the foams were significantly less stable in the presence of crude oil and oleophilic solid surfaces, compared with some crude oils and hydrophilic surfaces. Suffridge et al. (1989) reached the same conclusions on the basis of core-flood experiments. They found that the foams were more effective (stable) in water wet cores than in oil wet cores. Holt and Kristiansen (1991) studied foams flowing in cores under North Sea reservoir conditions that were either partially or completely oil wetted. They found that foam effectiveness was favored by water-wet conditions. Any degree of oil-wet character reduced the effectiveness of the flowing foam.

A complication is that the foam forming surfactants may adsorb onto the solid surfaces and may alter the wettability. In the microvisual experiments of Schramm and Mannhardt (1992), some of the foaming systems investigated appeared to change the wettability back to water-wet, in which case the foam sensitivities to oil reverted back to those appropriate to the water-wet cases. The result is consistent with the core-flood tests

of Sanchez and Hazlett (1992) in which foaming surfactants apparently caused wettability reversal in oil wet porous media. This reversal, in turn, was postulated to be the reason that stable foams could be generated and propagated in their oil-wetted cases.

3.2.3 INTENDED WORK

From the foregoing literature survey, it can be seen that the work done in oil-foam interaction mechanism studies gives us a direction, but definitely there is much to be studied with regard to the oil-foam interactions, the effects of wettability, and the processes governing them at the pore level.

With the micromodels, we intend studying the behavior of foam in the presence of oil using two specific surfactants, B-1333 and Servo AOS with a light crude oil from Norway, and possibly a Californian light crude. Different concentrations of surfactant and oil will be used in the micromodel displacement experiments.

It is felt that, with our new high-resolution micromodels, we are closer to the actual pore level phenomena than the previous models used to study oil-foam interactions at the pore scale.

The experimental procedure would consist of the following prominent steps:
(a) Oil flood
(b) Waterflood to residual oil saturation
(c) Surfactant injection
(d) Gas injection to generate foam

Steps (a) and (b) will be omitted when the experiments are performed with no crude oil present.

The following table lists the planned experiments:

Experiment Number	**Oil**	**Surfactant Concentration (%)**	
		AOS	**B-1333(Fluoro)**
1.	None	0.001	0.001
2.	None	0.01	0.01
3.	None	0.1	0.1
4.	None	1.0	1.0
5.	Crude A	0.1	0.1
6.	Crude A	1.0	1.0
7.	Crude B	0.1	0.1
8.	Crude B	1.0	1.0

3.2.4 REFERENCES

1. Bikerman, J.J.: "Foams;" Springer-Verlag : New York (1973).

2. Ross, S.: "Kirk -Othmer Encyclopedia of Chemical Technology," Third Ed; Wiley, New York (1980); Vol. 11, pp 127-145.

3. Robinson, J.W.;Woods,W.W. Soc. Chem. Ind. (1948), 67, 361-365.

4. Novosad, J.J.; Mannhardt, K.; Rendall, A. Proceedings of the 40th Annual Technical Meeting Of CIM; Calgary, Canada (1989); paper CIM 89-40-29.

5. Kuhlman, M,I. Proceedings of the SPE/DOE Enhanced Oil Recovery Symposium; Society Of Petroleum Engineers, Richardson,1988; SPE/DOE 17356.

6. Jensen, J.A. ; Friedmann, F. Proceedings of the California Regional Meeting of SPE; Society Of Petroleum Engineers : Richardson, TX, 1987; SPE/DOE 16375.

7. Kristiansen, T.S; Holt, T. Proceedings of the 12th International Workshop and symposium of the IEA Collaborative Project on Enhanced Oil Recovery; AEA Technology : Winfrith, UK, 1991.

8. Hanssen, J.E.; Dalland, M. Proceedings of the SPE/DOE 7th Enhanced Oil Recovery Symposium; Society Of Petroleum Engineers : Richardson, TX, 1990; paper CIM 86-37-01.

9. Schramm, L.L.; Turta, A.; Novosad, J.J. Proceedings of the SPE/DOE 7th Symposium on Enhanced Oil Recovery; Society Of Petroleum Engineers : Richardson, TX, 1990; SPE/DOE 20197.

10. Schramm, L.L. Foams: Fundamentals and Applications in the Petroleum Industry; American Chemical Society, Washington D.C. 1994.

11. Dalland, M.; Hanssen, J.E. Oil Interaction with foams at static and flowing conditions in porous media. Paper at the 13th EOR workshop and symposium, Banff 1992.

12. Hanssen, J.E.; Dalland, M. Foam barriers for thin oil rims : Gas Blockage at reservoir conditions. Paper, Sixth European Symposium on Improved Oil Recovery, Stavanger, 21-23 May 1991.

13. Meling, T.; Hanssen, J.E. Gas Blocking foams in porous media : effects of oil and surfactant hydrophobe carbon number Prog.Colloid Sci. 82:140-154, 1990.

14. Hanssen, J.E.; Dalland, M. Foams for effective gas blockage in the presence of crude oil. SPE/DOE 20193, 1990.

15. Woody, F.; Blunt, M.; Catanier, L.M. Pore level visualization of foam flow in a silicon Micromodel, SUPRI TR-100, Stanford University, 1995.

16. Marsden, S.S.; Foams In porous media, SUPRI TR-37, Stanford University, 1986.

17. Castanier, L.M.; Brigham,W.E. Annual Report SUPRI TR-99, Stanford University, (1995).

18. Owete, O.S.; Brigham, W.E. Flow of foam through porous media, SUPRI TR, Stanford University (1984).

PROJECT 4: RESERVOIR DEFINITION

To develop and improve techniques of formation evaluation such as tracer tests and pressure transient tests.

There are no students presently working on this project.

PROJECT 5: FIELD SUPPORT SERVICES

To provide technical support for design and monitoring of DOE sponsored or industry initiated field projects.

5.1 Water Influx Equations

(W. Brigham)

5.1.1 SUMMARY

The recovery from many oil reservoirs is affected by water influx, either from the perimeters of the oil reservoirs, or from below, or from both. In fact, worldwide, there is far more water produced from oil reservoirs than oil. Much of this is natural water influx. It is clear then, that an understanding of the interplay between aquifers and the oil reservoirs needs to be understood to properly perform oil recovery calculations.

Typically, when one looks at discussions of water influx in reservoir engineering texts, the subject is treated as though only the aquifer needs to be looked at. Various inner and outer boundary conditions and geometries are addressed, and solutions on the behavior of the aquifers are discussed. From these, various ways of solving these problems are presented, assuming one knows the inner boundary rate or pressure history.

In these notes I discuss these various problems in the order of their complexity of solution rather than in the chronological order in which they would be used by a reservoir engineer. The reason for this is simple. The ideas from one group of concepts can thus be built upon for the next group. In this portion of the notes I will only address the aquifer flow solutions.

This report shows that the results for all three geometries (linear, radial, and spherical) can be put into exact equation forms. Further, for all the possible inner and outer boundary conditions (Inner Boundary; constant rate or constant pressure; Outer Boundary; infinite, constant pressure or closed) the solutions behave in a logical manner for all these assumptions. We also show that the exact infinite series solutions can be transformed into very accurate closed form approximations which make calculations much easier, and which also give great insight into the behavior of the various solutions. We also show that superposition is an important way of handling real data which vary both in pressure and flow rate with time. Further notes on this subject will discuss how to relate these ideas to oil reservoir/aquifer systems, the ultimate goal for reservoir engineering applications.

☆U.S. GOVERNMENT PRINTING OFFICE: 1996 - 760-032/40018